Pediatric Reference Curves of Cardiac Parameters

Dissertation

zur Erlangung des Doktorgrades (PhD)

der Medizinischen Fakultät

der Rheinischen Friedrich-Wilhelms-Universität

Bonn

Christian Jürgen Winkler

aus Köln

2021

Angefertigt mit der Genehmigung

der Medizinischen Fakultät der Universität Bonn

1. Gutachter: Prof. Dr. med. Johannes Breuer

2. Gutachter: Prof. Dr. Thomas Schultz

Tag der Mündlichen Prüfung: 19.04.2021

Aus der Abteilung für Kinderkardiologie

Direktor: Prof. Dr. med. Johannes Breuer

Contents

1 Abstract **1**

2 Introduction **2**

3 Objectives **4**

4 Methods **5**
4.1 First study 5
4.1.1 Data for computing reference curves 5
4.1.2 Data acquisition for validating the stroke work estimation 7
4.1.3 Modeling of the pressure-volume loop 7
4.1.4 Model fitting 10
4.2 Second and third study 11
4.3 Reference curves for standard values 12

5 Results **14**
5.1 First study 14
5.2 Second study 15
5.3 Third study 16

6 Discussion **18**
6.1 Clinical implication 18
6.2 Limitations of the stroke work estimation 19
6.3 Limitations of left atrial and left ventricular volumes quantification 20
6.4 Limitations of the creation of reference curves 20
6.5 Conclusion 22

7 Appendix A - First study **30**

8 Appendix B - Second study **42**

9 Appendix C - Third study **62**

1 Abstract

In pediatric cardiology, the examination of cardiac parameters, such as the left ventricular volume and the stroke work, is essential to diagnose and treat patients with congenital heart disease. Pediatric standard values of cardiac parameters, which serve as a reference for examinations, are however scarce. The objective of this thesis is to determine pediatric reference curves of cardiac parameters by using a total of 497 healthy children's clinical data and mathematical modeling. This thesis contains three published studies, which provide computed and measured values of cardiac parameters. The first study estimates the left ventricular stroke work (SW) based on a data set of 340 healthy children and modeled pressure-volume loops from a lumped parameter model (LPM). As such, an LPM developed by Pironet et al. was extended by fitting it to the measured volumetric data. In the second study, pediatric reference curves were established for left atrial (LA) volumes based on the 3D echocardiography data of 432 healthy children. In the third study, reference curves were established for left ventricular (LV) volumes based on the data of 370 healthy children. The mentioned reference curves provide standard values of SW, LA volume, and LV volume for age, weight, and height of children.

2 Introduction

In Germany, about 1 in 100 children is born with a heart defect, while the spectrum ranges from mild to serious conditions. The most common heart defects are ventricular septal defects (49 %), atrial septal defects (17 %), valvular pulmonary stenoses (6 %), persistent ductus arteriosus (4 %), and aortic stenoses (4 %) (Lindinger et al., 2010). Patients with a single ventricle, who are examined in this work, have a prevalence of about 3 % of all congenital heart defects (CHD). By virtue of early diagnosis and treatment, 90 % of children with CHD reach adulthood today. The examination of cardiac parameters helps physicians to diagnose and treat these patients. A valuable method to obtain data is three-dimensional (3D) echocardiography, which is a non-invasive measurement technique. Common cardiac parameters, such as the volume of the heart chambers, can be derived from 3D echocardiographic images.

In addition to the assessment of common cardiac parameters, physicians aim to develop methods to extract more information from measured data. Indicators such as the left ventricular stroke work (SW) have gained interest in recent years (Ben-Assa et al., 2019; AbouEzzeddine et al., 2019; Gotzmann et al., 2019; Sprigings et al., 1990). SW represents the energy provided by the ventricle to pump blood into the arteries. With reduced energy, the heart is not capable of providing enough blood to the circulation. This can result in clinical symptoms of heart failure. SW is the integrated product of pressure and volume flow with respect to time. It can be visualized as the area within the pressure-volume loop (PV loop). The computation of SW requires information about left ventricular pressure and volume for the duration of one cardiac cycle. The gold standard measurement technology for the simultaneous measurement of pressure and volume in the ventricle is the conductance catheter technology. A catheter intervention is, however, risky and should not be performed in healthy subjects. Alternatively, non-invasive measurements in combination with modeling approaches have to be considered (Seemann et al., 2019). For the computation of blood pressure, lumped parameter models (LPM) have been established as an

efficient modeling approach (Mineroff et al., 2019; Kung et al., 2014; Neidlin et al., 2014; Hsia et al., 2011; Kaufmann et al., 2014). Pironet et al. (de Bournonville et al., 2019; Pironet et al., 2019) developed and validated a minimal cardiovascular model with animal data. Their proposed model contains 8 model parameters, which is a small number of parameters compared to the mentioned LPM. A model with small number of parameters is suitable for a parameter identification from a limited number of measurements. Based on the identification of the parameters, the SW computation and pressure-volume loop analysis can be performed.

Many computational models, such as the LPM mentioned above, focus on adult hemodynamics. However, approaches to compute cardiac parameters for pediatric patients, such as SW, have not been performed to such extent. Pediatric patients exhibit high variations in cardiac parameters and further mechanistic insights of variables that cannot be measured non-interventionally could ultimately improve current therapies. Such insights can be obtained via mathematical modeling and clinical data analysis based on LPM.

Another issue addressed in this thesis is the presentation of parameters. Measured and modeled cardiac parameters have to be presented in a way that clinical staff can access easily. Reference curves and charts have been established as a commonly used tool for pediatricians to describe the normal range of cardiac parameters. In clinical practice, physicians use percentile curves (or z-score curves) to evaluate the data gathered from patients. Comparing the measurement to a reference helps to quantify the severity of the disease and diagnose the condition of a patient. Therefore, the presentation as reference curves could be an appropriate way to provide computational results achieved by a cardiovascular model to clinical professionals.

3 Objectives

The overarching objective of this thesis is to determine pediatric reference curves of cardiac parameters by using clinical data of in total 497 healthy children and mathematical modeling. The reference curves were created over a biometric variable, such as age, weight, and height. Three published studies are parts of this thesis. The first study estimates the left ventricular stroke work (SW) based on a data set of 340 healthy children and modeled pressure-volume loops from a lumped parameter model (LPM). As such, an LPM developed by Pironet et al. was extended by fitting it to the measured volumetric data. In the second study, pediatric reference curves were established for left atrial (LA) volumes based on the 3D echocardiography data of 432 healthy children. As part of that, the volume before atrial contraction (VpreA) was determined. In the third study, reference curves were established for left ventricular (LV) volumes based on the data of 370 healthy children.

4 Methods

In a prospective multicenter design, 497 children and adolescents from birth to 18 years of age were enrolled to undergo 3D echocardiography examination. The age, body size, weight, and gender of each child were obtained. This data set served as the basis for all three studies. Normal cardiac anatomy and function as well as sinus rhythm were a precondition and confirmed by physical examination. 3D echocardiographical data sets were measured with two different sonographic units. On the one hand, iE33 (Philips, Andover, MA) with a matrix transducer X5-1 or X7-2 was used, on the other hand, Vivid E9 (GE Medical Systems, Milwaukee, WI) with a V4 transducer was used. The volumetric shapes of the left ventricle and the left atrium were determined for one heartbeat with two segmentation softwares (QLab and TomTec).

4.1 First study

For the SW estimation, left ventricular volume was measured non-invasively and left ventricular pressure was approximated by a regression model. The SW estimation was validated with patient data. Reference curves were created for the estimation of SW of healthy children.

4.1.1 Data for computing reference curves

The 3D shape of the left ventricle for 370 children was determined with the segmentation software QLab. QLab was also used to compute the volume-time curve, which shows the volumes over the period of one heart cycle. The maximal and minimal left ventricular volume during one heart cycle, $V_{lv,max}^{echo}$, and $V_{lv,min}^{echo}$, were determined using the volume-time curve. The RR duration, a measure of heart rate, was acquired simultaneously. The ventricular volume of 340 healthy children were used for the SW estimation. Volumetric data

of 156 girls and 184 boys were measured.

In this study, the assumption was made that the maximal blood pressure in the left ventricle, $P_{lv,max}$, can be approximated by the systolic systemic blood pressure ($P_{lv,max} \approx P_{sys,systolic}$). To estimate the systemic blood pressure, we used regression models to obtain clinical references of healthy children (50th percentile) (Neuhauser et al., 2013), with a distinction between girls and boys. For both girls and boys, the regression model estimates the systemic blood pressure with the input of age and body height.

To estimate left ventricular stroke work (SW), we considered the three methods SW_1, SW_2, and SW_3. SW_1 is a precise calculation, while SW_2 is a rough estimation. SW_3 is a clinical approach using commonly measured pressures.

The three different formulas were used to assess the range for SW computations. SW_2 is expected to mark the maximal possible value, while SW_1 and SW_3 should give lower values. Furthermore, a clinical study has shown that SW_3 underestimates SW (Topham, 1969), which we used for assessing the estimation results.

SW is defined as the integrated product of pressure and volume over one cardiac cycle

$$SW = \int P_{lv}(t)\, dV_{lv} = \int P_{lv}(t) \cdot Q_{lv}(t)\, dt \tag{4.1}$$

where P_{lv}, V_{lv}, and Q_{lv} are blood pressure, volume and flow, respectively. SW can be depicted as the area inside the pressure-volume loop.

This formula can be discretized by

$$SW_1 \approx \sum_{n=0}^{N} P_{lv}(t_n) \cdot Q_{lv}(t_n)\ \cdot (t_{n+1} - t_n) \approx \sum_{n=0}^{N-1} P_{lv}(t_n) \cdot (V_{lv}(t_{n+1}) - V_{lv}(t_n)) \tag{4.2}$$

for N time steps. For the bounds of integration, it must be considered that the ventricle pumps blood actively into the aorta during systole and is filled with blood passively during diastole. For a rough estimation, SW can be approximated by

$$SW_2 = \Delta P \cdot SV \tag{4.3}$$

where ΔP is the pressure difference between maximal and minimal ventricular pressure and SV is the stroke volume. SW_2 is represented by the rectangular area bordering the pressure-volume loop.

A formula for SW commonly used by clinicians is

$$SW_3 = MAP \cdot SV \tag{4.4}$$

where MAP is the mean arterial pressure (Klabunde, 2011). SW_1, SW_2, and SW_3 were computed from the model output (P_{lv}, V_{lv}, and MAP), which is described in Section 4.1.3.

4.1.2 Data acquisition for validating the stroke work estimation

Left ventricular volume and pressure were measured simultaneously in a patient group by a conductance catheter and used to validate the SW estimations. 18 measurement data sets were taken from a patient group of 11 children with congenital heart disease, which needed invasive cardiac catheterization due to clinical reasons.

4.1.3 Modeling of the pressure-volume loop

For the modeling of pressure-volume (PV) loops, we used a three-chamber cardiovascular model in the form of a lumped parameter model (LPM) by Pironet et al. (de Bournonville et al., 2019; Pironet et al., 2019, 2015). According to Pironet et al., the systemic and pulmonary circulations can be merged into a model that represents only one circulation. This kind of LPM with only one circulation has also been shown as suitable for other studies (Parlikar and Verghese, 2006; Olufsen et al., 2005). The LPM was used for both patients and healthy children.

Fig. 4.1 shows the structure of the LPM, while Table 4.1 lists the model parameters with description. The LPM includes the aorta (ao), one vena cava (vc), and the left ventricle (lv). It describes the relationship between the variables flow (Q), volume (V), and blood

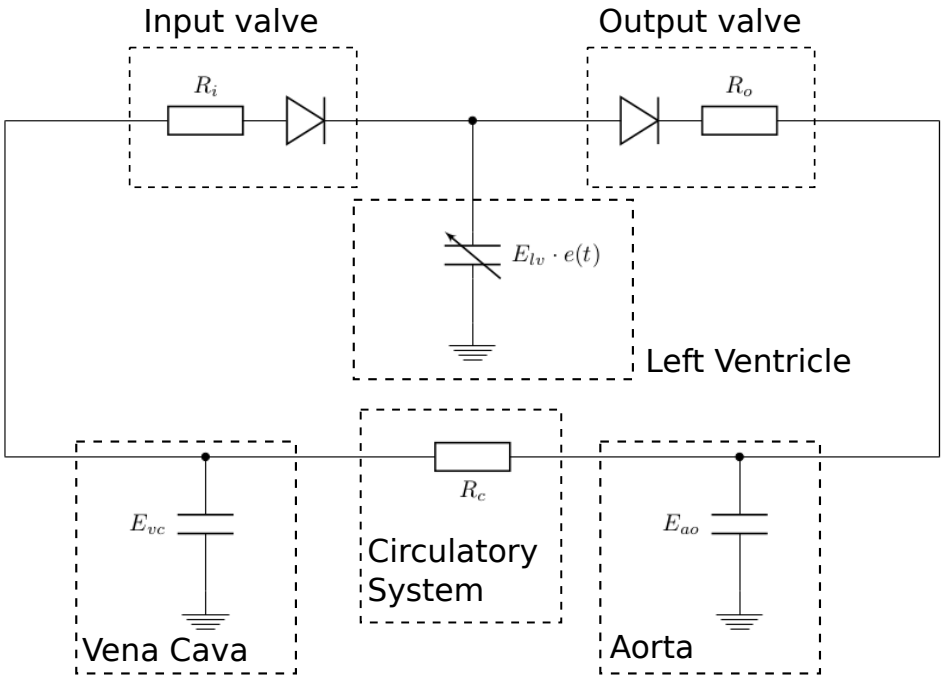

Figure 4.1: Lumped parameter model (LPM) represented by an electrical network. The left ventricle, aorta, and vena cava are modeled by conductors. The valves are represented by resistors and diodes. The circulatory system consists of a resistor.

pressure (P). The LPM is represented by a system of ordinary differential equations (ODE) and algebraic equations. The aorta, the vena cava and the circulatory system can be considered as abstract elements surrounding the left ventricle. They define the boundary conditions for the left ventricular behavior. The pressure in the left ventricle is given by

$$P_{lv}(t) = E_{lv}(t) \cdot (V_{lv}(t) - V_{U,lv}) \tag{4.5}$$

where $V_{lv}(t)$ is the volume, $V_{U,lv}$ is the unstressed blood volume, and $E_{lv}(t)$ is the time depending elastance, see Eq. 4.6.

$$E_{lv}(t) = E_{lv} \cdot e_{lv}(t, T) \tag{4.6}$$

with $e_{lv}(t, T)$ as the driver function. For this study, we used the driver function proposed by Korakianitis et al. (Korakianitis and Shi, 2006). The left ventricular unstressed blood vol-

Parameter	Description
E_{lv}	Maximal elastance of the left ventricle
E_{ao}	Elastance of the aorta
E_{vc}	Elastance of the vena cava
R_c	Resistance of the circulatory system
R_i	Resistance of the input valve
R_o	Resistance of the output valve
SBV	Stressed blood volume
T	Duration of a cardiac cycle

Table 4.1: The LPM is based on 8 model parameters (R_i, R_c, R_o, E_{ao}, E_{vc}, E_{lv}, SBV, T).

ume $V_{U,lv}$ is the blood volume that does not contribute to the pressure. It can be measured by preload reduction, which requires invasive intervention (Glower et al., 1985). We assumed it to be zero, which is commonly done for the analysis of cardiac dynamics (Stevenson et al., 2012; Seemann et al., 2019). Time alignment between model and measurement was achieved by adjusting the length of a heartbeat T in the driver function $e_{lv}(t, T)$ with the measured RR interval. To fit the model to the measurements, a subset selection of the model parameters was performed. As a result, we defined model parameters to be estimated as

$$p = [E_{lv}, R_c, SBV]^T \tag{4.7}$$

where $p \in \mathbb{R}_{>0}$. To obtain an overview about the parameter interaction, other parameters were assigned ($R_i = R_o = 0.1$ and $E_{vc} = E_{ao} = 1.0$) and kept constant during the estimation procedure.

The model output is defined as

$$y^{model}(p) = [P_{lv}(t), V_{lv}(t)]^T \tag{4.8}$$

depending on the vector of model parameters p. The mean atrial pressure, MAP, can be extracted from the model

$$MAP \approx \frac{1}{N} \sum_{n=0}^{N} P_{ao}(t_n) \tag{4.9}$$

where P_{ao} is the simulated aortic pressure.

4.1.4 Model fitting

For model fitting, we minimized a scalar function $f_{error}(p)$ that defines the deviation between measurement and model output

$$f_{error,i}(p) = (y_i^{measurement} - y_i^{model}(p))^2 \tag{4.10}$$

for the constraints i. In general, $V_{lv,min}$, $V_{lv,max}$ and the $P_{lv,max}$ were used as constraints

$$f_{error}(p) \quad = \quad f_{error,V_{lv,min}}(p) + f_{error,V_{lv,max}}(p) + f_{error,P_{lv,max}}(p) \tag{4.11}$$

where p represents the vector of model parameters to be estimated. For the validation of model fitting, conductance catheter measurements in patients ($V_{lv,min}^{\ cond}$, $V_{lv,max}^{\ cond}$, $P_{lv,max}^{\ cond}$) were used:

$$f_{error}^{patient}(p) \quad = \quad f_{error,V_{lv,min}^{\ cond}}(p) + f_{error,V_{lv,max}^{\ cond}}(p) + f_{error,P_{lv,max}^{\ cond}}(p) \tag{4.12}$$

For the SW estimation in the healthy cohort, ventricular volume measured by 3D echocardiography ($V_{lv,min}^{\ cond}$, $V_{lv,max}^{\ cond}$) and ventricular pressure computed by the regression model ($P_{lv,max}^{\ regression}$) were used.

$$f_{error}^{healthy}(p) \quad = \quad f_{error,V_{lv,min}^{\ echo}}(p) + f_{error,V_{lv,max}^{\ echo}}(p) + f_{error,P_{lv,max}^{\ regression}}(p) \tag{4.13}$$

The minimization is achieved by

$$\min_{p \in \mathbb{R}_{>0}} f_{error}(p) \tag{4.14}$$

to find a set of estimated model parameters $\hat{p} = [\hat{E}_{lv}, \hat{R}_c, \hat{SBV}]$. The estimated parameters have to be part of the positive real numbers due to their physical character. The Nelder-Mead method was used for minimization (Gao and Han, 2012). Initial conditions for $V_{S,lv}$, $V_{S,ao}$, and $V_{S,vc}$ were first set to $SBV/3$. We assumed a steady state after 20 heartbeats

and used the calculated state values as initial conditions for the main simulation. We developed a program for the model fitting in Python. The code can be found at https://github.com/xi2pi/SW_estimation.

4.2 Second and third study

The 3D echocardiographical image data of 497 healthy children were used to perform left atrial and left ventricular data analysis with two commercial softwares (QLab and TomTec). Following a standardized procedure, the shape of the left atrium (LA) and left ventricle (LV) were semi-automatically segmented, and the left ventricular cavity was displayed as a 3D model. Based on the 3D model, the volumes were computed.

In the second study, the maximal and minimal left atrial volume (Vmax and Vmin) were computed with TomTec 4D LV-Analysis. TomTec 4D LV-Analysis is originally designed for LV analysis but can also be used for LA analysis by following a protocol that was developed by our group and approved by the manufacturer TomTec. The result of the analysis was a volume-time curve (VTC) for LA. The LA volume before atrial contraction (VpreA) was determined manually by analyzing the VTC. The VTC was plotted and the VpreA was chosen to be at the end of the plateau during atrial emptying in agreement with clinical determination of VpreA. For the validation of the echocardiographical measurement, cardiovascular magnetic resonance (CMR) imaging was performed in 26 patients and 7 healthy children. Differences in Vmax and Vmin were compared by Bland-Altman analysis.

In the third study, the focus was on the end-diastolic volume (EDV), end-systolic volume (ESV), stroke volume (SV), and ejection fraction (EF) with QLab and TomTec. To determine the shape of the ventricle with TomTec, the software suggests an initial endocardial contour of the LV endocardial borders. This contour can be manually adjusted by the operator. In TomTec, two different settings for the sensitivity of the contour-finding algorithm with values of 30 and 75 were applied (TomTec30 and TomTec75). For the validation of the measurement, LV volumes were measured in 22 patients with CMR and compared to

the LV volumes measured with 3D echocardiography.

In both studies, intra and interobserver variabilities were assessed in randomly selected data sets. Intraobserver variability is the variability which occurs when the same observer repeats the measurement under the same conditions. Interobserver variability is the variability, which occurs between different observers. The agreement of intra and interobserver variabilities were analyzed with Bland-Altman analysis and the intraclass correlation coefficient (ICC).

4.3 Reference curves for standard values

For the computation of reference curves, univariate Generalized Additive Models for Location, Scale, and Shape (GAMLSS) were fitted to the SW estimations, LA volumes, and LV volumes of the healthy cohort. GAMLSS is a distribution-based approach to regression (Rigby and Stasinopoulos, 2005a). Reference curves represent the 3rd, 10th, 25th, 50th, 75th, 90th, and 97th percentile. For the application of GAMLSS, the “gamlss” framework in the environment R provides a broad set of functions and model types. For the choice of GAMLSS model settings, we focused on the LMS method (or Lambda-Mu-Sigma method) that has been applied in multiple studies and was recommended by the World Health Organization for pediatrics (Mul et al., 2001; Fredriks et al., 2000; Katzmarzyk, 2004; Nysom et al., 2001; Ataei et al., 2016; Hirschler et al., 2016; Khadilkar et al., 2014). The LMS method (or Lambda-Mu-Sigma method) is a type of GAMLSS with the following form:

- the Box-Cox Cole Green distribution $BCCG(y_i \mid \mu, \sigma, \lambda)$, depending on the three distribution parameters λ, μ, and σ, which are represented in the name of the method. The three parameters represent the skewness (λ), the median (μ) and the coefficient of variation (σ)
- link functions: identity for μ and λ, log function for σ
- smoothing functions are originally cubic splines $cs()$; the approach was extended

by Stasinopoulos et al. with penalized splines $pb()$, which we applied for all three distribution parameters

- transformation: covariate x can be transformed, e.g. logarithmic transformation $log(x)$

The model fitting was achieved by maximizing the penalized log likelihood function iteratively using the $RS()$ algorithm proposed by Rigby and Stasinopoulos (Rigby and Stasinopoulos, 2005b; Stasinopoulos et al., 2007). The used penalized Splines (or P-splines) are piecewise polynomials defined by B-spline basis functions in the explanatory variable, where the coefficients of the basis functions are penalized to guarantee sufficient smoothness (Stasinopoulos et al., 2007). The gamlss package provides the function $pb()$ for penalized splines where df is the desired equivalent number of degrees of freedom. For the LMS method, the degree of freedom for the penalized splines of L, M, and S are L_df, M_df, and S_df. To find the appropriate degrees of freedom L_df, M_df, and S_df the Bayesian information criterion (BIC) was used, which is also proposed by Stasinopoulos et al. (Stasinopoulos et al., 2007). The model with the lowest BIC is preferred. The BIC is defined as

$$BIC = \ln(n)k - 2\ln(\hat{l}_d) \tag{4.15}$$

where $\hat{l}_p$ is the maximized value of the likelihood function l_p. n is the number of observations and k is the number of parameters estimated by the model. The BIC helps to find a compromise between model complexity and goodness of fit. On the one hand, it penalizes high complexity with the term $\ln(n)k$ or $2k$. On the other hand, the goodness of fit is represented as $2\ln(\hat{l}_d)$.

For the creation of reference curves, we developed the software ”RefCurv” that enables the application of the presented methods (Winkler et al., 2020).

5 Results

In this section, the respective results of the three studies are summarized.

5.1 First study

The LPM was successfully fitted to 336 subjects by minimizing the error function $f_{error}^{healthy}$ (Eq. 4.13). The mean of the resulting error values was $2.4 \cdot 10^{-3}$ and the standard deviation was $4.4 \cdot 10^{-2}$, while 4 outliers were excluded. SW was estimated with three methods SW_1, SW_2, and SW_3 as presented in Section 4.1.1.

For validation of this method, we used 18 measurement data sets acquired by a conductance catheter in 11 patients. Each measurement data set contained multiple heartbeats during a steady-state condition. SW was estimated with the LPM using volume and pressure constraints by the conductance measurement (Eq. 4.12). For each measurement, SW_{cond} was averaged from multiple heartbeats. Fig. 5.1 shows the measured and modeled pressure-volume loops for one example patient. The method demonstrated a low

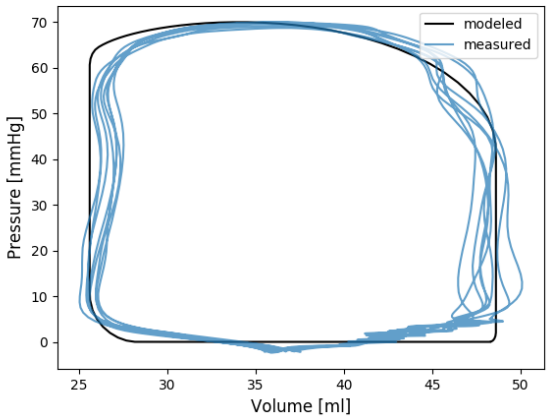

Figure 5.1: Measured and modeled PV loops for the patient group.

absolute mean difference of 0.033 J with a standard deviation (SD) of 0.031 J for SW between measurement and estimation, while the percentage error was 21.66 %. According

to the resulting reference curves, left ventricular SW of newborns has a median of 0.06 J and increases to 1.15 J at the age of 18 years. SW increases along with weight and height in a similar trend.

Reference curves were created with the LMS method. Table 5.1 shows the degrees of freedom L_df, M_df, and S_df for the lowest BIC, where the independent variables are age, height, and weight. The lowest BIC was found by grid search, where values for the

independent variable	L_df	M_df	S_df
Age	3	1	0
Height	3	1	0
Weight	1	2	0

Table 5.1: Degrees of freedom (L_df, M_df, S_df) for the independent variables age, height, and weight.

degrees of freedom were set $L\_df = \{0, 1, 2, 3\}$, $M\_df = \{0, 1, 2\}$, and $S\_df = \{0, 1, 2\}$. Table 5.2 exemplarily shows the four settings with the lowest BIC for the model with age as independent variable. The BIC is negative because the right side of the formula for BIC is higher than the left ($BIC = \ln(n)k - 2\ln(\hat{l}_d)$).

rank	BIC	L_df	M_df	S_df
1	-656.61	3	1	0
2	-656.03	3	2	0
3	-652.53	3	1	1
4	-652.16	3	2	1

Table 5.2: BIC for $L\_df = \{0, 1, 2, 3\}$, $M\_df = \{0, 1, 2\}$, and $S\_df = \{0, 1, 2\}$.

5.2 Second study

432 subjects provided adequate data sets for an LA volume quantification. The maximal and minimal LA volumes (Vmax, Vmin), the volume before atrial contraction (VpreA), and phasic function, such as active and passive emptying fraction (EF), were assessed. For LA volumes, sex-specific reference curves were created. Absolute volumes increased with age and body surface area. Active EF and relative duration of atrial emptying tended

to increase with increasing R-R intervals, while passive EF decreased. Reproducibility of volumes was promising with a low intraobserver variability for Vmax and Vmin (mean bias, Vmax = -0.03 ml, Vmin = -0.14 ml). Volumes showed a high correlation with cardiac magnetic resonance measurements (mean bias ± SD, △ Vmax = –14.2 ± 14 mL, △ Vmin = –11.5 ± 10 mL), while underestimation of volumes by 3DE was expected. Pediatric LA volumes and phasic function indices were reproducibly measured by 3D echocardiography.

5.3 Third study

370 of 497 subjects provided adequate data sets for an LV volume quantification (74.4 % feasibility). LV volumes had a significant association with age, body size, gender, and body surface area.

For intra and interobserver variability, the relative bias for end-systolic volume (ESV), end-diastolic volume (EDV), and stroke volume (SV) were determined in percentage. Table 5.3 shows interobserver variability for EDV. TomTec30 resulted in a bias of 1.2 % with limits of agreement (LOA) of – 8.7 % and 11.0 %, while TomTec75 resulted in a bias of 1.3 % with LOA of – 7.5 % and 10.1 %. Interobserver variability for QLab had a higher bias of 2.4 % compared to the other methods, with LOA of – 12.0 % and 17.0 %. The intraobserver

	Bias (%)	95% LOA (%)
QLab	2.4	- 12.0 to 17.0
TomTec30	1.2	- 8.7 to 11.0
TomTec75	1.3	- 7.5 to 10.1

Table 5.3: Interobserver variability for EDV.

variabilities of all three methods were in general low. For example, QLab resulted in a bias of 1.1 % for interobserver variability with LOA of - 9 % and 1.1 %. The exception was TomTec75, with resulted in a bias of - 5.5 % with LOA of – 21.6 % and 10.7 %.

The comparison with CMR showed that values obtained with QLab and TomTec are mostly smaller than CMR values, with the highest agreement between QLab and CMR. The result

for the intraobserver variability showed that 3D echocardiography allows reproducible non-invasive assessment of LV volumes and function. However, the interobserver variability between the two softwares TomTec and QLab was considered as significant. Therefore, separate reference curves were provided for both softwares (TomTec and QLab). Percentile curves were plotted over age, body size, gender, and body surface area.

6 Discussion

The objective of this thesis was to provide pediatric reference curves of cardiac parameters on the basis of data from 497 healthy children. We were able to create reference curves of the left ventricular stroke work (SW) by using an LPM. Standard values for SW were computed for a wide range of age, height, and weight of healthy children. Furthermore, reference curves for LA volumes (Vmax, Vmin, VpreA) were created over body surface area, while reference curves for LV volumes (EDV, ESV, SV) were created over age.

6.1 Clinical implication

The examination of LA volumes with the provided reference curves can help detecting increased LV volume loads by measuring the LA volume of the patient and comparing it against the reference. By doing this, pathological behavior such as shunt lesions as ventricular septal defect, a patent ductus arteriosus or elevated LV filling pressures could be detected in an early state.

The examination of LV volumes may also play an essential role in the longitudinal and horizontal follow-up of pediatric patients with, for example, cardiomyopathy, LV volume loads, or borderline left ventricle.

SW computations can be useful for comparison of simulated or measured results. In the specific case of Fontan patients, for example, there have been several studies to investigate the heart performance (Kung et al., 2014; Nogaki et al., 2000; Szabó et al., 2003). Some studies consider pressure, volume, and other medical parameters, such as oxygen consumption. Ideally, SW is also considered to understand the pump mechanics of the heart. Studies about the kinetic energy of the fluid are more common (Rodefeld et al., 2019; Rijnberg et al., 2018; Masutani and Senzaki, 2015), which is closely related to SW. With our study, we aimed to add valuable information about SW so that the acquisition of data in a control group might not be necessary anymore, saving effort and costs.

6.2 Limitations of the stroke work estimation

The primary limitation of SW estimation is the approximation of maximal left ventricular pressure by a regression model. Ventricular pressure highly depends on the individual situation. To overcome this limitation, we recommend using non-invasive cuff pressure measurements as an example, which were missing in this study.

A model-specific issue was the missing information about the unstressed blood volume in LV, $V_{U,lv}$ which was overcome by fixing it to zero. There are approaches for approximating $V_{U,lv}$ from single beat measurements (Senzaki et al., 1996). These methods are, however, of clinical nature and some propose a curve fitting to estimate the isovolumetric pressure. During clinical trials, we gained experience with these methods but we did not consider as helpful for this computational study. Kung et al. (Kung et al., 2014) and Davidson et al. (Davidson et al., 2018) used simple formulas or fixed values for $V_{U,lv}$, but evidence for its general usage is low. Furthermore, $V_{U,lv}$ is considered as a hyperparameter, meaning that it does not contribute to the model fitting. Therefore, fixing it to zero does not influence the model fitting and SW estimation. The validation could only be performed with invasive conductance catheter measurements in patients, which resulted in a relative difference of 21.66 % at its best. Due to the pathology, PV loops showed high variations, although the signals were already filtered against noise. Especially, the volume during the isovolumic contraction varied strongly. Apart from the pathology, the reasons for these differences might be the small heart size and the difficulties of the conductance catheter measurement technology. The application of the conductance catheter in children is challenging due to experimental noise, patient movement, and the technical difficulty in optimal catheter positioning.

6.3 Limitations of left atrial and left ventricular volumes quantification

For the validation of LA and LV volume quantification, 3D echocardiography and cardiovascular magnetic resonance imaging were obtained within one day but not simultaneously. Therefore, resulting values for volume may be affected by prolonged breath holding or sympathetic stimulation due to stress under CMR examination. Furthermore, CMR was obtained in a small number of volunteers but not in neonates or small children due to ethical reasons.

For the LA volume quantification, a commercial software (TomTec 4D LV Analysis) originally designed for LV analysis was used. The semi-automatic contour detection of TomTec 4D LV Analysis allows to rotate the view and treat a left atrium like a left ventricle. Our results for old age groups show similar LA values like other studies (Badano et al., 2016). Furthermore, the analysis of other cardiac parameters, such as VpreA, was possible in more detail because the contours of the LA could be adjusted manually. This was considered as a major advantage over LA specific software, which automatically calculates VpreA without further explanation of the underlying algorithm.

6.4 Limitations of the creation of reference curves

Limitations related to the creation of reference curves are based on the GAMLSS.

GAMLSS models and the R implementation were designed for a large set of continuous data points. Therefore, a high number of data points is preferred, such as the presented data sets in the GAMLSS repository (Stasinopoulos et al., 2007). In the presented studies a total number of 497 observations were available, where some cases had to be excluded because of bad image quality. This did not lead to computational problems but arose the question of how many observations are necessary to represent a study population, which we did not answer in this study.

We also found, that data points on the left and right borders determine the slope of the percentile curves on the borders and therefore can have a high impact on the outcome. For parameters, it is often expected that they increase during childhood and to reach a plateau for adults. This plateau is represented by a slope of zero degrees. The curves' behavior follows rather the data and thus the data define the slope on the edges. It was also found that GAMLSS models tend to fail for little data density on the edges. Single data points had to be removed consequently.

Another GAMLSS specific issue is the choice of hyperparameters, such as the degree of freedom for penalized splines. For the model selection, the BIC was used to find the balance between model complexity and goodness of fit. For this method, a grid search with discrete values for the model parameters was used. This approach seems arbitrary and does not guarantee the convergence or success of finding a good model setting.

6.5 Conclusion

The three presented studies provide pediatric reference curves of LA volumes, LV volumes, and SW based on echocardiographic data. While the computation of LA and LV volumes was achieved with commercial software, a model-based method to estimate the SW was developed and presented.

The presented reference curves can have a direct clinical impact. Physicians commonly assess the measured LA and LV volumes of adult patients. This thesis adds standard values over age for children that can be used as references for follow-up examinations.

This thesis also presented a new methodology to estimate the SW based on echocardiographical data and mathematical modeling of the cardiovascular system. This approach showed how cardiovascular modeling can be embedded to clinical studies and to which extent the lumped parameter approach contribute to the study.

For clinicians, the standard values of SW, which represent the energy provided by the left ventricle, can help to improve the treatment decisions of heart failures. Furthermore, the gained information about SW can help engineers to improve medical devices such as Ventricular Assist Devices or Extracorporal Membran Oxygenation systems. As these systems have a high impact on the cardiovascular system, the consideration of SW might help to design new concepts.

Acknowledgement

I would like to express my sincere gratitude to my advisor Professor Dr. Ulrike Herberg, who has supported me with this thesis from the beginning. Your expertise and endless energy is truly inspiring. Special thanks go to Dr. Katharina Linden and Prof. Dr. Johannes Breuer for their kind support. I would also like to thank Prof. Dr. Thomas Schultz for profound advises, his kindness and his generous help in reflecting the mathematical approaches.

I would like to thank all people working at the Department of Pediatric Cardiology and Stiftung kinderherzen, who I got in touch with during my time as a research assistant. Thank you for your support and kindness.

Of course, this thesis would not have been completed without the support and love of my family, who I want to thank with all my heart.

Bibliography

AbouEzzeddine, O. F., Kemp, B. J., Borlaug, B. A., Mullan, B. P., Behfar, A., Pislaru, S. V., Fudim, M., Redfield, M. M., and Chareonthaitawee, P. (2019). Myocardial energetics in heart failure with preserved ejection fraction. *Circulation: Heart Failure*, 12(10):e006240.

Ataei, N., Hosseini, M., Fayaz, M., Navidi, I., Taghiloo, A., Kalantari, K., and Ataei, F. (2016). Blood pressure percentiles by age and height for children and adolescents in tehran, iran. *Journal of human hypertension*, 30(4):268.

Badano, L. P., Miglioranza, M. H., Mihăilă, S., Peluso, D., Xhaxho, J., Marra, M. P., Cucchini, U., Soriani, N., Iliceto, S., and Muraru, D. (2016). Left atrial volumes and function by three-dimensional echocardiography: reference values, accuracy, reproducibility, and comparison with two-dimensional echocardiographic measurements. *Circulation: Cardiovascular Imaging*, 9(7):e004229.

Ben-Assa, E., Brown, J., Keshavarz-Motamed, Z., Jose, M., Leiden, B., Olender, M., Kallel, F., Palacios, I. F., Inglessis, I., Passeri, J. J., et al. (2019). Ventricular stroke work and vascular impedance refine the characterization of patients with aortic stenosis. *Science translational medicine*, 11(509):eaaw0181.

Davidson, S., Pretty, C., Kamoi, S., Desaive, T., and Chase, J. G. (2018). Beat-by-beat estimation of the left ventricular pressure–volume loop under clinical conditions. *Annals of biomedical engineering*, 46(1):171–185.

de Bournonville, S., Pironet, A., Pretty, C., Chase, J. G., and Desaive, T. (2019). Parameter estimation in a minimal model of cardio-pulmonary interactions. *Mathematical biosciences*, 313:81–94.

Fredriks, A. M., Van Buuren, S., Burgmeijer, R. J., Meulmeester, J. F., Beuker, R. J., Brugman, E., Roede, M. J., Verloove-Vanhorick, S. P., and Wit, J.-M. (2000). Continu-

ing positive secular growth change in the netherlands 1955–1997. *Pediatric research*, 47(3):316.

Gao, F. and Han, L. (2012). Implementing the nelder-mead simplex algorithm with adaptive parameters. *Computational Optimization and Applications*, 51(1):259–277.

Glower, D. D., Spratt, J. A., Snow, N. D., Kabas, J., Davis, J., Olsen, C., Tyson, G., Sabiston Jr, D., and Rankin, J. (1985). Linearity of the frank-starling relationship in the intact heart: the concept of preload recruitable stroke work. *Circulation*, 71(5):994–1009.

Gotzmann, M., Hauptmann, S., Hogeweg, M., Choudhury, D. S., Schiedat, F., Dietrich, J. W., Westhoff, T. H., Bergbauer, M., and Mügge, A. (2019). Hemodynamics of paradoxical severe aortic stenosis: insight from a pressure–volume loop analysis. *Clinical Research in Cardiology*, pages 1–9.

Hirschler, V., Molinari, C., Maccallini, G., Hidalgo, M., Gonzalez, C., and de los Cobres Study Group, S. A. (2016). Waist circumference percentiles in indigenous argentinean school children living at high altitudes. *Childhood Obesity*, 12(1):77–85.

Hsia, T.-Y., Cosentino, D., Corsini, C., Pennati, G., Dubini, G., Migliavacca, F., and of Congenital Hearts Alliance (MOCHA) Investigators, M. (2011). Use of mathematical modeling to compare and predict hemodynamic effects between hybrid and surgical norwood palliations for hypoplastic left heart syndrome. *Circulation*, 124(11_suppl_1):S204–S210.

Katzmarzyk, P. (2004). Waist circumference percentiles for canadian youth 11–18 y of age. *European journal of clinical nutrition*, 58(7):1011.

Kaufmann, T. A., Neidlin, M., Büsen, M., Sonntag, S. J., and Steinseifer, U. (2014). Implementation of intrinsic lumped parameter modeling into computational fluid dynamics studies of cardiopulmonary bypass. *Journal of biomechanics*, 47(3):729–735.

Khadilkar, A., Ekbote, V., Chiplonkar, S., Khadilkar, V., Kajale, N., Kulkarni, S., Parthasarathy, L., Arya, A., Bhattacharya, A., and Agarwal, S. (2014). Waist circumference percentiles in 2-18 year old indian children. *The Journal of pediatrics*, 164(6):1358–1362.

Klabunde, R. (2011). *Cardiovascular physiology concepts*. Lippincott Williams & Wilkins.

Korakianitis, T. and Shi, Y. (2006). Effects of atrial contraction, atrioventricular interaction and heart valve dynamics on human cardiovascular system response. *Medical engineering & physics*, 28(8):762–779.

Kung, E., Pennati, G., Migliavacca, F., Hsia, T.-Y., Figliola, R., Marsden, A., and Giardini, A. (2014). A simulation protocol for exercise physiology in fontan patients using a closed loop lumped-parameter model. *Journal of biomechanical engineering*, 136(8):081007.

Lindinger, A., Schwedler, G., and Hense, H.-W. (2010). Prevalence of congenital heart defects in newborns in germany: Results of the first registration year of the pan study (july 2006 to june 2007). *Klinische Pädiatrie*, 222(05):321–326.

Masutani, S. and Senzaki, H. (2015). Assessment of ventricular function using the pressure-volume relationship. In *Congenital Heart Disease*, pages 97–126. Springer.

Mineroff, J., McCulloch, A. D., Krummen, D., Ganapathysubramanian, B., and Krishnamurthy, A. (2019). Optimization framework for patient-specific cardiac modeling. *Cardiovascular engineering and technology*, 10(4):553–567.

Mul, D., Fredriks, A. M., Van Buuren, S., Oostdijk, W., Verloove-Vanhorick, S. P., and Wit, J. M. (2001). Pubertal development in the netherlands 1965–1997. *Pediatric research*, 50(4):479.

Neidlin, M., Steinseifer, U., and Kaufmann, T. A. (2014). A multiscale 0-d/3-d approach to patient-specific adaptation of a cerebral autoregulation model for computational fluid

dynamics studies of cardiopulmonary bypass. *Journal of biomechanics*, 47(8):1777–1783.

Neuhauser, H., Schienkiewitz, A., Rosario, A. S., Dortschy, R., and Kurth, B.-M. (2013). Referenzperzentile für anthropometrische Maßzahlen und Blutdruck aus der Studie zur Gesundheit von Kindern und Jugendlichen in Deutschland (KiGGS).

Nogaki, M., Senzaki, H., Masutani, S., Kobayashi, J., Kobayashi, T., Sasaki, N., Asano, H., Kyo, S., and Yokote, Y. (2000). Ventricular energetics in fontan circulation: evaluation with a theoretical model. *Pediatrics International*, 42(6):651–657.

Nysom, K., Mølgaard, C., Hutchings, B., and Michaelsen, K. F. (2001). Body mass index of 0 to 45-y-old danes: reference values and comparison with published european reference values. *International journal of obesity*, 25(2):177.

Olufsen, M. S., Ottesen, J. T., Tran, H. T., Ellwein, L. M., Lipsitz, L. A., and Novak, V. (2005). Blood pressure and blood flow variation during postural change from sitting to standing: model development and validation. *Journal of Applied Physiology*, 99(4):1523–1537.

Parlikar, T. A. and Verghese, G. C. (2006). A simple cycle-averaged model for cardiovascular dynamics. In *2005 IEEE Engineering in Medicine and Biology 27th Annual Conference*, pages 5490–5494. IEEE.

Pironet, A., Desaive, T., Dauby, P. C., Chase, J. G., and Docherty, P. D. (2015). Parameter identification methods in a model of the cardiovascular system. *IFAC-PapersOnLine*, 48(20):366–371.

Pironet, A., Docherty, P. D., Dauby, P. C., Chase, J. G., and Desaive, T. (2019). Practical identifiability analysis of a minimal cardiovascular system model. *Computer methods and programs in biomedicine*, 171:53–65.

Rigby, R. A. and Stasinopoulos, D. M. (2005a). Generalized additive models for location,

scale and shape. *Journal of the Royal Statistical Society: Series C (Applied Statistics)*, 54(3):507–554.

Rigby, R. A. and Stasinopoulos, D. M. (2005b). Generalized additive models for location, scale and shape. *Journal of the Royal Statistical Society: Series C (Applied Statistics)*, 54(3):507–554.

Rijnberg, F. M., Hazekamp, M. G., Wentzel, J. J., De Koning, P. J., Westenberg, J. J., Jongbloed, M. R., Blom, N. A., and Roest, A. A. (2018). Energetics of blood flow in cardiovascular disease: concept and clinical implications of adverse energetics in patients with a fontan circulation. *Circulation*, 137(22):2393–2407.

Rodefeld, M. D., Marsden, A., Figliola, R., Jonas, T., Neary, M., and Giridharan, G. A. (2019). Cavopulmonary assist: Long-term reversal of the fontan paradox. *The Journal of Thoracic and Cardiovascular Surgery*, 158(6):1627–1636.

Seemann, F., Arvidsson, P., Nordlund, D., Kopic, S., Carlsson, M., Arheden, H., and Heiberg, E. (2019). Noninvasive quantification of pressure-volume loops from brachial pressure and cardiovascular magnetic resonance. *Circulation: Cardiovascular Imaging*, 12(1):e008493.

Senzaki, H., Chen, C.-H., and Kass, D. A. (1996). Single-beat estimation of end-systolic pressure-volume relation in humans: a new method with the potential for noninvasive application. *Circulation*, 94(10):2497–2506.

Sprigings, D. C., Chambers, J. B., Cochrane, T., Allen, J., and Jackson, G. (1990). Ventricular stroke work loss: validation of a method of quantifying the severity of aortic stenosis and derivation of an orifice formula. *Journal of the American College of Cardiology*, 16(7):1608–1614.

Stasinopoulos, D. M., Rigby, R. A., et al. (2007). Generalized additive models for location scale and shape (gamlss) in r. *Journal of Statistical Software*, 23(7):1–46.

Stevenson, D., Revie, J., Chase, J. G., Hann, C. E., Shaw, G. M., Lambermont, B., Ghuysen, A., Kolh, P., and Desaive, T. (2012). Beat-to-beat estimation of the continuous left and right cardiac elastance from metrics commonly available in clinical settings. *Biomedical engineering online*, 11(1):73.

Szabó, G., Buhmann, V., Graf, A., Melnitschuk, S., Bährle, S., Vahl, C. F., and Hagl, S. (2003). Ventricular energetics after the fontan operation: contractility-afterload mismatch. *The Journal of thoracic and cardiovascular surgery*, 125(5):1061–1069.

Topham, W. S. (1969). Comparison of methods for calculation of left ventricular stroke work. *Journal of applied physiology*, 27(5):767–769.

Winkler, C., Linden, K., Mayr, A., Schultz, T., Welchowski, T., Breuer, J., and Herberg, U. (2020). Refcurv: A software for the construction of pediatric reference curves. *Software Impacts*, page 100040.

7 Appendix A - First study

Winkler, C., Neidlin, M., Sonntag, S.J., Grünwald, A., Groß-Hardt, S., Breuer, J., Linden, K. and Herberg, U. (2020). Estimation of left ventricular stroke work based on a large cohort of healthy children. Computers in Biology and Medicine, 123, p.103908.

Computers in Biology and Medicine 123 (2020) 103908

Contents lists available at ScienceDirect

Computers in Biology and Medicine

journal homepage: www.elsevier.com/locate/compbiomed

Estimation of left ventricular stroke work based on a large cohort of healthy children

Christian Winkler [a,*], Michael Neidlin [b,d], Simon J. Sonntag [c], Anna Grünwald [d], Sascha Groß-Hardt [d], Johannes Breuer [a], Katharina Linden [a], Ulrike Herberg [a]

[a] Department of Pediatric Cardiology, University Hospital of Bonn, Germany
[b] Department of Mechanical Engineering, National Technical University of Athens, Greece
[c] Virtonomy GmbH, Munich, Germany
[d] Department of Cardiovascular Engineering, Institute of Applied Medical Engineering, Helmholtz Institute, Medical Faculty, RWTH Aachen University, Germany

ARTICLE INFO

Keywords:
Cardiovascular modeling
Lumped parameter model
Cardiac mechanics
Parameter estimation
Pediatric cardiology

ABSTRACT

Left ventricular stroke work is an important prognostic marker to analyze cardiac function. Standard values for children are, however, missing. For clinicians, standards can help to improve the treatment decision of heart failures. For engineers, they can help to optimize medical devices.

In this study, we estimated the left ventricular stroke work for children based on modeled pressure–volume loops. A lumped parameter model was fitted to clinical data of 340 healthy children. Reference curves for standard values were created over age, weight, and height. Left ventricular volume was measured with 3D echocardiography, while maximal ventricular pressure was approximated with a regression model from the literature.

For validation of this method, we used 18 measurements acquired by a conductance catheter in 11 patients. The method demonstrated a low absolute mean difference of 0.033 J (SD: 0.031 J) for stroke work between measurement and estimation, while the percentage error was 21.66 %.

According to the resulting reference curves, left ventricular stroke work of newborns has a median of 0.06 J and increases to 1.15 J at the age of 18 years. Stroke work increases over weight and height in a similar trend. The percentile curves depict the distribution.

We demonstrate how reference curves can be used for quantification of differences and comparison in patients.

1. Introduction

Left ventricular stroke work (SW) is an important prognostic marker to determine cardiac function [1–3]. For patients with a Fontan circulation, SW has been proven to reflect the degree of the disease [4–6]. Furthermore, recent studies have assessed SW as a medical parameter for other pathologies, especially aortic stenosis [7–10].

While SW has been investigated in patients, standard values of healthy people are missing, most likely because its determination requires an invasive catheter intervention. Especially in children, the standard values of SW for different ages, weights, and heights could improve clinical decision-making by monitoring cardiac function during the growth process [11]. From an engineering point of view, knowledge about the range of SW can be helpful to control mechanical circulatory support devices, such as ventricular assist devices (VAD) [12–14].

SW represents the energy provided by the ventricle to pump blood into the arteries. With reduced energy, the heart is not capable of providing enough blood to the circulation that can lead to heart failure. SW is the integrated product of pressure and volume flow with respect to time. It can be visualized as the area within the pressure–volume loop (PV loop).

The computation of SW requires information about left ventricular pressure and volume for the duration of one cardiac cycle. The gold standard measurement technology for the simultaneous measurement of pressure and volume in the ventricle is the conductance catheter. A catheter intervention is, however, risky and should not be performed in healthy subjects. Alternatively, noninvasive measurements have to be considered [15].

Ventricular blood flow can be easily approximated with information about the heart volume. 3D echocardiography has been established as an accurate cardiac imaging technology and the according ventricular volumes can be extracted with the help of image segmentation algorithms [16,17].

* Corresponding author.
E-mail address: s6cnwink@uni-bonn.de (C. Winkler).

https://doi.org/10.1016/j.compbiomed.2020.103908
Received 14 April 2020; Received in revised form 4 July 2020; Accepted 4 July 2020
Available online 9 July 2020

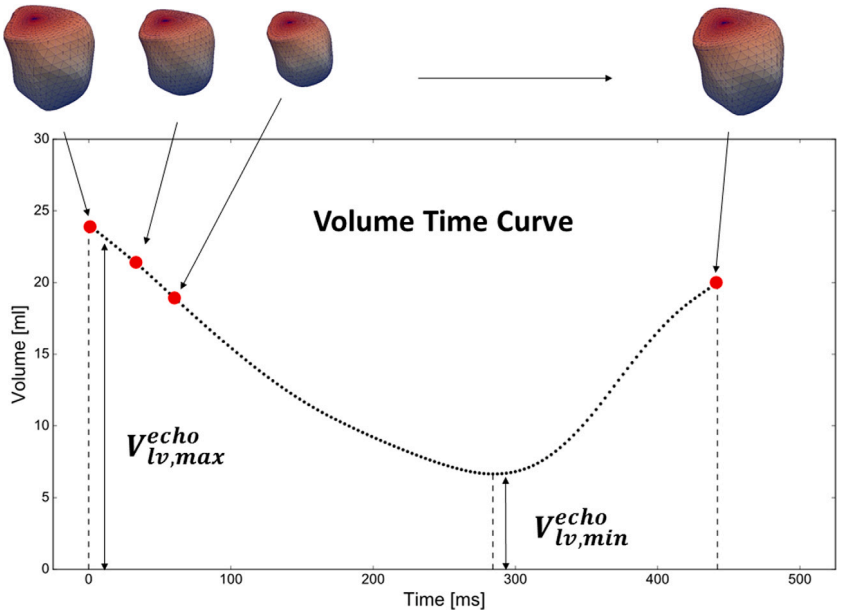

Fig. 1. Left ventricular volume approximation with segmented volumetric shape models derived from 3D echocardiography.

Ventricular blood pressure, however, can only be measured during a catheter intervention [18]. Information about pressure during the cardiac cycle are often missing in practice. In many cases, an invasive intervention may not be possible due to ethical reasons.

For the computation of blood pressure, lumped parameter models (LPM) have been established as an efficient modeling approach [19–23]. The studies by Pironet et al. [24,25] developed and validated a minimal cardiovascular model with animal data. Their proposed model has a small number of parameters and is therefore suitable for fitting to a limited number of measurements and a pressure–volume loop analysis.

1.1. Aim of this study

In this study, left ventricular stroke work (SW) was estimated based on modeled pressure–volume loops from an LPM. As such, a lumped parameter model developed by Pironet et al. was extended by fitting it to measured volumetric data for a cohort of 340 healthy children.

Noninvasive 3D echocardiography was used for the acquisition of volume data, while maximal left ventricular pressure was approximated with a regression model taken from the literature. Different methods of SW computation were compared. Reference curves of standard values were created over age, weight, and height.

For validation of the method, we used 18 conductance catheter measurements in 11 patients.

2. Material and methods

2.1. Data acquisition for validating the estimation

Left ventricular volume and pressure were measured in a patient group and used to validate the SW estimations. 18 measurements were taken from a patient group of 11 children with congenital heart disease, which needed catheterization due to clinical reasons. The study was approved by the local ethics institutional review committee (Registration No. 007/15) and conformed to the principles of the Declaration of Helsinki as well as the German law. Table 1 gives a statistical overview about age, weight, height, and heart rate (RR interval) of the patient group.

Table 1
Study group of patients ($n = 11$). Age, weight, height, RR interval of the patient group are summarized as mean, standard deviation (Std), and range (Min–Max).

	Mean	Std	Min–Max
Age [years]	5.93	2.81	2.25–11
Weight [kg]	19.12	7.06	10.40–32.30
Height [cm]	109.25	18.45	81–139
RR [s]	1.76	0.48	0.93–2.51

2.2. Data acquisition for computing reference curves

Invasive measurements in healthy humans are risky. Therefore, left ventricular volume and pressure had to be measured noninvasively or approximated from regression models.

Data of healthy children ($n = 340$) were acquired with 3D echocardiography (iE33, Philips, Andover, MA), and the volumetric shape of the left ventricle for one heartbeat was determined with segmentation software (QLab 9.0, Philips, Andover, MA) [17]. Fig. 1 shows exemplary how the volume time curve is derived for one subject. The maximal and minimal left ventricular volume during one heart cycle, $V^{echo}_{lv,max}$, and $V^{echo}_{lv,min}$, can be easily determined with the volume time curve. The RR duration, a measure of heart rate, was acquired simultaneously.

In this study, the assumption was made that the maximal blood pressure in the left ventricle, $P_{lv,max}$, can be approximated by the systolic systemic blood pressure ($P_{lv,max} \approx P_{sys,systolic}$). For the systemic blood pressure, we used regression models for clinical references of healthy children (50th percentile) [26], with a distinction between girls and boys.

$$\begin{aligned} P_{sys,systolic,girls}(age, height) = {} & 83.37 - 0.9057 \cdot age + 0.05795 \cdot (age - 10)^2 \\ & + 0.09447 \cdot height + 0.01101 \cdot height \cdot age \\ & + 0.00006818 \cdot height \cdot (age - 10)^2 \end{aligned} \tag{1}$$

$$\begin{aligned} P_{sys,systolic,boys}(age, height) = {} & exp(4.163 + 0.01409 \cdot age + 0.003363 \cdot (age - 10)^2 \\ & + 0.003189 \cdot height - 0.00007603 \cdot height \cdot age \\ & - 0.00001816 \cdot height \cdot (age - 10)^2) \end{aligned} \tag{2}$$

Table 2
Study group of healthy children (n = 340), which included 156 girls and 184 boys. Age, weight, height, RR interval, $V_{lv,max}^{echo}$, and $V_{lv,min}^{echo}$ of the study group are summarized as mean, standard deviation (Std), and range (Min–Max).

	Mean	Std	Min–Max
Age [years]	7.97	5.03	0.0–18.25
Weight [kg]	30.52	18.80	2.16–88.3
Height [cm]	126.07	35.34	46.0–192.0
RR [s]	0.69	0.16	0.33–1.4
$V_{lv,min}^{echo}$ [ml]	26.58	15.46	0.84–73.17
$V_{lv,max}^{echo}$ [ml]	68.52	39.33	3.17–250.52
BSA [m^2]	1.01	0.45	0.1–2.13

For both girls and boys, the regression model depends on age and body height.

Volumetric data of 156 girls and 184 boys were measured. The study was approved by the local ethics institutional review committee (Registration No. 245/10) and conformed to the principles of the Declaration of Helsinki as well as the German law. Table 2 gives an overview of all included subjects (n = 340) and a statistical summary on age, weight, height, heart rate (RR interval), $V_{lv,max}^{echo}$, and $V_{lv,min}^{echo}$.

The demographic data of both groups, patients and healthy children, can be found in Supplement S1, S3 and S9.

2.3. Estimation of left ventricular stroke work

For the estimation of left ventricular stroke work (SW), we considered the three methods SW_1, SW_2, and SW_3. SW_1 is a precise calculation, while SW_2 is a rough estimation. SW_3 is a clinical approach using commonly measured pressures.

The three different formulas were used to assess the range for SW computations. SW_2 is expected to mark the maximal possible value, while SW_1 and SW_3 should give lower values. Furthermore, a clinical study has shown that SW_3 underestimates SW [27], which we used for assessing the estimation results.

SW is defined as the integrated product of pressure and volume over one cardiac cycle

$$SW = \int P_{lv}(t)\, dV_{lv} = \int P_{lv}(t) \cdot Q_{lv}(t)\, dt \tag{3}$$

where P_{lv}, V_{lv}, and Q_{lv} are blood pressure, volume and flow, respectively. SW can be depicted as the area inside the pressure–volume loop (Supplement S5).

This formula can be discretized by

$$SW_1 \approx \sum_{n=0}^{N} P_{lv}(t_n) \cdot Q_{lv}(t_n) \cdot (t_{n+1} - t_n) \approx \sum_{n=0}^{N-1} P_{lv}(t_n) \cdot (V_{lv}(t_{n+1}) - V_{lv}(t_n)) \tag{4}$$

for N time steps. For the bounds of integration, it has to be considered that the ventricle pumps blood actively into the aorta during systole and is filled with blood passively during diastole.

For a rough estimation, SW can be approximated by

$$SW_2 = \Delta P \cdot SV \tag{5}$$

where ΔP is the pressure difference between maximal and minimal ventricular pressure and SV is the stroke volume. SW_2 is represented by the rectangular area bordering the pressure–volume loop and has been shown to overestimate SW (Supplement S5).

A formula for SW commonly used by clinicians is

$$SW_3 = MAP \cdot SV \tag{6}$$

where MAP is the mean arterial pressure.

SW_1, SW_2, and SW_3 were computed from the model output (P_{lv}, V_{lv}, and MAP) that is described in the next section.

Table 3
The LPM is based on 8 model parameters (R_i, R_c, R_o, E_{ao}, E_{vc}, E_{lv}, SBV, T).

Parameter	Description
E_{lv}	Maximal elastance of the left ventricle
E_{ao}	Elastance of the aorta
E_{vc}	Elastance of the vena cava
R_c	Resistance of the circulatory system
R_i	Resistance of the input valve
R_o	Resistance of the output valve
SBV	Stressed blood volume
T	Duration of a cardiac cycle

2.4. Modeling of the pressure–volume loop

For the modeling of pressure–volume (PV) loops, we used a three-chamber cardiovascular model in the form of a lumped parameter model (LPM), which was developed and validated in previous studies by Pironet et al. [24,25,28].

According to the work of Pironet et al. the systemic and pulmonary circulations can be merged into a model that represents only one circulation. This kind of LPM with only one circulation was also developed and applied by others [29,30].

LPM was used for both, patients and healthy children. The difference of both groups in SW is mainly determined by the measurements (V_{max}, V_{min}, P_{max}) and there is evidence that left ventricular SW of the single ventricle circulation differs the SW of healthy subjects. In one case, the left ventricle is pumping blood through the systemic and pulmonary circulation, whereas in healthy subjects, the ventricle is pumping blood through the systemic circulation.

Despite this difference in the structure of the circulations, we applied the LPM for both groups because the focus of the model is on the ventricular function and its elastance function, while the surrounding model compartments are concatenated and modeled abstractly as an inlet compliance (vena cava) and an outlet compliance (aorta) both connected by a flow resistance (resistance of the circulatory system). In this context, the behavior of the PV loop and the related SW can be analyzed in detail, while the behavior of the surrounding system are represented by abstract formulations of the systemic resistance, the aorta and the vena cava.

Fig. 2 shows the structure of the LPM, while Table 3 lists the model parameters with description. The LPM includes the aorta (ao), one vena cava (vc), and the left ventricle (lv). It describes the relationship between the variables flow (Q), volume (V), and blood pressure (P). The LPM is represented by a system of ordinary differential equations (ODE) and algebraic equations, which can be found as supplementary material (Supplement S3). As mentioned before, the aorta, the vena cava and the circulatory system should be considered as abstract elements surrounding the left ventricle. They define the boundary conditions for the left ventricular behavior.

The pressure in the left ventricle is given by

$$P_{lv}(t) = E_{lv}(t) \cdot (V_{lv}(t) - V_{U,lv}) \tag{7}$$

where $V_{lv}(t)$ is the volume, $V_{U,lv}$ is the unstressed blood volume, and $E_{lv}(t)$ is the time depending elastance, see Eq. (8).

$$E_{lv}(t) = E_{lv} \cdot e_{lv}(t, T) \tag{8}$$

with $e_{lv}(t, T)$ as the driver function. For this study, we used the driver function proposed by Korakianitis et al. [31].

The left ventricular unstressed blood volume $V_{U,lv}$ is the blood volume that does not contribute to the pressure. It is usually measured by preload reduction and requires invasive intervention. We assumed it to be zero, which is commonly done for the analysis of cardiac dynamics [15,32].

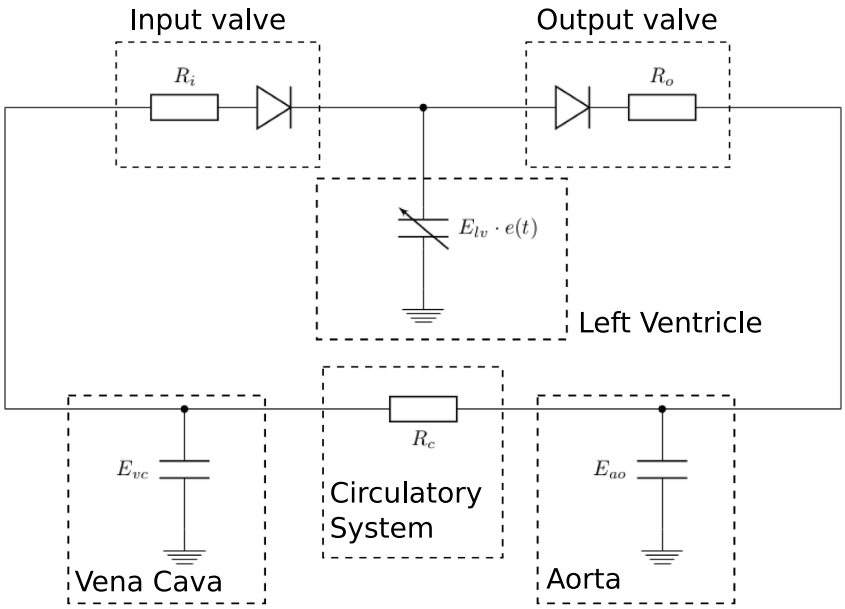

Fig. 2. Lumped parameter model (LPM) represented by an electrical network. The left ventricle, aorta, and vena cava are modeled by conductors. The valves are represented by resistors and diodes. The circulatory system consists of a resistor.

Time alignment between model and measurement was achieved by adjusting the length of a heartbeat T in the driver function $e_{lv}(t, T)$ with the measured RR interval.

To fit the model to the measurements, a subset selection of the model parameters was performed. As a result, we defined model parameters to be estimated as

$$p = [E_{lv}, R_c, SBV]^T \tag{9}$$

where $p \in \mathbb{R}_{>0}$. To obtain an overview about the parameter interaction, other parameters were assigned ($R_i = R_o = 0.1$ and $E_{vc} = E_{ao} = 1.0$) and were kept constant during the estimation procedure.

A detailed description of the subset selection and parameter assignment can be found in Supplement S4.

The model output is defined as

$$y^{model}(p) = [P_{lv}(t), V_{lv}(t)]^T \tag{10}$$

depending on the vector of model parameters p.

The mean atrial pressure, MAP, can be extracted from the model

$$MAP \approx \frac{1}{N} \sum_{n=0}^{N} P_{ao}(t_n) \tag{11}$$

where P_{ao} is the simulated aortic pressure.

2.5. Model fitting

For model fitting, we minimized a scalar function $f_{error}(p)$ that defines the deviation between measurement and model output

$$f_{error,i}(p) = (y_i^{measurement} - y_i^{model}(p))^2 \tag{12}$$

for the constraints i.

In general, $V_{lv,min}$, $V_{lv,max}$ and the $P_{lv,max}$ were used as constraints

$$f_{error}(p) = f_{error,V_{lv,min}}(p) + f_{error,V_{lv,max}}(p) + f_{error,P_{lv,max}}(p) \tag{13}$$

where p represents the vector of model parameters to be estimated.

For the validation of model fitting, conductance catheter measurements in patients ($V_{lv,min}^{cond}$, $V_{lv,max}^{cond}$, $P_{lv,max}^{cond}$) were used:

$$f_{error}^{patient}(p) = f_{error,V_{lv,min}^{cond}}(p) + f_{error,V_{lv,max}^{cond}}(p) + f_{error,P_{lv,max}^{cond}}(p) \tag{14}$$

For the SW estimation in the healthy cohort, ventricular volume measured by 3D echocardiography ($V_{lv,min}^{cond}$, $V_{lv,max}^{cond}$) and ventricular pressure computed by the regression model ($P_{lv,max}^{regression}$) were used.

$$f_{error}^{healthy}(p) = f_{error,V_{lv,min}^{echo}}(p) + f_{error,V_{lv,max}^{echo}}(p) + f_{error,P_{lv,max}^{regression}}(p) \tag{15}$$

The minimization is achieved by

$$\min_{p \in \mathbb{R}_{>0}} f_{error}(p) \tag{16}$$

to find a set of estimated model parameters $\hat{p} = [\hat{E}_{lv}, \hat{R}_c, \hat{SBV}]$. The estimated parameters have to be part of the positive real numbers due to their physical character. The Nelder–Mead method was used for minimization [33].

Initial conditions for $V_{S,lv}$, $V_{S,ao}$, and $V_{S,vc}$ were first set to $SBV/3$. We assumed a steady state after 20 heartbeats and used the calculated state values as initial conditions for the main simulation.

We developed a program for the model fitting in Python. The code can be found at https://github.com/xi2pi/SW_estimation.

2.6. Reference curves for standard values

The central aim of this study is to present the estimated values of SW as reference curves, where the curves represent the percentiles of a distribution. The intention is to show how SW is distributed over age or anthropometric variables like body height.

For the computation of reference curves, univariate Generalized Additive Models for Location, Scale, and Shape (GAMLSS) were fitted to the resulting SW estimations of the healthy cohort. GAMLSS is a distribution-based approach to regression [34]. Reference curves represent the 3rd, 10th, 25th, 50th, 75th, 90th, and 97th percentile. The software environment R provides a package for the application of GAMLSS.

3. Results

LPM was successfully fitted to 336 subjects by minimizing the error function $f_{error}^{healthy}$ (Eq. (15)). The mean of the resulting error values was

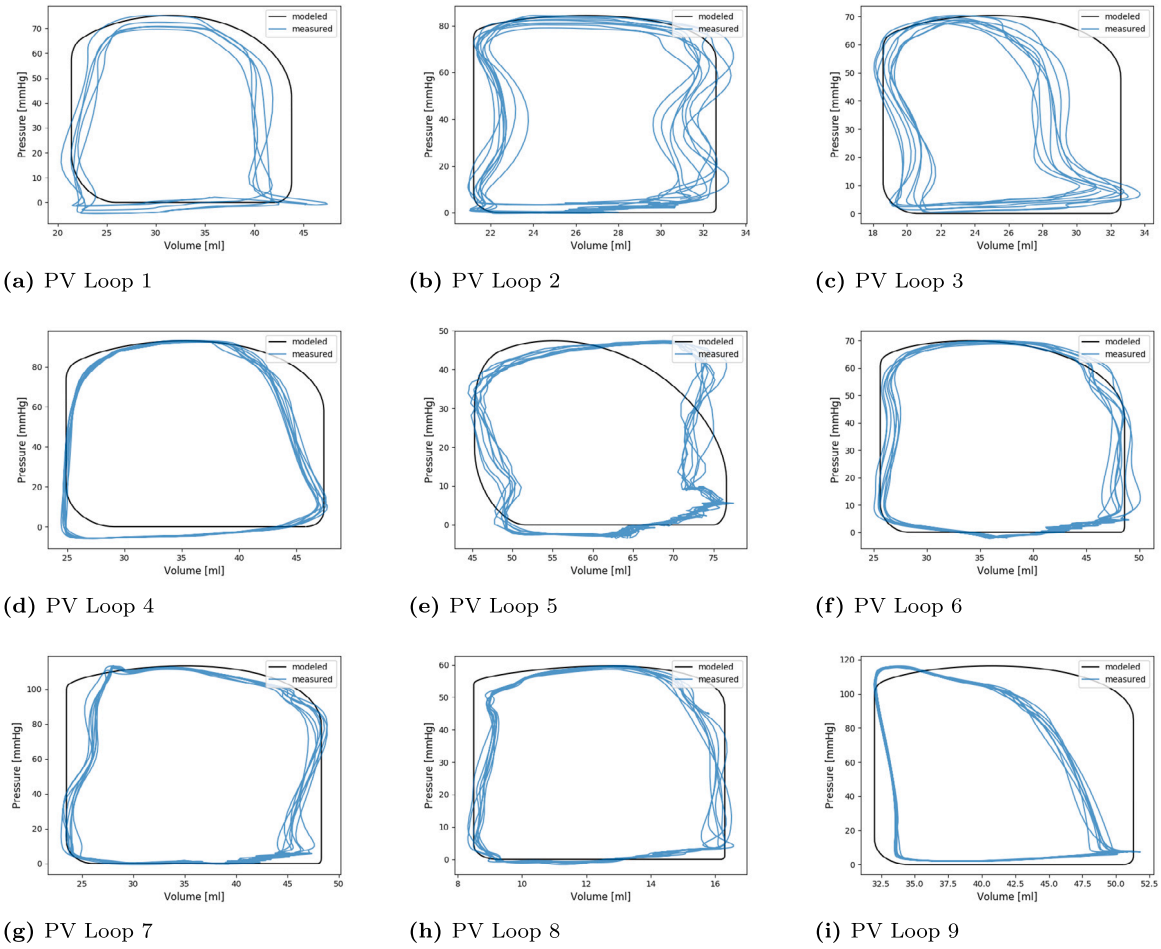

(a) PV Loop 1 (b) PV Loop 2 (c) PV Loop 3

(d) PV Loop 4 (e) PV Loop 5 (f) PV Loop 6

(g) PV Loop 7 (h) PV Loop 8 (i) PV Loop 9

Fig. 3. Measured and modeled PV loops for the patient group.

$2.4 \cdot 10^{-3}$ and the standard deviation was $4.4 \cdot 10^{-2}$, while 4 outliers were excluded.

SW was estimated with three methods SW_1, SW_2, and SW_3 as presented in Section 2.3. Detailed results of the SW estimation for one example subject are given in Supplement S5. In addition, we analyzed the model parameter distribution and the PV loop in the left ventricle. Scatter plots of the fitted model parameters ($\hat{p} = [\hat{E}_{lv}, \hat{R}_c, \hat{SBV}]$) are given as supplementary material (Supplement S6).

For the validation of the method, SW was measured by a conductance catheter in patients and SW_{cond} was compared to the estimated SWs (SW_1, SW_2, SW_3).

3.1. Validation with conductance catheter measurements

18 conductance catheter measurements were acquired from single-ventricle patients. Multiple heartbeats were recorded during a steady-state condition. SW was estimated with the LPM using volume and pressure constraints by the conductance measurement (Eq. (14)). For each measurement, SW_{cond} was averaged from multiple heart beats. Figs. 3 and 4 show the measured and modeled pressure–volume loops for the patient group.

Table 4 gives a statistical summary of the percentage error between model and measurement ($|SW_i - SW_{cond}|/SW_{cond} \cdot 100$). SW_1 has the lowest median of 21.66%, followed by SW_3 with a median of 25.44%. SW_2 has the highest median of 37.96%.

Fig. 5 shows box-plots of the absolute differences of SW_1, SW_2, and SW_3 compared to SW_{cond}. The mean difference and standard deviations (SD) were 0.033 J (SD: 0.031 J) for SW_1 versus SW_{cond}, 0.055 J (SD: 0.037 J) for SW_2 versus SW_{cond}, and −0.007 J (SD: 0.037 J) for SW_3 versus SW_{cond}.

Table 4
Percentage error of SW_1, SW_2, and SW_3 compared to SW_{cond}. The mean difference and standard deviations (SD) were 0.033 J (SD: 0.031 J) for SW_1 versus SW_{cond}, 0.055 J (SD: 0.037 J) for SW_2 versus SW_{cond}, and −0.007 J (SD: 0.037 J) for SW_3 versus SW_{cond}.

	SW_1 vs. SW_{cond}	SW_2 vs. SW_{cond}	SW_3 vs. SW_{cond}
Median	21.66%	37.96%	25.44%
25th percentile	12.50%	24.50%	13.34%
75th percentile	53.87%	68.04%	31.36%

To test the differences between the groups (SW_1, SW_2, SW_3, SW_{cond}), the Friedman test in combination with post hoc tests and a significance level of 0.05 was conducted. The resulting p-value of $3.71 \cdot 10^{-10}$ showed that the differences between all groups are significant. The post hoc tests showed that there are significant differences between SW_1 and SW_{cond} (p-value = 0.0044), and SW_2 and SW_{cond} (p-value = $3.71 \cdot 10^{-10}$). Results did not provide any evidence whether differences between SW_3 and SW_{cond} exist or not (p-value = 0.9992).

In summary, the analysis showed that SW_3 has the highest accuracy because of its low mean difference of −0.007 J. Fig. 5 however revealed that the precision is low due to the high SD. SW_1 has a better precision with low SD, but a slightly higher mean difference of 0.033 J. These findings were supported by a Bland–Altman analysis for SW_1, SW_2, and SW_3 compared to SW_{cond} (Supplement S7).

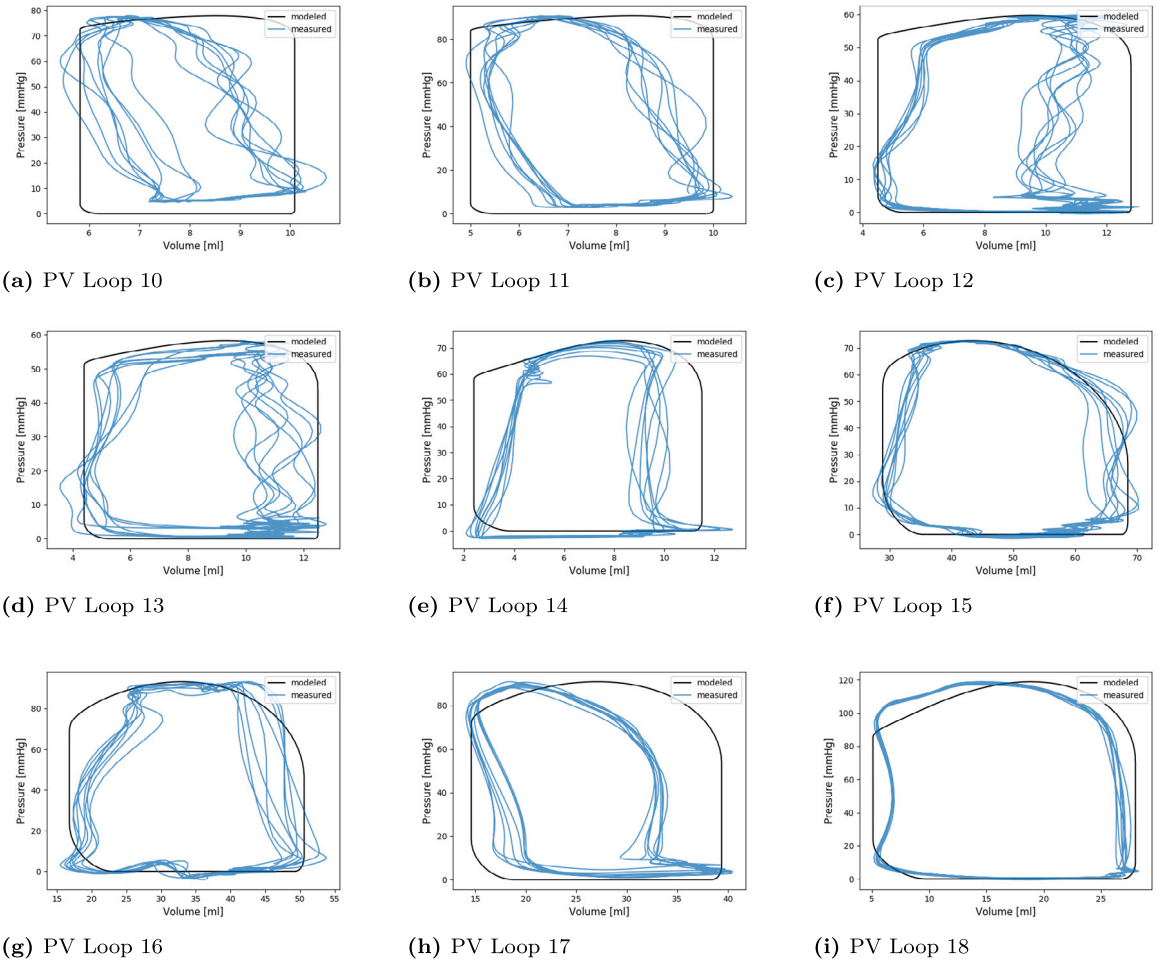

(a) PV Loop 10 (b) PV Loop 11 (c) PV Loop 12

(d) PV Loop 13 (e) PV Loop 14 (f) PV Loop 15

(g) PV Loop 16 (h) PV Loop 17 (i) PV Loop 18

Fig. 4. Measured and modeled PV loops for the patient group.

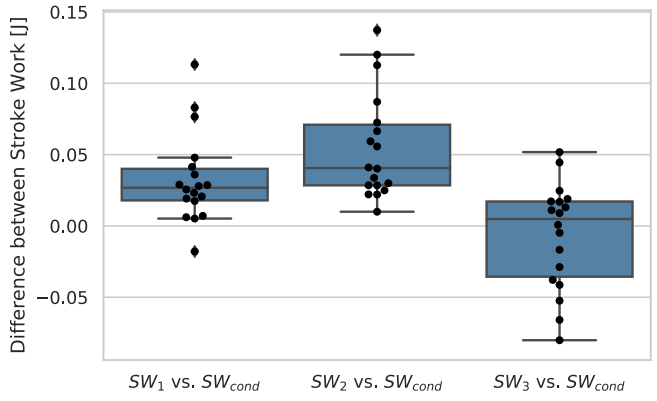

Fig. 5. Box-plot for the absolute differences of the estimated SW, SW_1, SW_2, and SW_3, compared to the conductance measurements SW_{cond}.

3.2. Comparison of SW_1, SW_2, and SW_3

Differences between SW_1, SW_2, and SW_3 for the subject group of 336 healthy children were analyzed. Fig. 6 shows scatter and Bland–Altman plots for each combination.

The limits of agreement (LOA) are reference intervals (mean ± 1.96 x standard deviation), which are highlighted in the Bland–Altman plots. The mean differences between SW_1 and SW_2 was −0.0835 J and LOA were −0.2416 J and 0.0746 J (Fig. 6(b)). For each subject, SW_2 had bigger values than SW_1. Differences increased systematically for higher average values of SW.

SW_3 was smaller than SW_1 and SW_2. Comparing SW_3 and SW_1, LOA were −0.119 J and 0.4588 J and mean was 0.1699 J (Fig. 6(c)). Absolute difference increased for higher average values of SW. Analogously, comparing SW_3 and SW_2, LOA were −0.1913 J and 0.698 J and mean was 0.2534 J (Fig. 6(d)).

3.3. Reference curves for standard values

The validation and comparison showed that SW_1 gave the best approximation of SW because of its low percentage error and low SD. SW_2 overestimated SW with high differences while SW_3 performed better but showed high standard deviations and a higher percentage error than SW_1.

Reference curves were created for SW_1 by fitting a GAMLSS model to the data over age, height, and weight, respectively. Curves (P3, P10, P25, P50, P75, P90) represent the distribution of the population as 3rd, 10th, 25th, 50th, 75th, 90th, and 97th percentile. Model selection was performed by choosing the model with the lowest Bayesian Information Criterion (BIC).

Fig. 7 shows the resulting reference curves for SW_1. SW of a standard newborn is 0.06 J and increases to 1.15 J at the age of 18 years. Stroke work increases over weight and height in a similar trend. The percentile curves depict the distribution of SW.

In Fig. 8, it is exemplarily demonstrated how to compare SW of patient hearts to normal values for the respective age (50th percentile) and to quantify the differences. Differences were quantified as absolute

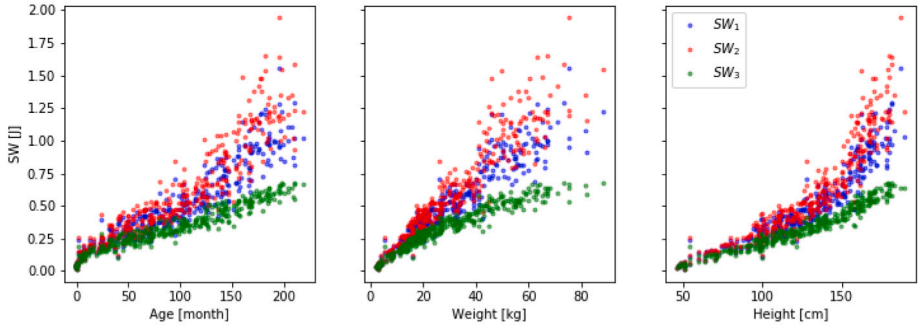

(a) SW over age, weight, and height

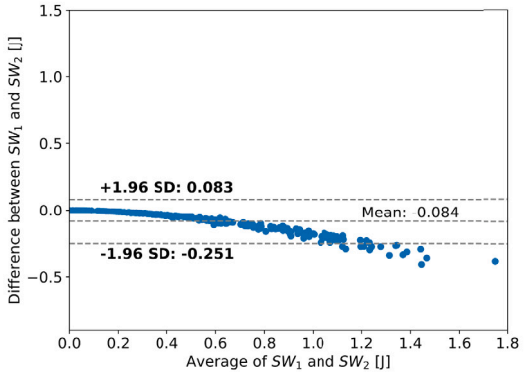

(b) Abs. differences - SW_1 and SW_2

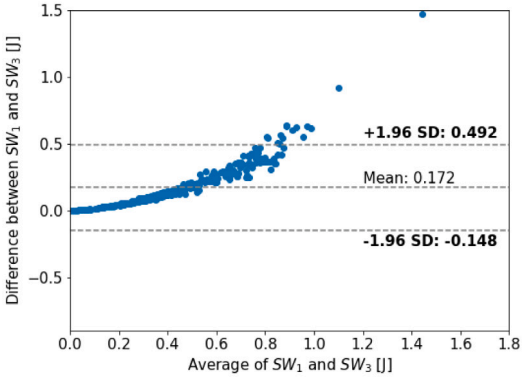

(c) Abs. differences - SW_1 and SW_3

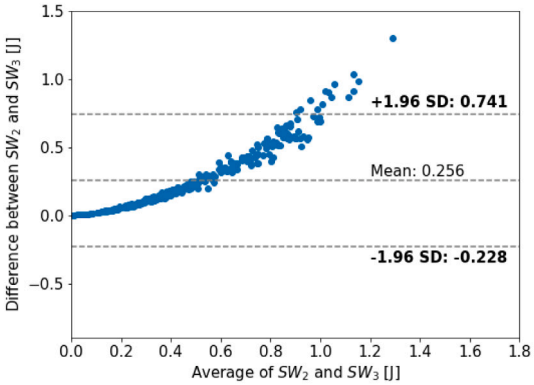

(d) Abs. differences - SW_2 and SW_3

Fig. 6. Comparison of SW_1, SW_2, and SW_3. SW is plotted over age, weight and height (a). Absolute differences are shown for SW_1 and SW_2, SW_1 and SW_3, and SW_2 and SW_3 respectively (b–d).

values and standard z score, which can be computed with the formula and tables given in Supplement S8. An example patient (132 months old) with a stroke work of 0.33 J is highlighted in the figure, where the absolute difference (ΔSW) was determined as −0.31 J, and the z score is −3.81.

SW of patients were lower than the norm. The z score was in a range between −9.21 to 0.38, with a mean of −3.73.

4. Discussion

In this study, we were able to create reference curves of the left ventricular stroke work for a wide range of age, height, and weight in healthy children. Stroke work was estimated and compared with three different methods (SW_1, SW_2, SW_3), which are commonly used by researchers and practitioners.

Comparing SW estimation among different methods (SW_1, SW_2, SW_3), absolute differences between SW_1, SW_2, and SW_3 showed a systematic trend, where differences increased with average values of SW (Fig. 6). Also, differences increased with age, weight, and height, so that heart size can be assumed to affect the differences between SW_1, SW_2, and SW_3. Reasons for this effect can be the different inputs for SW_1, SW_2, and SW_3. The differences between SW_1 and SW_2 can be visualized in the pressure–volume diagram as difference area (Supplement S5). It seems plausible that this area will increase for higher pressures and volumes. SW_3 is smaller than SW_2 or SW_3 for all cases. Therefore, it underestimates SW, which is matching with the clinical findings by Topham et al. [27].

By validating the methods with 18 invasive measurements in patients, we can show that measured and modeled SW have small absolute

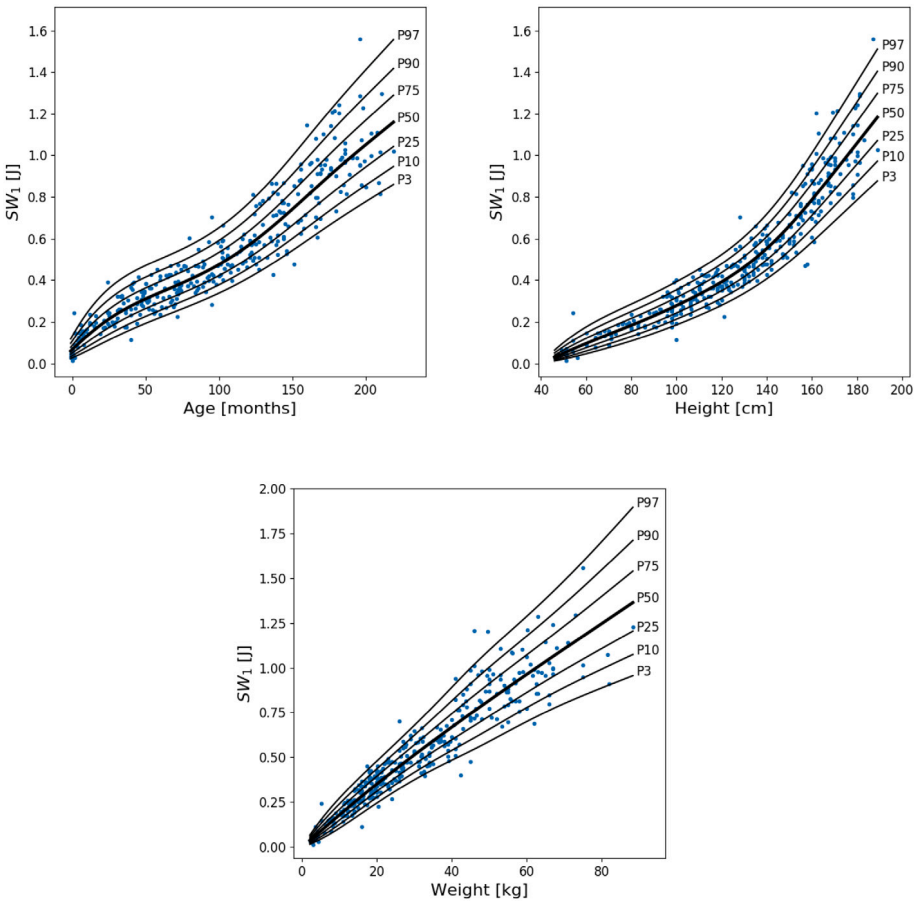

Fig. 7. Reference curves for SW_1 over age, height, weight. Curves (P3, P10, P25, P50, P75, P90) represent the distribution of the population as 3rd, 10th, 25th, 50th, 75th, 90th, and 97th percentile.

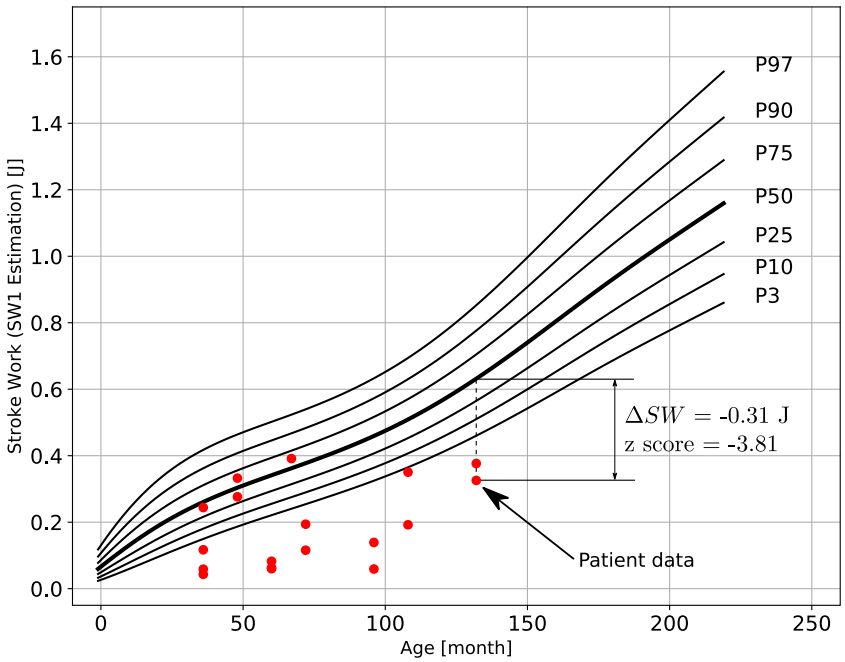

Fig. 8. Comparison of patient data (red data points) and normal values. Percentile curves (P3, P10, P25, P50, P75, P90) represent the group of healthy children. An example patient (132 months old) with a stroke work of 0.33 J is highlighted in the figure, where the absolute difference (ΔSW) was determined as −0.31 J, and the z score is −3.81.

differences. Estimations with SW_1 resulted in a mean difference of 0.033 J, for example. In general, SW_1 and SW_2 tend to overestimate SW, while SW_3 tends to slightly underestimate SW. Percentage errors are however high with median values from 21.66% to 37.96%

(Table 4). These relative differences highly depend on the heart size of the patients. We found that for all methods (SW_1, SW_2, SW_3), small hearts had a higher percentage error and a higher variation than large hearts.

In a similar study by Davidson et al. [35], a new method was proposed to estimate left ventricular work, where percentage errors of 23.2% were received. Davidson et al. acquired about 5000 heartbeats in piglets, while we were able to receive up to 7 heartbeats in our study group. The similar value for the error shows that our method can compete with modern approaches for stroke work estimation.

Currently, norm values for the work or power of the human heart only exist for adults and are given in physiological textbooks. Comparing our values for healthy teenagers ($SW \approx 1$ J) and literature values for adults ($SW = 1.07$ J) [36], we found them to match closely. Furthermore, the created reference curves for SW_1 present not only the trend over age, weight, and height, but also give information about the distribution.

The utilized LPM, which was developed by Pironet et al. is an abstract model of the cardiovascular system with a concatenated circulation. This approach is justified by the focus of this study on the PV loop of the ventricle. The shape of the PV loop is mainly described by the modeled driver function (or normalized elastance function) $e_{lv}(t, T)$ (Eq. (8)) [37,38]. The surrounding elements, which are modeled to describe the circulation, are responsible for the position of the loop in the pressure–volume diagram (maximal pressure, maximal volume and minimal volume). From a technical point of view, the surroundings (systemic and pulmonary circulation) can be merged into one circulation, which reduces the number of model parameters and enables an easier model fitting with the limited number of measurements. For the focus on ventricular behavior, this abstraction does not limit the quality of the SW estimation. However, the model parameters of surroundings like aorta or vena cava are difficult to interpret as real clinical values, which we found to be discussed as a general issue and limitation for most modeling approaches.

A set of model parameters (R_i, R_o, E_{vc}, E_{ao}) was fixed at chosen values during the estimation process. The assignment of these parameters was done by analyzing their impact on the estimation results (Supplement S4). It could be shown that R_i, R_o, E_{vc}, and E_{ao} have only little impact on the SW estimation and can be fixed at plausible values. However, they determine the shape of the PV loop and therefore should be analyzed further. As a future work, one could consider to tune R_i, R_o, E_{vc}, E_{ao} for each model fitting. This could be achieved by using two nested loops, an inner loop for the estimation of E_{lv}, R_c, and SBV and an outer loop for the remaining parameters. The information taken from the volume time curve (Fig. 1) could serve as constraints for the outer loop.

As a result of the SW estimation, model parameters were estimated for a large cohort of children. These information are valuable for multiscale modeling, as they can be used to describe the global mechanical behavior of the heart or the boundaries of Computational Fluid Dynamics (CFD) models [21,39,40]. The given model parameters distributions can be a helpful reference for such modeling approaches.

There are mainly two sources of errors in our approach: the measurement error and modeling error. The measurement error depends on the measurement technology and devices, which were used to acquire the data. The 3D echocardiography technology for volumetric data acquisition has been validated in multiple studies [41,42]. Furthermore, the used conductance catheter for volume and pressure measurements was tested over the last decades [43,44]. The maximal left ventricular pressure was approximated by a regression model, which accounts as a limitation of the study as it was not validated. Modeling errors occur due to oversimplification of the cardiovascular system. The simplifying assumptions of the LPM are justified by the chosen focus on the left ventricular PV loop and a detailed analysis of its global behavior, whereas the hemodynamics of the remaining circulation were not investigated. Comparing conductance catheter measurements and model output (Figs. 3 and 4), we found that the LPM was able to capture the behavior of the left ventricular pressure and volume in all aspects. For future work, it has to be proven whether the model error in our approach is smaller than the measurement error of the conductance catheter.

Our findings can be useful for comparison of simulated or measured results, as shown in Fig. 8. In the specific case of Fontan patients, for example, there have been several studies to investigate the heart performance [5,6,20]. Most studies consider pressure, volume, and other medical parameters, such as oxygen consumption. Ideally, stroke work is also considered to understand the pump mechanics of the heart. Studies about the kinetic energy of the fluid are more common [45–47], which is closely related to stroke work. With our study, we aimed to add valuable information about stroke work so that the acquisition of data in a control group might not be necessary anymore, saving effort and costs.

For the optimization of medical devices, the presented standard values can be profitable, too. In ventricular assist devices (VAD), for example, modern approaches consider SW to improve the control mechanism [48,49]. In the study by Rüschen et al. [13], an algorithm is presented to control a VAD by minimizing SW. Our study contributes information about the absolute values of SW in children. Especially in small patients, an accurate adjustment is required.

4.1. Limitation

The primary limitation of this study is the approximation of maximal left ventricular pressure by a regression model. Ventricular pressure highly depends on the individual situation. To overcome this limitation, we recommend using non-invasive cuff pressure measurements, as an example, which were missing in this study.

A model-specific issue was the missing information about the unstressed blood volume in LV, $V_{U,lv}$, which was overcome by fixing it to zero. There are approaches for approximating $V_{U,lv}$ from single beat measurements [37]. These methods are, however, of clinical nature and most propose a curve fitting to estimate the isovolumetric pressure. During clinical trials, we gained experience with these methods, which we did not consider helpful for this computational study. Kung et al. [20] and Davidson et al. [35] used simple formulas or fixed values for $V_{U,lv}$, but evidence for its general usage is low. Furthermore, $V_{U,lv}$ is considered as a hyperparameter, meaning that it does not contribute to the model fitting. Therefore, fixing it to zero does not influence the model fitting and SW estimation.

The validation could only be performed with measurements in patients, which resulted in a relative difference of 21.66% at its best. Due to the pathology, PV loops showed high variations, although the signals were already filtered for noise. Especially, the volume during the isovolumic contraction varied strongly. Apart from the pathology, the reasons for these significant differences might be the small heart size and the difficulties of the conductance catheter measurement technology (Figs. 3 and 4). The application of the conductance catheter in children is challenging due to experimental noise, patient movement, and optimal catheter positioning.

4.2. Conclusion

This is the first study to provide pediatric reference curves for standard values of left ventricular stroke work, allowing comparison with simulation results or clinical measurements. Despite the discussed limitations, we showed how these standard values can potentially help to impact clinical decision-making. The presented model-based method has the capability to estimate stroke work with only non-invasive data.

Ethical approval

All procedures followed were in accordance with the ethical standards of the responsible committee on human experimentation (institutional and national) and with the Helsinki Declaration of 1975, as revised in 2000 (5). Informed consent was obtained from all patients for being included in the study.

Declaration of competing interest

The authors declare that they have no known competing financial interests or personal relationships that could have appeared to influence the work reported in this paper.

Acknowledgments

This study was supported by Fördergemeinschaft Deutsche Kinderherzzentren e.V.

Michael Neidlin acknowledges financial support through the "Return Fellowship" of the German Research Foundation (DFG).

Appendix A. Supplementary data

Supplementary material related to this article can be found online at https://doi.org/10.1016/j.compbiomed.2020.103908.

References

[1] K.R. Walley, Left ventricular function: time-varying elastance and left ventricular aortic coupling, Crit. Care 20 (1) (2016) 270.

[2] G. Cotter, S.G. Williams, Z. Vered, L.B. Tan, Role of cardiac power in heart failure, Curr. Opin. Cardiol. 18 (3) (2003) 215–222.

[3] G. Elzinga, N. Westerhof, How to quantify pump function of the heart. the value of variables derived from measurements on isolated muscle, Circ. Res. 44 (3) (1979) 303–308.

[4] H. Saiki, B.W. Eidem, T. Ohtani, M.A. Grogan, M.M. Redfield, Ventricular-arterial function and coupling in the adult Fontan Circulation, J. Am. Heart Assoc. 5 (9) (2016) e003887.

[5] G. Szabó, V. Buhmann, A. Graf, S. Melnitschuk, S. Bährle, C.F. Vahl, S. Hagl, Ventricular energetics after the Fontan operation: contractility-afterload mismatch, J. Thorac. Cardiovasc. Surg. 125 (5) (2003) 1061–1069.

[6] M. Nogaki, H. Senzaki, S. Masutani, J. Kobayashi, T. Kobayashi, N. Sasaki, H. Asano, S. Kyo, Y. Yokote, Ventricular energetics in Fontan circulation: evaluation with a theoretical model, Pediatr. Int. 42 (6) (2000) 651–657.

[7] E. Ben-Assa, J. Brown, Z. Keshavarz-Motamed, M. Jose, B. Leiden, M. Olender, F. Kallel, I.F. Palacios, I. Inglessis, J.J. Passeri, et al., Ventricular stroke work and vascular impedance refine the characterization of patients with aortic stenosis, Sci. Transl. Med. 11 (509) (2019) eaaw0181.

[8] O.F. AbouEzzeddine, B.J. Kemp, B.A. Borlaug, B.P. Mullan, A. Behfar, S.V. Pislaru, M. Fudim, M.M. Redfield, P. Chareonthaitawee, Myocardial energetics in heart failure with preserved ejection fraction, Circ.: Heart Fail. 12 (10) (2019) e006240.

[9] M. Gotzmann, S. Hauptmann, M. Hogeweg, D.S. Choudhury, F. Schiedat, J.W. Dietrich, T.H. Westhoff, M. Bergbauer, A. Mügge, Hemodynamics of paradoxical severe aortic stenosis: insight from a pressure–volume loop analysis, Clin. Res. Cardiol. (2019) 1–9.

[10] D.C. Sprigings, J.B. Chambers, T. Cochrane, J. Allen, G. Jackson, Ventricular stroke work loss: validation of a method of quantifying the severity of aortic stenosis and derivation of an orifice formula, J. Am. Coll. Cardiol. 16 (7) (1990) 1608–1614.

[11] G. de Simone, R.B. Devereux, T.R. Kimball, G.F. Mureddu, M.J. Roman, F. Contaldo, S.R. Daniels, Interaction between body size and cardiac workload: influence on left ventricular mass during body growth and adulthood, Hypertension 31 (5) (1998) 1077–1082.

[12] D. Burkhoff, G. Sayer, D. Doshi, N. Uriel, Hemodynamics of mechanical circulatory support, J. Am. Coll. Cardiol. 66 (23) (2015) 2663–2674.

[13] D. Rüschen, F. Prochazka, R. Amacher, L. Bergmann, S. Leonhardt, M. Walter, Minimizing left ventricular stroke work with iterative learning flow profile control of rotary blood pumps, Biomed. Signal Process. Control 31 (2017) 444–451.

[14] E.L. Wu, M.C. Stevens, F. Nestler, J.P. Pauls, A.P. Bradley, G. Tansley, J.F. Fraser, S.D. Gregory, A Starling-like total work controller for rotary blood pumps: An in vitro evaluation, Artif. Organs (2019).

[15] F. Seemann, P. Arvidsson, D. Nordlund, S. Kopic, M. Carlsson, H. Arheden, E. Heiberg, Noninvasive quantification of pressure-volume loops from brachial pressure and cardiovascular magnetic resonance, Circ.: Cardiovasc. Imaging 12 (1) (2019) e008493.

[16] U. Herberg, E. Gatzweiler, T. Breuer, J. Breuer, Ventricular pressure–volume loops obtained by 3D real-time echocardiography and mini pressure wire—a feasibility study, Clin. Res. Cardiol. 102 (6) (2013) 427–438.

[17] K. Krell, K.T. Laser, R. Dalla-Pozza, C. Winkler, U. Hildebrandt, D. Kececioglu, J. Breuer, U. Herberg, Real-time three-dimensional echocardiography of the left ventricle—Pediatric percentiles and head-to-head comparison of different contour-finding algorithms: A multicenter study, J. Am. Soc. Echocardiogr. 31 (6) (2018) 702–711.

[18] P. Steendijk, S.A. Tulner, M. Wiemer, R.A. Bleasdale, J.J. Bax, E.E. van der Wall, J. Vogt, M.J. Schalij, Pressure–volume measurements by conductance catheter during cardiac resynchronization therapy, Eur. Heart J. Suppl. 6 (suppl_D) (2004) D35–D42.

[19] J. Mineroff, A.D. McCulloch, D. Krummen, B. Ganapathysubramanian, A. Krishnamurthy, Optimization framework for patient-specific cardiac modeling, Cardiovasc. Eng. Technol. 10 (4) (2019) 553–567.

[20] E. Kung, G. Pennati, F. Migliavacca, T.-Y. Hsia, R. Figliola, A. Marsden, A. Giardini, A simulation protocol for exercise physiology in Fontan patients using a closed loop lumped-parameter model, J. Biomech. Eng. 136 (8) (2014) 081007.

[21] M. Neidlin, U. Steinseifer, T.A. Kaufmann, A multiscale 0-D/3-D approach to patient-specific adaptation of a cerebral autoregulation model for computational fluid dynamics studies of cardiopulmonary bypass, J. Biomech. 47 (8) (2014) 1777–1783.

[22] T.-Y. Hsia, D. Cosentino, C. Corsini, G. Pennati, G. Dubini, F. Migliavacca, M. of Congenital Hearts Alliance (MOCHA) Investigators, Use of mathematical modeling to compare and predict hemodynamic effects between hybrid and surgical Norwood palliations for hypoplastic left heart syndrome, Circulation 124 (11_suppl_1) (2011) S204–S210.

[23] T.A. Kaufmann, M. Neidlin, M. Büsen, S.J. Sonntag, U. Steinseifer, Implementation of intrinsic lumped parameter modeling into computational fluid dynamics studies of cardiopulmonary bypass, J. Biomech. 47 (3) (2014) 729–735.

[24] S. de Bournonville, A. Pironet, C. Pretty, J.G. Chase, T. Desaive, Parameter estimation in a minimal model of cardio-pulmonary interactions, Math. Biosci. 313 (2019) 81–94.

[25] A. Pironet, P.D. Docherty, P.C. Dauby, J.G. Chase, T. Desaive, Practical identifiability analysis of a minimal cardiovascular system model, Comput. Methods Prog. Biomed. (2017).

[26] H. Neuhauser, A. Schienkiewitz, A.S. Rosario, R. Dortschy, B.-M. Kurth, Referenzperzentile für anthropometrische Maßzahlen und Blutdruck aus der Studie zur Gesundheit von Kindern und Jugendlichen in Deutschland, KiGGS, Robert Koch-Institut, 2013.

[27] W. Topham, Comparison of methods for calculation of left ventricular stroke work, J. Appl. Physiol. 27 (5) (1969) 767–769.

[28] A. Pironet, T. Desaive, P.C. Dauby, J.G. Chase, P.D. Docherty, Parameter identification methods in a model of the cardiovascular system, IFAC-PapersOnLine 48 (20) (2015) 366–371.

[29] T.A. Parlikar, G.C. Verghese, A simple cycle-averaged model for cardiovascular dynamics, in: 2005 IEEE Engineering in Medicine and Biology 27th Annual Conference, IEEE, 2006, pp. 5490–5494.

[30] M.S. Olufsen, J.T. Ottesen, H.T. Tran, L.M. Ellwein, L.A. Lipsitz, V. Novak, Blood pressure and blood flow variation during postural change from sitting to standing: model development and validation, J. Appl. Physiol. 99 (4) (2005) 1523–1537.

[31] T. Korakianitis, Y. Shi, Effects of atrial contraction, atrioventricular interaction and heart valve dynamics on human cardiovascular system response, Med. Eng. Phys. 28 (8) (2006) 762–779.

[32] D. Stevenson, J. Revie, J.G. Chase, C.E. Hann, G.M. Shaw, B. Lambermont, A. Ghuysen, P. Kolh, T. Desaive, Beat-to-beat estimation of the continuous left and right cardiac elastance from metrics commonly available in clinical settings, Biomed. Eng. Online 11 (1) (2012) 73.

[33] F. Gao, L. Han, Implementing the Nelder–Mead simplex algorithm with adaptive parameters, Comput. Optim. Appl. 51 (1) (2012) 259–277.

[34] R.A. Rigby, D. Stasinopoulos, Generalized additive models for location, scale and shape, J. R. Stat. Soc. Ser. C. Appl. Stat. 54 (3) (2005) 507–554.

[35] S. Davidson, C. Pretty, S. Kamoi, T. Desaive, J.G. Chase, Beat-by-beat estimation of the left ventricular pressure–volume loop under clinical conditions, Ann. Biomed. Eng. 46 (1) (2018) 171–185.

[36] S. Silbernagl, A. Despopoulos, Taschenatlas Physiologie, Georg Thieme Verlag, 2007.

[37] H. Senzaki, C.-H. Chen, D.A. Kass, Single-beat estimation of end-systolic pressure-volume relation in humans: a new method with the potential for noninvasive application, Circulation 94 (10) (1996) 2497–2506.

[38] J.-W. Lankhaar, F.A. Rövekamp, P. Steendijk, T.J. Faes, B.E. Westerhof, T. Kind, A. Vonk-Noordegraaf, N. Westerhof, Modeling the instantaneous pressure–volume relation of the left ventricle: a comparison of six models, Ann. Biomed. Eng. 37 (9) (2009) 1710–1726.

[39] C. Corsini, C. Baker, A. Baretta, G. Biglino, A.M. Hlavacek, T.-Y. Hsia, E. Kung, A. Marsden, F. Migliavacca, I. Vignon-Clementel, et al., Integration of clinical data collected at different times for virtual surgery in single ventricle patients: a case study, Ann. Biomed. Eng. 43 (6) (2015) 1310–1320.

[40] S. Sankaran, M.E. Moghadam, A.M. Kahn, E.E. Tseng, J.M. Guccione, A.L. Marsden, Patient-specific multiscale modeling of blood flow for coronary artery bypass graft surgery, Ann. Biomed. Eng. 40 (10) (2012) 2228–2242.

[41] U. Herberg, M. Brand, C. Bernhardt, H.G. Trier, J. Breuer, Variables influencing the accuracy of 2-dimensional and real-time 3-dimensional echocardiography for assessment of small volumes, areas, and distances: An in vitro study using static tissue-mimicking phantoms, J. Ultrasound Med. 30 (7) (2011) 899–908.

[42] S.M. Chowdhury, R.J. Butts, C.L. Taylor, V.M. Bandisode, K.S. Chessa, A.M. Hlavacek, G.S. Shirali, G.H. Baker, Validation of noninvasive measures of left ventricular mechanics in children: a simultaneous echocardiographic and conductance catheterization study, J. Am. Soc. Echocardiogr. 29 (7) (2016) 640–647.

[43] J. Baan, E.T. Van Der Velde, H.G. De Bruin, G.J. Smeenk, J. Koops, A.D. Van Dijk, D. Temmerman, J. Senden, B. Buis, Continuous measurement of left ventricular volume in animals and humans by conductance catheter, Circulation 70 (5) (1984) 812–823.

[44] D. Burkhoff, E. Van Der Velde, D. Kass, J. Baan, W. Maughan, K. Sagawa, Accuracy of volume measurement by conductance catheter in isolated, ejecting canine hearts, Circulation 72 (2) (1985) 440–447.

[45] M.D. Rodefeld, A. Marsden, R. Figliola, T. Jonas, M. Neary, G.A. Giridharan, Cavopulmonary assist: Long-term reversal of the Fontan paradox, J. Thorac. Cardiovasc. Surg. (2019).

[46] F.M. Rijnberg, M.G. Hazekamp, J.J. Wentzel, P.J. De Koning, J.J. Westenberg, M.R. Jongbloed, N.A. Blom, A.A. Roest, Energetics of blood flow in cardiovascular disease: concept and clinical implications of adverse energetics in patients with a Fontan circulation, Circulation 137 (22) (2018) 2393–2407.

[47] S. Masutani, H. Senzaki, Assessment of ventricular function using the pressure-volume relationship, in: Congenital Heart Disease, Springer, 2015, pp. 97–126.

[48] G.A. Giridharan, M. Ising, M.A. Sobieski, S.C. Koenig, J. Chen, S. Frankel, M.D. Rodefeld, Cavopulmonary assist for the failing Fontan circulation: impact of ventricular function on mechanical support strategy, ASAIO J. (Am. Soc. Artif. Internal Organs: 1992) 60 (6) (2014) 707.

[49] R.F. Salamonsen, E. Lim, N. Gaddum, A.-H.H. AlOmari, S.D. Gregory, M. Stevens, D.G. Mason, J.F. Fraser, D. Timms, M.K. Karunanithi, et al., Theoretical foundations of a Starling-like controller for rotary blood pumps, Artif. Organs 36 (9) (2012) 787–796.

8 Appendix B - Second study

Linden, K., Goldschmidt, F., Laser, K.T., Winkler, C., Körperich, H., Dalla-Pozza, R., Breuer, J. and Herberg, U., (2019). Left atrial volumes and phasic function in healthy children: reference values using real-time three-dimensional echocardiography. Journal of the American Society of Echocardiography, 32(8), pp.1036-1045.

Left Atrial Volumes and Phasic Function in Healthy Children: Reference Values Using Real-Time Three-Dimensional Echocardiography

Katharina Linden, MD, Franziska Goldschmidt, MD, Kai Thorsten Laser, MD, PhD, Christian Winkler, MSc, Hermann Körperich, PhD, Robert Dalla-Pozza, MD, PhD, Johannes Breuer, MD, PhD, and Ulrike Herberg, MD, PhD, *Bonn, Bad Oeynhausen, and Munich, Germany*

Background: Evaluation of left atrial (LA) size and function is important in congenital and acquired pediatric cardiac disease. Real-time three-dimensional echocardiography (3DE) offers noninvasive assessment of cardiac volumes and phasic function independent of geometric assumptions. The aim of this prospective multicenter study was to establish pediatric reference values for LA 3DE volumes and phasic function based on a large cohort of healthy children.

Methods: LA data sets of 432 subjects (0 days-222 months) were analyzed prospectively using a vendor-independent software. LA volumes (maximal [Vmax], minimal [Vmin], and before atrial contraction) as well as phasic function (active and passive emptying fraction [EF]) were assessed. For volumes, sex-specific reference values, percentiles, and *z*-scores were calculated by the LMS method of Cole and Green.

Results: Absolute volumes increased with age and body surface area. Active EF and relative duration of atrial emptying tended to increase with increasing R-R intervals, while passive EF decreased. Reproducibility of volumes was very good (intra- and interobserver variability for Vmax and Vmin (mean bias ± SD, 0.1 ± 0.9 mL and 0.7 ± 2.8 mL). Volumes were well correlated with cardiac magnetic resonance measurements showing known underestimation of volumes by 3DE (mean bias ± SD, Vmax –14.2 ± 14 mL; Vmin –11.5 ± 10 mL).

Conclusions: Pediatric LA volumes and phasic function indices were reproducibly measured by 3DE. The provided pediatric reference values can be the basis for evaluation of the LA by 3DE and contribute to detection of LA dysfunction and follow-up of patients with congenital heart diseases. (J Am Soc Echocardiogr 2019;32:1036-45.)

Keywords: Left atrium, Phasic function, Three-dimensional echocardiography, Reference values, Pediatric

The role of left atrial (LA) volumes and function as a prognostic marker for cardiac outcome and a parameter for follow-up has been of growing interest in recent years. Studies in adults show that LA size and function can serve as a marker for diastolic dysfunction.[1-6] In children, only few and small studies exist. Taggart *et al.*[7] and Sakata *et al.*[8] showed that situations with a left-to-right-shunt leading to a left ventricular (LV) volume load are reflected by enlarged LA volumes. In children with hypertrophic cardiomyopathy LA volumes were enlarged, and this was found to be a potential marker of elevated LV end-diastolic pressure and diastolic dysfunction.[7,9] The different phases of LA function play important roles in cardiac performance as there is interplay between the LA and the LV. The LA reservoir function is determined by atrial relaxation and compliance as well as LV systolic function. The conduit function is determined by LA compliance and LV relaxation and early filling. LA contractility and LV diastolic compliance are determinants of

From the Department of Pediatric Cardiology, Children's Hospital, University of Bonn (K.L., F.G., C.W., J.B., U.H.), Bonn; Department of Congenital Heart Defects (K.T.L.) and Institute for Radiology, Nuclear Medicine and Molecular Imaging, Heart and Diabetes Center, North Rhine Westphalia Ruhr University Bochum (H.K.), Bad Oeynhausen; and Department of Pediatric Cardiology and Pediatric Intensive Care, Ludwig Maximilians University, Medical Hospital of the University of Munich (R.D.-P.), Munich, Germany.

Drs. Linden and Goldschmidt contributed equally.

Conflicts of Interest: None.

This study was part of the project Validation and Standardization of Real-Time-3D Echocardiography for the Functional Analysis of Pediatric Cardiac Valves, sponsored by the Fördergemeinschaft Deutsche Kinderherzzentren (Project No. W-BN/M/BAD-009/2009).

Reprint requests: Katharina Linden, Department of Pediatric Cardiology, University of Bonn, Adenauerallee 119, 53113 Bonn, Germany (E-mail: *Katharina.Linden@ukbonn.de*).

0894-7317

https://doi.org/10.1016/j.echo.2019.03.018

Abbreviations

2D = Two-dimensional

3D = Three-dimensional

2DE = Two-dimensional echocardiography

3DE = Three-dimensional echocardiography

AE = Active emptying

BIC = Bayesian information criterion

BSA = Body surface area

CMR = Cardiac magnetic resonance

e.d.f. = Equivalent degree of freedom

EV = Emptying volume

HR = Heart rate

ICC = Intraclass correlation coefficient

LA = Left atrial, atrium

LV = Left ventricular, ventricle

PE = Passive emptying

Vmax = Maximum left atrial volume

Vmin = Minimum left atrial volume

VpreA = Volume before atrial contraction

VTC = Volume-time curve

the contractile function. Therefore, accurate assessment and reference values of LA volume and phasic function may be of value and can increase our ability to detect diastolic dysfunction of the LV.[1]

Measurement of LA volumes, rather than area or diameter, is recommended for LA assessment (Simpson rule).[10] However, two-dimensional (2D) echocardiographic methods are dependent on geometric assumptions and are prone to errors associated with foreshortening.[10,11] As shown in adults, real-time three-dimensional echocardiography (3DE) offers an assessment of LA volumes independent of geometric assumptions, correlates better with cardiac magnetic resonance (CMR), and has superior prognostic abilities.[6,12]

Unfortunately, in children, reference values for LA volumes using up-to-date 3DE are scarce. Tanaka *et al.*[13] reports pediatric LA reference volumes in a Japanese population using a vendor-specific software. Ghelani *et al.*[14] published pediatric normal maximal and minimal LA volumes and strain measured by 3DE in 196 children, mainly older than 2.5 years, in a retrospective single-center study.

The aim of our study was to establish pediatric reference values for LA phasic volumes and phasic function indices measured by 3DE based on a large cohort of healthy Caucasian children in a prospective multicenter study. Moreover, we wanted to evaluate the duration of the different phases in regard to heart rate (HR). We focused on including an adequate number of infants and toddlers as previous studies were often limited regarding that group.

METHODS

Study Design

We enrolled 497 healthy Caucasian children (ages 0 days to 222 months) between April 2011 and November 2013 in a prospective multicenter design including three centers. All healthy subjects included in this study were in sinus rhythm, and cardiac disease was ruled out by history, physical examination, and 2DE according to standard recommendations.[15] Age, sex, weight, and height were measured at the time of the examination. Body surface area (BSA) was calculated using the Haycock formula according to American Society of Echocardiography recommendations.[15] The study was approved by the local ethics institutional review committee (Registration No. 226/06) and representative boards of all participating centers and conformed to the principles of the Declaration of Helsinki as well as German law. Written consent was given by the legal guardian or in person by the 18-year-olds.

Three-Dimensional Echocardiography

Acquisition. The 3DE data sets were obtained using iE33 (Philips, Andover, MA) with a matrix transducer X5-1 or X7-2 or using Vivid E9 (GE Medical Systems, Milwaukee, WI) with a V4 transducer. Prior to the start of the study, standardization of the acquisition procedure, including presets and operator training, took place.[16,17] Full-volume 3DE data sets were obtained from an apical approach based on standard recommendations.[18] A full-volume scan was acquired from four to seven R-wave triggered subvolumes. In those children who were able to perform breath holding, this acquisition was done during end-expiratory breath holding. In the core lab, 3DE data were rated for quality and were subsequently quantified. Data sets containing artifacts or incomplete depiction of the LA were excluded.

Analysis. The 3DE LA analysis was performed in the core lab using TomTec 4D LV-Analysis software 3.1 (Image-Arena version 4.6; Build 4.6.3.9, TomTec, Unterschleißheim, Germany).

First, the frame corresponding to the maximum LA volume (Vmax), just before the mitral valve opening, was identified and chosen as the reference frame. Second, the LA data set was aligned to obtain an optimal nonforeshortened view of the LA in all three apical reference views (apical two-chamber, three-chamber, and four-chamber view). The marker for the apex was set at the roof of the LA, and the three-dimensional (3D) data set was rotated 60° counterclockwise according to the recommendations of the software developer. This way the shape of the LA better resembled the respective shape of the LV in the three apical views, facilitating automated border detection and tracing (Figure 1). After identifying and marking the mitral valve and the roof of the LA, the automated border detection traced the contours of the LA first in the frame of the maximal volume (reference frame). Manual adjustments to these traced contours were made as needed (example in Supplemental Figure 1; available at www.onlinejase.com). Pulmonary veins and the LA appendage were excluded. Then the software was allowed to trace the contours in the frame of the minimal LA volume (Vmin) semiautomatically. Here manual adjustments were made only if necessary. In the next step an interpolated volume-time curve (VTC) is computed by the software (Figure 2).

Determination of time-specific events in echocardiography is not trivial and temporal resolution especially can lead to limitation. Different approaches have been published to determine the volume before atrial contraction (VpreA): the frame before mitral valve reopening,[19-21] the time of the p-wave on the surface electrocardiogram[11] or the plateau during atrial emptying.[22] We determined all three time points. For the establishment of the most reliable reference values we decided to only define VpreA and time of VpreA in the VTC when all three time points or at least the last frame before mitral valve reopening and the plateau of the curve were matching. The VTC is displayed by the software as a curve. Data can be exported as discrete values in the form of a table. We designed a tool to plot these values with the feature to set a cursor at any point of the curve and read time and corresponding volume (Figure 3). This way we were able to determine time of VpreA and VpreA more accurately.

Each data set was analyzed twice, and the mean of these two measurements was used for further analysis to minimize random error.

HIGHLIGHTS

- 3D Echocardiographic pediatric percentiles for left atrial volumes are presented.
- The percentiles are sex specific and based on a large cohort of 432 subjects.
- 3D Echocardiographic reference values for left atrial phasic function are provided.
- Data for the calculation of *z*-scores are provided.

LA phasic function can be assessed noninvasively by echocardiography by calculating certain key volumetric parameters as described elsewhere.[5,23,24] As a measure for the LA reservoir function we calculated total emptying volume (EV; Vmax − Vmin) and total emptying fraction (EF; (EV/Vmax) × 100). To assess LA conduit function, the passive EV (Vmax − VpreA), the passive EF ((passive EV/Vmax) × 100), and the passive emptying (PE) percentage (passive EV/EV) were computed. As a measure for the LA pump function, active EV (VpreA − Vmin), active EF ((active EV/VpreA) × 100), and active emptying (AE) percentage (active EV/EV) were calculated (Figure 2).

We measured the duration of atrial filling and atrial emptying absolute and as a fraction of the cardiac cycle. Moreover, we measured the duration of AE and PE absolute and as a fraction of the cardiac cycle as well as a fraction of the atrial emptying period. Earlier studies showed that duration of ventricular systole and diastole is mainly correlated with the duration of the R-R interval rather than age or BSA.[25,26] Therefore, we related durations of the different atrial phases to R-R interval. Linear regression was used to model this relationship.

CMR Image Acquisition and Analysis

CMR and 3DE were carried out prospectively in one of the centers to compare volume measurements by 3DE and CMR. In small children, sedation or general anesthesia is needed to perform a CMR. In addition to seven older healthy children, who also participated in the reference value study, we included 26 patients with congenital heart disease who were referred for routine CMR. By this we sought to cover as much as possible the whole LA range of shapes and sizes that can be expected in the clinical routine work. The volumetric CMR data acquisition was performed in breathing arrest.

Volumetric measurements were performed using a clinical 3.0-T whole-body magnetic resonance imaging system (Achieva 3.0T TX; Philips Medical Systems) equipped with parallel radiofrequency signal transmission technology to enhance image uniformity (maximum gradient performance, 80 mT/m; slew rate, 200 T/m/sec) using vector electrocardiography. A 32-element phased-array receive-only surface coil was used for signal detection. To assess the LA volume a stack of 15-21 short-axis or axial view slices was acquired by applying a segmented multislice, multiphase, triggered steady-state free precession gradient-echo sequence (repetition time, 2.7 msec; echo time, 1.35 msec; excitation angle, 40°; slice thickness, 5-6 mm; no slice gap; matrix size, 160 × 240; field of view, 384 mm; in-plane resolution, 1.6 × 1.6 mm; 25 cardiac phases under short breath-holding periods of <12 seconds in duration).

Quantification of the volumetric CMR data was performed offline on a workstation using the threshold-based HDZ MR-Tools software package (HDZ, Bad Oeynhausen, Germany).[27,28] LA volumes were generated from the summation of the cavity areas multiplied by the slice thickness in an algorithm for semiautomatic vessel border detection without geometric models or assumptions. The LA appendage and pulmonary veins were excluded in conformance with the analysis of 3DE data.

Statistical Analysis—Reference Percentiles

For the computation of reference curves, we fitted smooth curves applying the LMS methods of Cole and Green.[29] We used the GAMLSS package in R for the computation.[30] For the model fitting, the GAMLSS function fits a regression model to the data by minimizing the likelihood function. For the LMS method, the regression model is based on the Box-Cox Cole and Green distribution with the parameters L (Box-Cox power), M (median), and S (coefficient of variation). While L is the skewness parameter, S defines the scale parameter and M establishes the location parameter. Penalized splines were used for L, M, and S to create smooth percentile curves. The smoothness of the penalized splines can be configured by their equivalent degree of freedom (e.d.f.). Vmax, Vmin, total EV, and VpreA were chosen as dependent variables. We defined age, body height, and BSA as independent variables. Male and female subjects were considered separately as we saw statistically significant differences between the sexes. For each setting of dependent and independent variable, we applied the LMS method for different settings of e.d.f. for each parameter L, M, and S. We limited the range for e.d.f. from 0 to 5. We compared the resulting different models by the Bayesian information criterion (BIC).[31] The model with the lowest BIC was considered the best model. The BIC served also as selection criterion regarding the independent variable.

Intra- and Interobserver Variability

Intraobserver variability was tested on 147 data sets by reanalysis at least 4 weeks apart and blinded from the first analysis. Interobserver variability was assessed in 48 randomly selected data sets, which were analyzed independently by a different researcher blinded to the other's measurement. Agreement was expressed by Bland-Altman analysis (Graph Pad Prism 6, GraphPad Software, San Diego, CA) as well as by intraclass correlation coefficient (ICC) with 95% CI (two-way mixed-effects model, absolute-agreement; SPSS Statistical Package, version 25, SPSS, Chicago, IL).

RESULTS

We were able to analyze the LA in 432 subjects of all 497 children enrolled in the study (87%). Exclusion of subjects was due to inadequate image quality or trigger artifacts that would have led to unreliable measurements. Another reason was incomplete capture of the LA. Of these 432 subjects, we determined VpreA in 350 (81%) subjects using the criteria mentioned above. Subject characteristics and frame rates are presented in Table 1. We had a fairly uniform distribution between the sexes in every age group. HR did not differ between the sexes in any age groups.

Reference Values for LA Measured by 3DE

Figure 4 shows percentiles for boys and girls for Vmax, Vmin, total EV, and VpreA. BSA was a better predictor of volume compared with height or age.

All volumes increased significantly with increasing BSA. Percentiles show increasing volumes with an increasing heteroskedasticity with

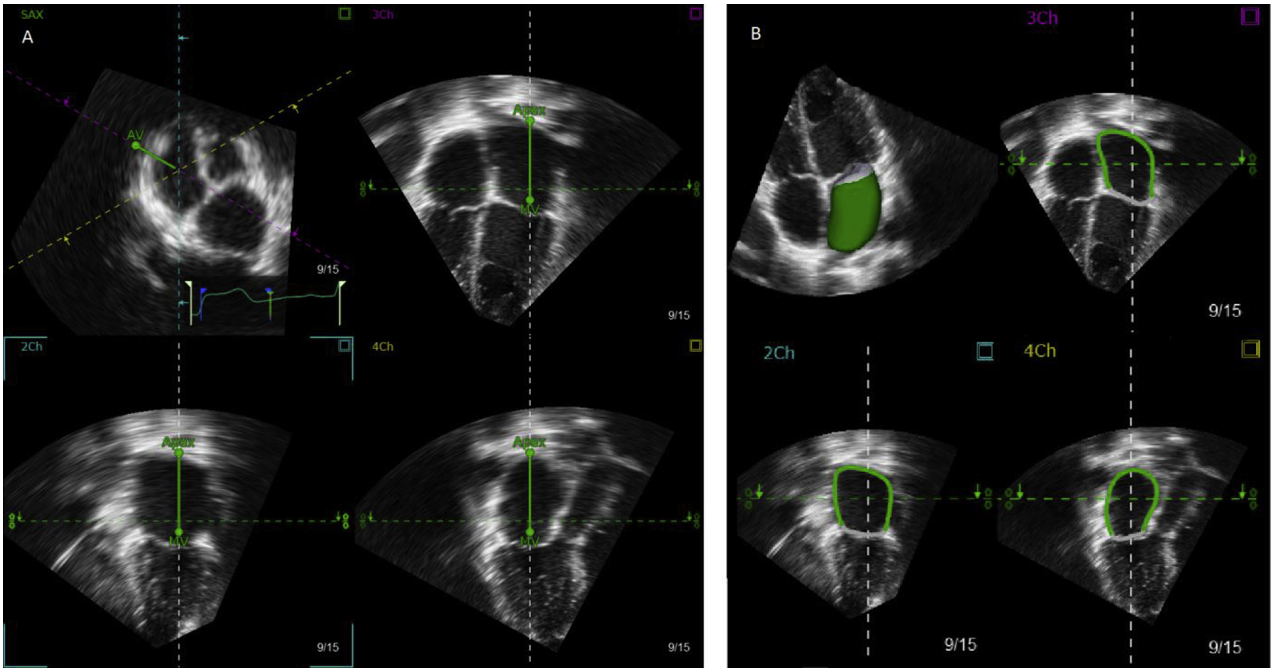

Figure 1 Three-dimensional echocardiography analysis of the LA with TomTec 4D LV-Analysis software 3.1. Panel **(A)** shows the alignment of the LA at the frame of maximal volume. The marker for the mitral valve (MV) was set at the mitral valve. The marker for the apex was set at the roof of the LA, and the 3D data set was rotated 60° counterclockwise. Therefore, the marker for the aortic valve (AV), which was originally set at the aortic valve, is no longer in this position. In this way, the shape of the LA better resembles the respective shape of the LV in the three apical views to allow for better automated border detection and tracing. Panel **(B)** shows the LA with endocardial contouring and the LA cast reconstruction. *2Ch*, Two-chamber; *3Ch*, three-chamber; *4Ch*, four-chamber.

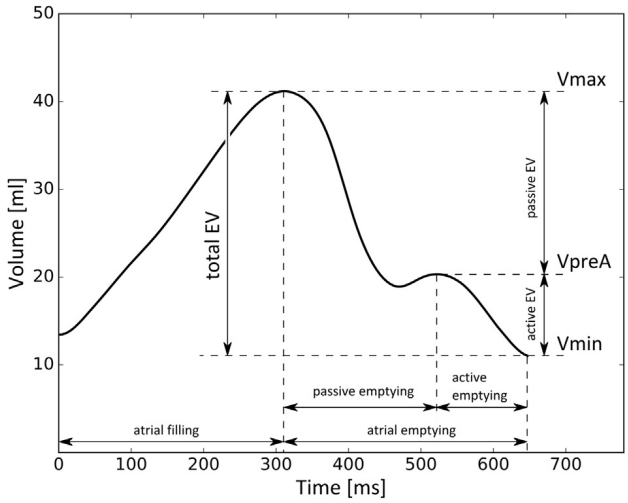

Figure 2 Example of a VTC of the LA showing the different phases and volumes of the cardiac cycle. EV = Vmax − Vmin, total EF = (EV/Vmax) × 100, passive EV = Vmax − VpreA, passive EF = (passive EV/Vmax) × 100, PE percentage = passive EV/EV, active EV = VpreA − Vmin, active EF = (active EV/VpreA) × 100, AE percentage = active EV/EV.

increasing BSA. The female percentiles begin with a more shallow slope than do the male percentiles, resulting in a bit more wavy curve. Female percentiles showed lower volumes when compared with the corresponding male percentile. For example, the Vmax 50th percentile for girls differs >5% from the Vmax 50th percentile for boys.

To calculate *z* scores, Supplemental Table 1 and Equations 1 and 2 (available at www.onlinejase.com) are given in the supplemental materials. For example, they can be used for automated computation of *z*-scores of LA volumes.

Supplemental Tables 2 and 3 (available at www.onlinejase.com) show absolute values, values indexed to BSA, and ejection fractions for all volumes measured grouped by age. Moreover, they show statistical differences between sexes and age groups. These tables can be used as an overview.

Figure 5 shows the linear regressions of the different atrial phases as fractions of the cardiac cycle or fraction of the atrial emptying period with increasing R-R intervals. Moreover, linear regressions of active and passive EF and active and PE percentage with increasing R-R intervals are displayed in Figure 5 as well. Because we did not find significant differences between the sexes, male and female subjects are displayed together. Duration of atrial filling as a fraction of the cardiac cycle decreased with increasing R-R interval. On the other hand, duration of atrial emptying as a fraction of the cardiac cycle increased with increasing R-R interval. Both phases of atrial emptying, AE and PE as fractions of the cardiac cycle, increased. Looking at the duration of AE and PE as a fraction of the atrial emptying period we found that the AE tended to take an increasing part with increasing R-R interval. Active EF and percentage showed a trend toward increasing with increasing R-R interval, while the passive EF and percentage decreased. Durations of atrial emptying and filling grouped by R-R intervals are also given in Supplemental Table 4 (available at www.onlinejase.com).

Intra- and Interobserver Variability

Intraobserver variability was excellent with a small bias of 0.03 mL and narrow limits of agreement [−2.2 to 2.2 mL] for Vmax and −0.14 mL [−1.4 to 1.2 mL] for Vmin, respectively. ICC and 95% CI were 0.998 (0.997-0.999) for Vmax and 0.995 (0.993-0.997) for

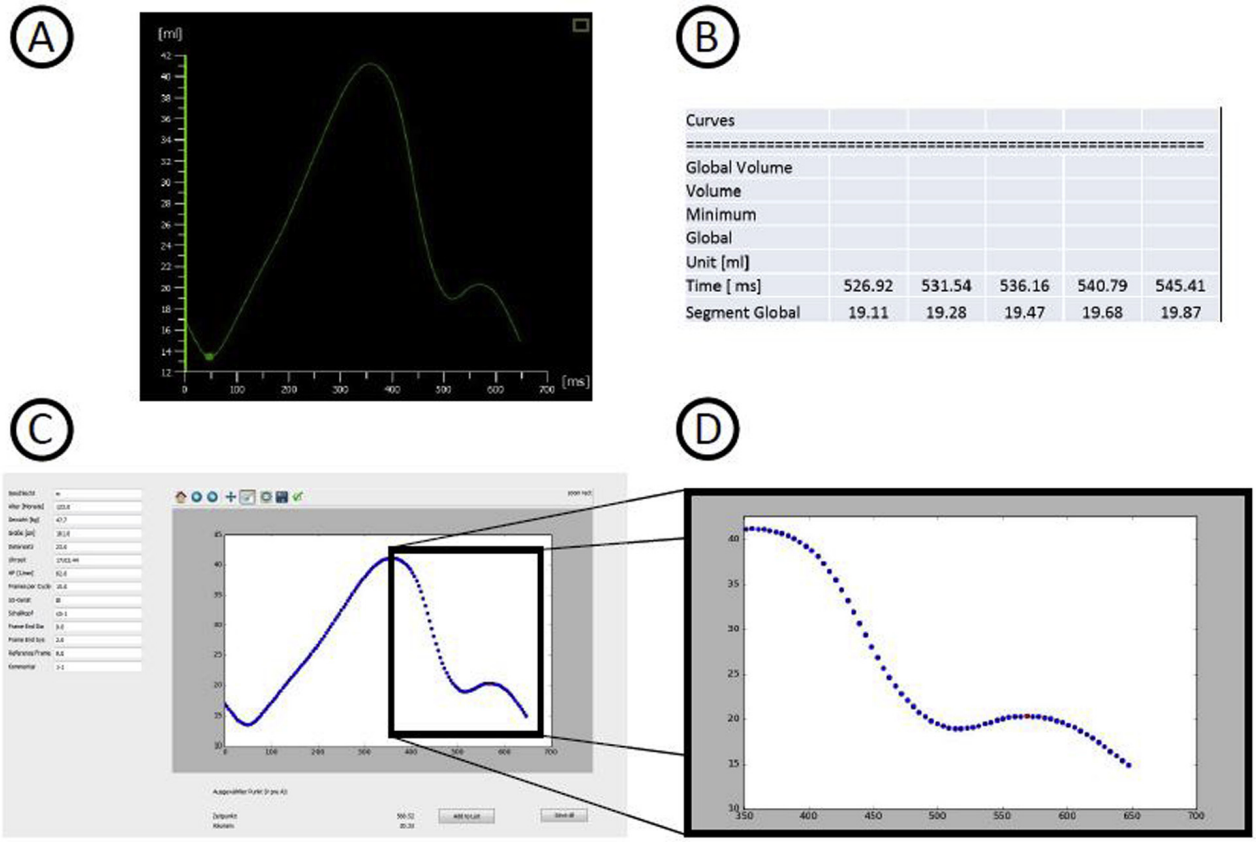

Figure 3 Example of a VTC as displayed by the software TomTec **(A)** and the exported table with the discrete values **(B)**. The tool we designed plots these values **(C)**, and one can zoom into the curve and mark one discrete point with corresponding volume and time **(D)**.

Vmin, indicating excellent reliability. Intraobserver variability was also small for VpreA with a bias of 0.3 mL and limits of agreement of [−2.4 to 3.0 mL] as well as an ICC and 95% CI of 0.992 (0.989-0.995). Interobserver variability was good with slightly wider limits of agreement with Bland-Altman analysis showing 0.9 mL [−5.0 to 6.8 mL] for Vmax, 0.2 mL [−3.7 to 4.1 mL] for Vmin, and 0.8 mL [−3.7 to 5.4 mL] for VpreA (bias and limits of agreement). ICC and 95% CI showed excellent reliability with 0.99 (0.982-0.995) for Vmax, 0.968 (0.943-0.982) for Vmin, and 0.968 (0.935-0.984) for VpreA.

Comparison with CMR

CMR was performed in 26 patients and seven healthy children (12 boys and 21 girls; median age, 14 years; range, 2.2-29 years; median BSA, 1.3 m^2; range, 0.5-2.7 m^2). Bland-Altman analysis showed an underestimation of LA size measured by 3DE compared with CMR. Bias and limits of agreement for Vmax were −14.2 mL (−41.7 to 13.3), and for Vmin −11.5 mL (−31.0 to 8.1; Supplemental Figure 2; available at www.onlinejase.com). ICC and 95% CI were 0.828 (0.181-0.942) for Vmax and 0.795 (0.0-0.934) for Vmin.

DISCUSSION

This study is the first to provide pediatric sex-related reference values of LA phasic volumes and function indices using real-time 3DE. Moreover, for the first time, normal durations of atrial filling and emptying are reported. The results are based on a large cohort of healthy Caucasian children, including a representative sample of children younger than 2 and up to 5 years of age. Availability of these reference values and percentiles for 3DE may play an essential role in the longitudinal as well as cross-sectional evaluation and follow-up of pediatric patients and may enable clinicians to better identify LA dysfunction and disease progression.

Reference Values

We found that volumes for Vmax, Vmin, and VpreA measured by 3DE increased with increasing BSA. Using the same analysis software, Ghelani *et al.*[14] studied 196 subjects ages 4 days to 20 years and presented median and ± 2 *z*-scores for Vmax, Vmin, and EV. It is unknown to the reader whether the study population had a defined ethnicity or was mixed. Our 50th percentiles are similar to their median, also showing increasing heteroskedasticity with increasing BSA. Their median begins with a bit more shallow slope than our male percentiles, which might be related to the fact that they did not differentiate between the sexes due to a smaller study population. They included 10 newborns or small infants, but from then on data for children up to 2.5 years are missing. Hence the median and *z*-scores for these ages and corresponding BSA might not be very precise. They found a decreasing EF with age, which we also saw, although not as distinctly as they did.

The 3DE LA data of Japanese children have been analyzed by Tanaka *et al.*[13] using the vendor-dependent software QLab. Their results for LA volumes are smaller than ours. However, their study population consisted of Asian children and ours of Caucasian children. The EchoNoRMAL Collaboration[32] points out that ethnicity-

Table 1 Subjects' characteristics and 3DE acquisition parameters presented by sex and age groups

	All (N = 432) (M = 227, F = 205)	0-24 mo (n = 55) (M = 24, F = 31)	>2-5 years (n = 82) (M = 46, F = 36)	>5-10 years (n = 130) (M = 60, F = 70)	>10-14 years (n = 95) (M = 53, F = 42)	>14-18 years (n = 70) (M = 44, F = 26)
Age, mo:						
M	106 (0.03; 222)	7.5 (0.03; 24)	43.5 (25; 60)	95.0 (62; 120)	142 (121; 168)	190.5 (169; 222)
F	84 (0.03; 216)	6.0 (0.03; 23)	42.0 (27; 60)	84.0 (62; 119)	144 (121; 168)	189.0 (170; 216)
Overall	95 (0.03; 222)	7.0 (0.03; 24)	43.0 (25; 60)	89.5 (62; 120)	143 (121; 168)	190.5 (169; 222)
Weight, kg:						
M	30.0 (2.4; 93.0)	8.0 (2.4; 12.5)	16.1 (10.2; 46.0)	27.0 (11.5; 40.9)*	43.8 (27.0; 65.2)	67.0 (41.0; 93.0)*
F	23.0 (2.4; 81.6)	8.1 (2.4; 13.0)	15.0 (10.0; 23.5)	22.9 (15.9; 42.3)*	40.8 (26.4; 62.0)	56.0 (45.0; 81.6)*
Overall	27.0 (2.4; 92.0)	8.0 (2.4; 13.0)	15.6 (10.0; 46.0)	24.9 (11.5; 42.3)	42.0 (26.4; 65.2)	63.0 (41.0; 93.0)
Height, cm:						
M	135 (46; 192)	70.5 (46; 92)	100 (86; 119)	129.5 (94; 150.0)*	157.0 (134.5; 180)	177.5 (156; 192)*
F	124 (48; 183)	70.0 (48; 90)	100 (80; 118)	124.0 (96; 147.5)*	151.6 (128.0; 175)	168.0 (158; 183)*
Overall	130 (46; 192)	70.0 (46 92)	100 (80; 119)	126.8 (94; 150.0)	155.0 (128.0; 180)	172.0 (156; 192)
BSA, m^2:						
M	1.07 (0.18; 2.19)	0.40 (0.18; 0.56)	0.67 (0.50; 1.18)	0.98 (0.55; 1.26)*	1.38 (1.01; 1.80)	1.82 (1.34; 2.20)*
F	0.88 (0.18; 2.04)	0.40 (0.18; 0.57)	0.63 (0.48; 0.87)	0.88 (0.66; 1.29)*	1.30 (0.99; 1.72)	1.61 (1.42; 2.04)*
Overall	0.98 (0.18; 2.19)	0.40 (0.18; 0.57)	0.67 (0.48; 1.18)	0.94 (0.55; 1.29)	1.34 (0.99; 1.79)	1.80 (1.34; 2.19)
HR, 1/min:						
M	82 (47; 169)	134 (80; 169)	99 (66; 133)	82 (64; 105)	78 (57; 108)	69 (47; 114)
F	88 (53; 173)	127 (102; 173)	101 (79; 138)	86 (64; 115)	77 (55; 109)	70 (53; 96)
Overall	85 (47; 173)	132 (80; 173)	101 (66; 138)	85 (64; 115)	77 (55; 109)	69 (47; 114)
Frames per cycle:						
M	15 (10; 44)	13 (10; 20)	15 (11; 33)	16 (10; 32)	16 (10; 35)	18 (11; 44)
F	16 (10; 46)	13 (10; 27)	15 (10; 30)	16 (11; 33)	18 (13; 32)	18 (13; 46)
Overall	16 (10; 46)	13 (10; 27)	15 (10; 30)	16 (10; 33)	17 (10; 35)	18 (11; 46)
Frames per second, 1/sec:						
M	24.7 (14.5; 53.0)	28.3 (19.6; 37.6)	25.6 (21.1; 53.1)	23.8 (16.7; 49.1)	22.1 (16.8; 46.8)	20.5 (14.5; 44.5)
F	25.5 (15.3; 62.1)	29.8 (19.2; 62,1)	25.9 (16.8; 52.2)	24.8 (15.9; 52.2)	24.3 (16.0; 43.4)	22.0 (15.3; 42.4)
Overall	25.0 (14.5; 62.1)	29.0 (19.2; 62.0)	25.8 (16.8; 53.1)	24.2 (15.9; 52.2)	23.0 (16.0; 46.8)	20.6 (14.5; 44.5)

F, Female; *M*, male.
Values are presented as medians (range).
*P <.05 for sex differences.

appropriate echocardiographic reference values are indicated for measurements of LA volumes as these values differ even after indexing by BSA or height. Additionally, Buechel *et al.*[33] as well as our working group demonstrated that vendor-dependent and vendor-independent software can have an impact on the resulting data derived from 3DE.[16,32] Therefore, it might be suggested that the same software should be used for longitudinal analysis in the same subjects and for cross-sectional studies.

Phasic function indices for the LA determined by real-time 3DE have not been described for children so far. In adults, Badano *et al.*[11] used customized software designed for the LA by TomTec to assess reference values for LA volumes including phasic function. We can compare our eldest age group (>14-18 years) with their youngest group (18-29 years). Here we found very good agreement with their values indexed to BSA for Vmax, Vmin, VpreA, passive EV, active EV, passive EF, and active EF. They described an increasing active EF and active EV counterbalanced by a decreasing passive EF with increasing age. Poutanen *et al.*[34] were one of the first to describe increasing AE percentage and decreasing PE percentage with increasing BSA in children using the early technique of 3D reconstructive echocardiography with rotational acquisition of planes. Friedberg and Silverman[26] showed a decreasing ventricular systolic fraction of the cardiac cycle with increasing R-R interval in healthy children. Our results for the atrial filling fraction are in line with this observation, so with this study, we can confirm these observations and give the first pediatric reference values for these phasic function volumes as well as absolute durations for atrial and emptying phases.

Clinical Implications

LA volumes are of interest and may contribute to the detection of increased LV volume load (e.g., ventricular septal defect or patent ductus arteriosus) or elevated LV filling pressures (e.g., cardiomyopathy). Here studies showed enlarged LA volume indexed to BSA.[7,8]

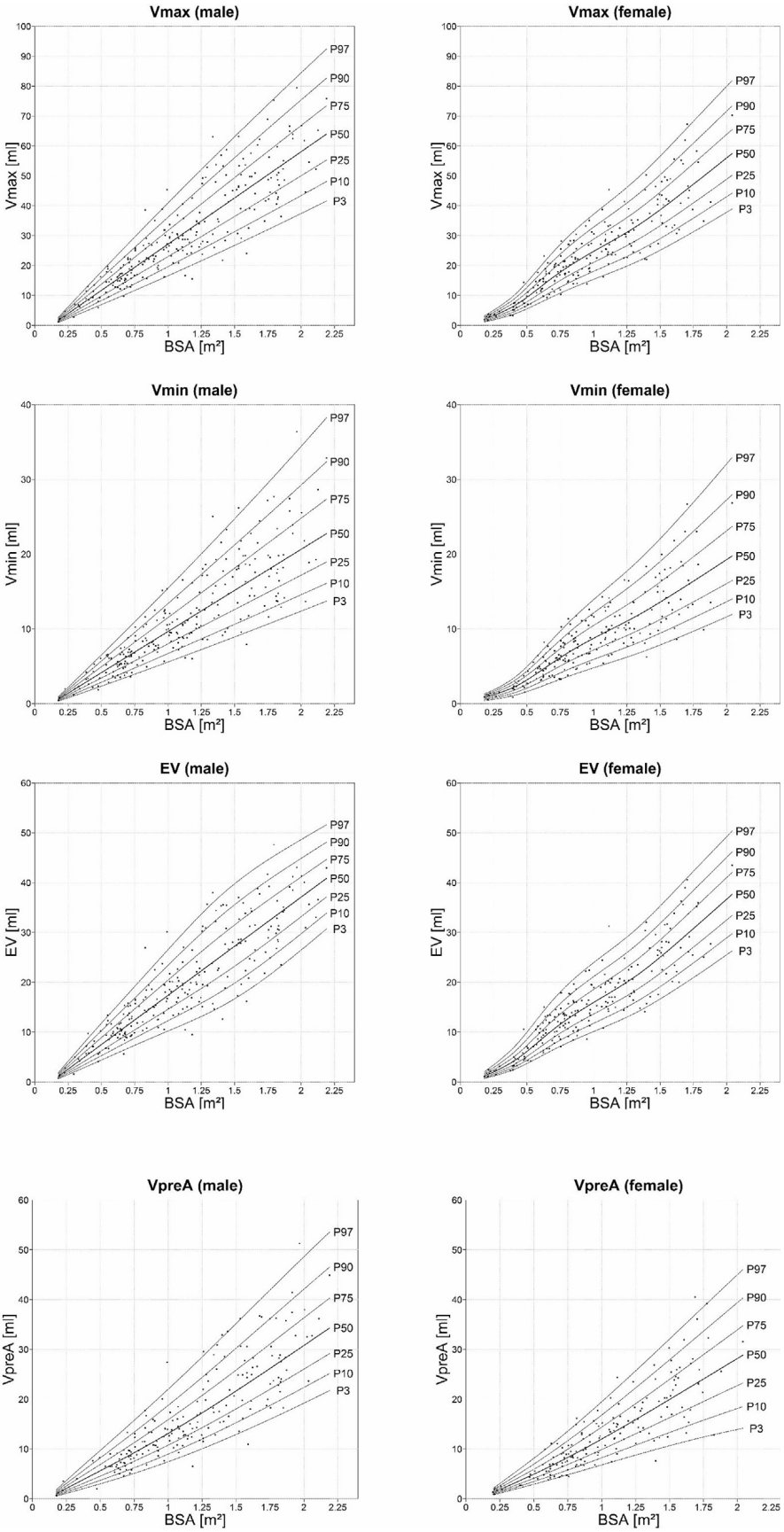

Figure 4 Sex-related percentiles for Vmax, Vmin, EV, and VpreA. P indicates the percentile value, e.g., P50 = 50th percentile value.

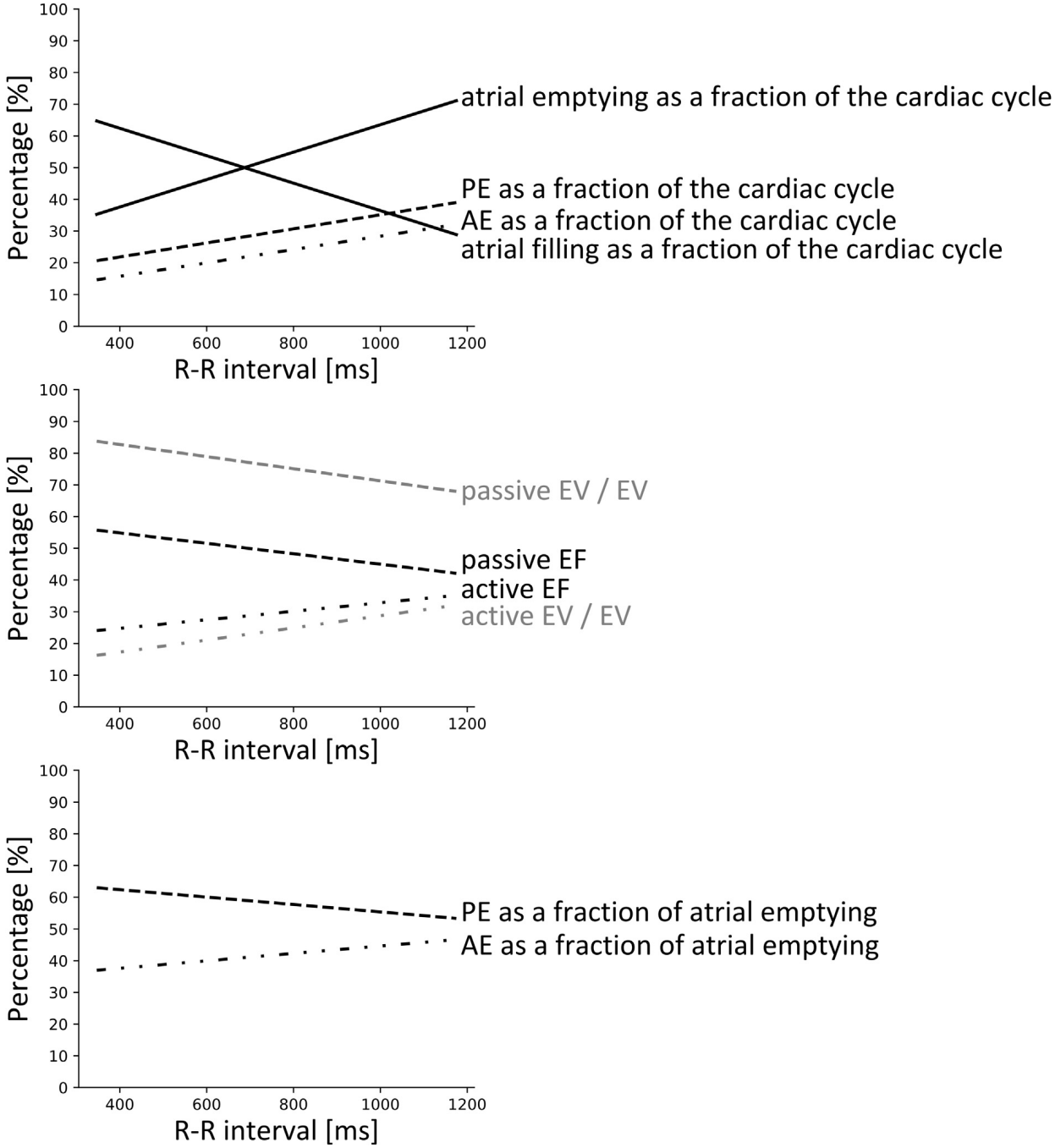

Figure 5 Relationships between the different atrial phases as fractions of the cardiac cycle or fractions of the atrial emptying period and R-R intervals modeled by linear regression. passive EF = (passive EV/Vmax) × 100, PE percentage = passive EV/EV, active EF = (active EV/VpreA) × 100, AE percentage = active EV/EV.

Moreover, in children with hypertrophic cardiomyopathy, LA volume has been reported to have significant diagnostic and prognostic value as a marker of elevated LV end-diastolic pressure and diastolic dysfunction.[9]

Badano *et al.*[11] found that underestimation of LA volumes with 2DE compared with 3DE increased with larger LA. So especially in conditions of disease with enlarged and probably deformed LA, 3DE can serve as a method without geometric assumption and less underestimation as in 2DE compared with CMR.[11]

Due to the interaction of the LA and LV, absolute and fractional durations of the phases of the LA are of interest. Friedberg and Silverman[26] showed that in children with heart failure secondary to idiopathic dilated cardiomyopathy, ventricular systole was prolonged at the expense of ventricular diastole. Ventricular diastole corresponds to the atrial emptying. Therefore, one might expect changes in the durations of atrial phases in sick children. Our results show that the active EF that augments late LV filling especially seems to get more important with increasing R-R intervals (Figure 5). One reason might be that the increasing LA contractile function reflects greater LA volumes at the onset of LA contraction (Starling effect). Moreover, this atrial phase is determined by LV compliance, so changes in the LV compliance might be reflected in duration and volumes of this atrial phase.

Further studies are planned to compare LA volumes and phasic function determined by 3DE in children with heart diseases, such as cardiomyopathy or mitral valve disease, with these reference values.

Comparison with CMR

To cover a larger range of LA shapes and sizes, representing the clinical routine, we included patients with congenital heart diseases. Some of them had enlarged LA due to their disease. In accordance with other studies, we found an underestimation of LA volumes measured by 3DE in comparison with CMR. The average discrepancy of −14.2 mL is somewhat higher than, for example, in the study of Badano *et al.*[11] but in a clinically realistic order. It shows that volumes measured by the two techniques cannot be used interchangeably without care. The rather wide limits of agreement and 95% CI underline this. However, they are similar to the ones of Badano *et al.* and are also owing to the fact that underestimation of volumes increased with increasing LA size. By including patients in this comparison, we could see that LAs rated as enlarged by CMR[35] were also rated as enlarged when measured by 3DE and compared with our reference values.

The 3DE and CMR were obtained within 1 day, but not simultaneously. Therefore, and due to breath holding or sympathetic stimulation due to stress under CMR examination, HR and volume status may vary and account for some differences between both methods. In echocardiography, spatial resolution, especially lateral resolution, decreases with increasing depth, while resolution stays constant in every region in CMR. Different approaches of analysis, border detection, and summation of discs may have contributed to differences between the methods.

Limitations

We used vendor-independent commercial software designed for LV analysis to measure the LA. Although we tried to account for this by rotation of the views as described above, this might have led to slight deviations. On the other hand, we could show that our results in the oldest age group (>14-18 years) are consistent with Badano *et al.*, who used a customized LA-specific software from the same vendor. Many echocardiography laboratories working with 3DE might not possess LA-specific software but the more common LV tool. This work enables them to use this tool for measurement of the LA. A general limitation of echocardiography is the temporal resolution and spatial lateral resolution in the depth. The temporal resolution especially can be a limitation when determining time-specific events like VpreA. Moreover, as explained in the methods section, different approaches have been used. Moreover, LA-specific software automatically calculates VpreA without further explanation of the underlying algorithmus.[11] The work of Mada *et al.*[36] describes very honestly the problems of defining time points within the cardiac cycle in echocardiography. Often the automatic approaches are not disclosed to the user. Also, electrocardiogram signals can differ in the different leads. Therefore, different approaches to define VpreA, including an automated approach by the software, might lead to slightly different values for VpreA and other phasic function indices. We decided to only include VpreA when p-wave, frame before mitral valve reopening, and shape of the curve, or at least the latter two, were matching. This had the result that determination of VpreA and phasic function was only possible in 81% of our subjects. Especially in the group of children <2 years old, an exact determination of the temporal definition of VpreA was not possible in all cases, so the data for this age-group might be less robust.

CONCLUSION

This study provides pediatric sex-specific reference values and percentiles for LA 3DE volumes and phasic function from the largest cohort of healthy subjects to date. These data can be the basis for evaluation of the LA by 3DE and can contribute to a better longitudinal as well as horizontal follow-up of pediatric patients with congenital heart diseases, such as cardiomyopathy, left-to-right shunts, or mitral valve disease. Further studies are planned to compare LA volumes and phasic function determined by 3DE in children with heart diseases to these reference values.

ACKNOWLEDGMENTS

The authors thank Ute Baur (study nurse) for her support and Andrea Kelter-Kloepping (medical technical assistant) for CMR analysis.

SUPPLEMENTARY DATA

Supplementary data to this article can be found online at https://doi.org/10.1016/j.echo.2019.03.018.

REFERENCES

1. Hatipoglu S, Ozdemir N, Babur Guler G, Omaygenc MO, Bakal RB, Kahveci G, et al. Left atrial expansion index is an independent predictor of diastolic dysfunction in patients with preserved left ventricular systolic function: a three dimensional echocardiography study. Int J Cardiovasc Imaging 2014;30:1315-23.
2. Boyd AC, Thomas L. Left atrial volumes. Curr Opin Cardiol 2014;29:408-16.
3. Leung DY, Boyd A, Ng A, Chi C, Thomas L. Echocardiographic evaluation of left atrial size and function: Current understanding, pathophysiologic correlates, and prognostic implications. Am Heart J 2008;156:1056-64.
4. Murata M, Iwanaga S, Tamura Y, Kondo M, Kouyama K, Murata M, et al. A real-time three-dimensional echocardiographic quantitative analysis of left atrial function in left ventricular diastolic dysfunction. Am J Cardiol 2008;102:1097-102.
5. To ACY, Flamm SD, Marwick TH, Klein AL. Clinical utility of multimodality LA imaging: assessment of size, function, and structure. JACC Cardiovasc Imaging 2011;4:788-98.
6. Caselli S, Canali E, Foschi ML, Santini D, Di Angelantonio E, Pandian NG, et al. Long-term prognostic significance of three-dimensional echocardiographic parameters of the left ventricle and left atrium. Eur J Echocardiogr 2010;11:250-6.
7. Taggart NW, Cetta F, O'Leary PW, Seward JB, Eidem BW. Left atrial volume in children without heart disease and in those with ventricular septal defect or patent ductus arteriosus or hypertrophic cardiomyopathy. Am J Cardiol 2010;106:1500-4.
8. Sakata M, Hayabuchi Y, Inoue M, Onishi T, Kagami S. Left atrial volume change throughout the cardiac cycle in children with congenital heart disease associated with increased pulmonary blood flow: evaluation using a novel left atrium-tracking method. Pediatr Cardiol 2013;34:105-11.

9. Menon SC, Ackerman MJ, Cetta F, O'Leary PW, Eidem BW. Significance of left atrial volume in patients < 20 years of age with hypertrophic cardiomyopathy. Am J Cardiol 2008;102:1390-3.
10. Lang RM, Badano LP, Mor-Avi V, Afilalo J, Armstrong A, Ernande L, et al. Recommendations for cardiac chamber quantification by echocardiography in adults: an update from the American Society of echocardiography and the European Association of Cardiovascular Imaging. J Am Soc Echocardiogr 2015;28:1-39.e14.
11. Badano LP, Miglioranza MH, Mihăilă S, Peluso D, Xhaxho J, Marra MP, et al. Left atrial volumes and function by three-dimensional echocardiography: reference values, accuracy, reproducibility, and comparison with two-dimensional echocardiographic measurements. Circ Cardiovasc Imaging 2016;9:e004229.
12. Mor-Avi V, Yodwut C, Jenkins C, Khl H, Nesser HJ, Marwick TH, et al. Real-time 3D echocardiographic quantification of left atrial volume: multicenter study for validation with CMR. JACC Cardiovasc Imaging 2012;5:769-77.
13. Tanaka N, Takigiku K, Takahashi K, Kuraoka A, Matsui K, Iwashima S, et al. Assessment of the developmental change in the left atrial volume using real time three-dimensional echocardiography. Echocardiography 2015;32:1131-9.
14. Ghelani SJ, Brown DW, Kuebler JD, Perrin D, Shakti D, Williams DN, et al. Left atrial volumes and strain in healthy children measured by three-dimensional echocardiography: normal values and maturational changes. J Am Soc Echocardiogr 2018;31:187-93.e1.
15. Lopez L, Colan SD, Frommelt PC, Ensing GJ, Kendall K, Younoszai AK, et al. Recommendations for quantification methods during the performance of a pediatric echocardiogram: a report from the Pediatric Measurements Writing Group of the American Society of Echocardiography Pediatric and Congenital Heart Disease Council. J Am Soc Echocardiogr 2010;23:465-95. quiz 576-77.
16. Krell K, Laser KT, Dalla-Pozza R, Winkler C, Hildebrandt U, Kececioglu D, et al. Real-time three-dimensional echocardiography of the left ventricle—pediatric percentiles and head-to-head comparison of different contour-finding algorithms: a multicenter study. J Am Soc Echocardiogr 2018;31:702-11.e13.
17. Laser KT, Karabiyik A, Körperich H, Horst J-P, Barth P, Kececioglu D, et al. Validation and reference values for three-dimensional echocardiographic right ventricular volumetry in children: a multicenter study. J Am Soc Echocardiogr 2018;31:1050-63.
18. Lang RM, Badano LP, Tsang W, Adams DH, Agricola E, Buck T, et al. EAE/ASE recommendations for image acquisition and display using three-dimensional echocardiography. J Am Soc Echocardiogr 2012;25:3-46.
19. Anwar AM, Soliman OII, Geleijnse ML, Nemes A, Vletter WB, ten Cate FJ. Assessment of left atrial volume and function by real-time three-dimensional echocardiography. Int J Cardiol 2008;123:155-61.
20. Aggeli C, Felekos I, Poulidakis E, Aggelis A, Tousoulis D, Stefanadis C. Quantitative analysis of left atrial function in asymptomatic patients with b-thalassemia major using real-time three-dimensional echocardiography. Cardiovasc Ultrasound 2011;9:38.
21. Buechel RR, Sommer G, Leibundgut G, Rohner A, Riede F, Kessel-Schaefer A, et al. Assessment of left atrial functional parameters using a novel dedicated analysis tool for real-time three-dimensional echocardiography: validation in comparison to magnetic resonance imaging. Int J Cardiovasc Imaging 2013;29:601-8.
22. Peluso D, Badano LP, Muraru D, Dal Bianco L, Cucchini U, Kocabay G, et al. Right atrial size and function assessed with three-dimensional and speckle-tracking echocardiography in 200 healthy volunteers. Eur Hear J Cardiovasc Imaging 2013;14:1106-14.
23. Shin M-S, Fukuda S, Song J-M, Tran H, Oryszak S, Thomas JD, et al. Relationship between left atrial and left ventricular function in hypertrophic cardiomyopathy: a real-time 3-dimensional echocardiographic study. J Am Soc Echocardiogr 2006;19:796-801.
24. Blume GG, McLeod CJ, Barnes ME, Seward JB, Pellikka PA, Bastiansen PM, et al. Left atrial function: Physiology, assessment, and clinical implications. Eur J Echocardiogr 2011;12:421-30.
25. Sarnari R, Kamal RY, Friedberg MK, Silverman NH. Doppler assessment of the ratio of the systolic to diastolic duration in normal children: Relation to heart rate, age and body surface area. J Am Soc Echocardiogr 2009;22:928-32.
26. Friedberg MK, Silverman NH. Cardiac ventricular diastolic and systolic duration in children with heart failure secondary to idiopathic dilated cardiomyopathy. Am J Cardiol 2006;97:101-5.
27. Laser KT, Barth P, Bunge M, Dachner G, Esdorn H, Fischer M, et al. Model versus non-model based left ventricular volumetry: a matter of imaging modality or quantification software? J Biomed Graph Comput 2013;3.
28. Laser KT, Bunge M, Hauffe P, Argueta JRP, Kelter-Klopping A, Barth P, et al. Left ventricular volumetry in healthy children and adolescents: Comparison of two different real-time three-dimensional matrix transducers with cardiovascular magnetic resonance. Eur J Echocardiogr 2010;11:138-48.
29. Cole TJ, Green PJ. Smoothing reference centile curves: the LMS method and penalized likelihood. Stat Med 1992;11:1305-19.
30. Rigby RA, Stasinopoulos DM. Generalized additive models for location, scale and shape (with discussion). J R Stat Soc Ser C (Applied Statistics) 2005;54:507-54.
31. Kobayashi T, Fuse S, Sakamoto N, Mikami M, Ogawa S, Hamaoka K, et al. A new Z score curve of the coronary arterial internal diameter using the lambda-mu-sigma method in a pediatric population. J Am Soc Echocardiogr 2016;29:794-801.e29.
32. Poppe KK, Doughty RN, Gardin JM, Nagueh SF, Whalley GA, Cameron V, et al. Ethnic-specific normative reference values for echocardiographic LA and LV size, LV mass, and systolic function: the EchoNoRMAL study. JACC Cardiovasc Imaging 2015;8:656-65.
33. Buechel RR, Stephan FP, Sommer G, Bremerich J, Zellweger MJ, Kaufmann BA. Head-to-head comparison of two-dimensional and three-dimensional echocardiographic methods for left atrial chamber quantification with magnetic resonance imaging. J Am Soc Echocardiogr 2013;26:428-35.
34. Poutanen T, Jokinen E, Sairanen H, Tikanoja T. Left atrial and left ventricular function in healthy children and young adults assessed by three dimensional echocardiography. Heart 2003;89:544-9.
35. Sarikouch S, Koerperich H, Boethig D, Peters B, Lotz J, Gutberlet M, et al. Reference values for atrial size and function in children and young adults by cardiac MR: a study of the German competence network congenital heart defects. J Magn Reson Imaging 2011;33:1028-39.
36. Mada RO, Lysyansky P, Daraban AM, Duchenne J, Voigt J-U. How to define end-diastole and end-systole? Impact of timing on strain measurements. JACC Cardiovasc Imaging 2015;8:148-57.

APPENDIX

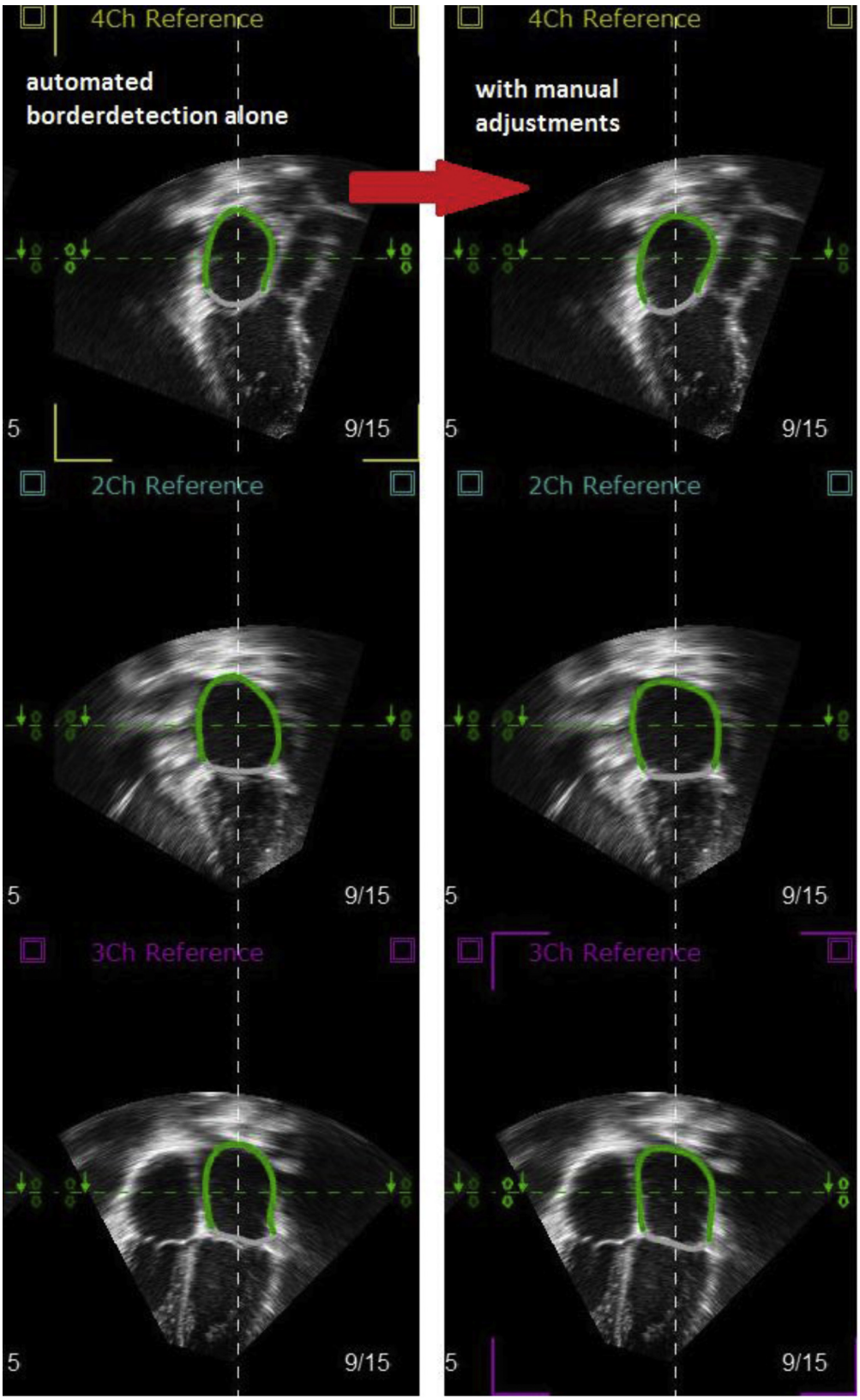

Supplemental Figure 1 Example of manual adjustment to the contours traced by the automated border detection. The left side shows how the automated border detection traced the contours of the LA in the three apical views. The right side shows the contours after manual adjustment. *2Ch*, Two-chamber; *3Ch*, three-chamber; *4Ch*, four-chamber.

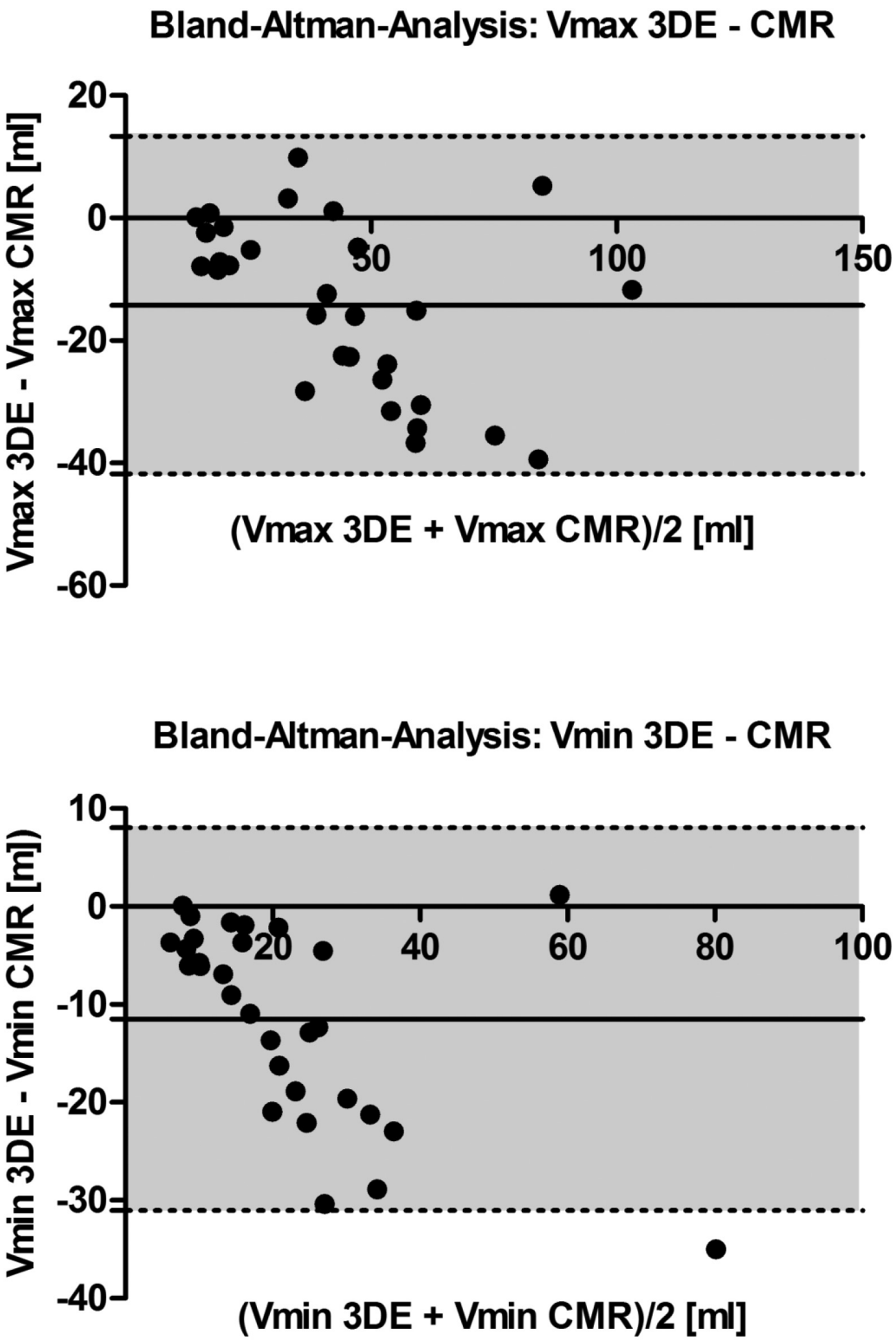

Supplemental Figure 2 Comparison of Vmax and Vmin volumes assessed by 3DE and CMR using Bland-Altman analysis.

Supplemental Table 1 L, M, and S Values according to BSA for Calculation of *z*-Scores

Vmax male			
M	S	L	BSA
2.41	0.26	0.43	0.20
3.96	0.26	0.43	0.25
5.51	0.26	0.43	0.30
7.05	0.25	0.43	0.35
8.60	0.25	0.43	0.40
10.14	0.25	0.43	0.45
11.69	0.25	0.42	0.50
13.24	0.25	0.42	0.55
14.78	0.25	0.42	0.60
16.33	0.25	0.42	0.65
17.88	0.25	0.42	0.70
19.42	0.24	0.42	0.75
20.97	0.24	0.42	0.80
22.51	0.24	0.42	0.85
24.06	0.24	0.42	0.90
25.61	0.24	0.42	0.95
27.15	0.24	0.41	1.00
28.70	0.24	0.41	1.05
30.25	0.24	0.41	1.10
31.79	0.23	0.41	1.15
33.34	0.23	0.41	1.20
34.88	0.23	0.41	1.25
36.43	0.23	0.41	1.30
37.98	0.23	0.41	1.35
39.52	0.23	0.41	1.40
41.07	0.23	0.41	1.45
42.62	0.23	0.40	1.50
44.16	0.22	0.40	1.55
45.71	0.22	0.40	1.60
47.25	0.22	0.40	1.65
48.80	0.22	0.40	1.70
50.35	0.22	0.40	1.75
51.89	0.22	0.40	1.80
53.44	0.22	0.40	1.85
54.98	0.22	0.40	1.90
56.53	0.22	0.40	1.95
58.08	0.21	0.39	2.00
59.62	0.21	0.39	2.05
61.17	0.21	0.39	2.10
62.72	0.21	0.39	2.15
64.26	0.21	0.39	2.20

Vmax female			
M	S	L	BSA
2.36	0.26	0.45	0.20
3.22	0.26	0.44	0.25
4.14	0.26	0.43	0.30

(*Continued*)

Supplemental Table 1 (*Continued*)

Vmax female			
M	S	L	BSA
5.17	0.26	0.43	0.35
6.38	0.26	0.42	0.40
7.78	0.25	0.41	0.45
9.35	0.25	0.41	0.50
11.04	0.25	0.40	0.55
12.77	0.25	0.40	0.60
14.49	0.25	0.39	0.65
16.16	0.24	0.38	0.70
17.76	0.24	0.38	0.75
19.28	0.24	0.37	0.80
20.72	0.24	0.37	0.85
22.10	0.24	0.36	0.90
23.43	0.23	0.36	0.95
24.72	0.23	0.35	1.00
25.98	0.23	0.35	1.05
27.23	0.23	0.34	1.10
28.49	0.23	0.34	1.15
29.77	0.23	0.33	1.20
31.09	0.22	0.33	1.25
32.47	0.22	0.32	1.30
33.92	0.22	0.32	1.35
35.43	0.22	0.31	1.40
37.01	0.22	0.31	1.45
38.64	0.21	0.30	1.50
40.30	0.21	0.30	1.55
42.00	0.21	0.29	1.60
43.72	0.21	0.29	1.65
45.45	0.21	0.28	1.70
47.18	0.21	0.28	1.75
48.93	0.20	0.28	1.80
50.68	0.20	0.27	1.85
52.44	0.20	0.27	1.90
54.21	0.20	0.26	1.95
55.98	0.20	0.26	2.00

Vmin male			
M	S	L	BSA
0.84	0.27	0.55	0.20
1.39	0.27	0.53	0.25
1.94	0.27	0.52	0.30
2.49	0.27	0.50	0.35
3.04	0.27	0.49	0.40
3.60	0.27	0.47	0.45
4.15	0.27	0.46	0.50
4.70	0.27	0.44	0.55
5.25	0.27	0.43	0.60
5.80	0.27	0.41	0.65
6.35	0.27	0.40	0.70

(*Continued*)

Supplemental Table 1 (*Continued*)

Vmin male

M	S	L	BSA
6.90	0.27	0.38	0.75
7.45	0.27	0.37	0.80
8.00	0.27	0.35	0.85
8.55	0.27	0.34	0.90
9.10	0.27	0.32	0.95
9.65	0.27	0.30	1.00
10.20	0.27	0.29	1.05
10.75	0.27	0.27	1.10
11.30	0.27	0.26	1.15
11.85	0.27	0.24	1.20
12.40	0.27	0.23	1.25
12.95	0.27	0.21	1.30
13.50	0.27	0.20	1.35
14.05	0.27	0.18	1.40
14.60	0.27	0.17	1.45
15.15	0.27	0.15	1.50
15.70	0.27	0.14	1.55
16.25	0.27	0.12	1.60
16.80	0.27	0.11	1.65
17.35	0.27	0.09	1.70
17.90	0.27	0.08	1.75
18.45	0.27	0.06	1.80
19.00	0.27	0.05	1.85
19.55	0.27	0.03	1.90
20.10	0.27	0.02	1.95
20.65	0.27	0.00	2.00
21.20	0.27	-0.01	2.05
21.75	0.27	-0.03	2.10
22.30	0.27	-0.04	2.15
22.85	0.27	-0.06	2.20

Vmin female

M	S	L	BSA
0.94	0.28	0.92	0.20
1.19	0.28	0.89	0.25
1.47	0.28	0.86	0.30
1.79	0.28	0.84	0.35
2.18	0.28	0.81	0.40
2.64	0.28	0.78	0.45
3.17	0.28	0.75	0.50
3.74	0.28	0.73	0.55
4.35	0.28	0.70	0.60
4.96	0.28	0.67	0.65
5.56	0.28	0.65	0.70
6.15	0.28	0.62	0.75
6.71	0.28	0.59	0.80
7.25	0.28	0.57	0.85
7.77	0.28	0.54	0.90

(*Continued*)

Supplemental Table 1 (*Continued*)

Vmin female

M	S	L	BSA
8.26	0.28	0.51	0.95
8.74	0.28	0.49	1.00
9.20	0.28	0.46	1.05
9.65	0.28	0.44	1.10
10.11	0.28	0.41	1.15
10.56	0.28	0.39	1.20
11.02	0.28	0.36	1.25
11.50	0.27	0.34	1.30
12.00	0.27	0.31	1.35
12.51	0.27	0.29	1.40
13.04	0.27	0.26	1.45
13.58	0.27	0.24	1.50
14.13	0.27	0.21	1.55
14.69	0.27	0.19	1.60
15.25	0.27	0.16	1.65
15.81	0.27	0.14	1.70
16.38	0.27	0.11	1.75
16.95	0.27	0.09	1.80
17.52	0.27	0.06	1.85
18.10	0.27	0.04	1.90
18.68	0.27	0.01	1.95
19.26	0.27	-0.01	2.00

EV male

M	S	L	BSA
1.59	0.28	0.27	0.20
2.57	0.27	0.29	0.25
3.56	0.27	0.30	0.30
4.55	0.27	0.31	0.35
5.53	0.26	0.32	0.40
6.52	0.26	0.34	0.45
7.50	0.26	0.35	0.50
8.49	0.26	0.36	0.55
9.48	0.25	0.37	0.60
10.46	0.25	0.39	0.65
11.45	0.25	0.40	0.70
12.44	0.25	0.41	0.75
13.42	0.25	0.42	0.80
14.41	0.25	0.44	0.85
15.40	0.25	0.45	0.90
16.38	0.25	0.46	0.95
17.37	0.25	0.47	1.00
18.35	0.25	0.49	1.05
19.34	0.25	0.50	1.10
20.33	0.25	0.51	1.15
21.31	0.25	0.52	1.20
22.30	0.25	0.54	1.25
23.29	0.24	0.55	1.30

(*Continued*)

Supplemental Table 1 (*Continued*)

EV male

M	S	L	BSA
24.27	0.24	0.56	1.35
25.26	0.24	0.57	1.40
26.25	0.23	0.59	1.45
27.23	0.23	0.60	1.50
28.22	0.22	0.61	1.55
29.20	0.21	0.62	1.60
30.19	0.21	0.64	1.65
31.18	0.20	0.65	1.70
32.16	0.19	0.66	1.75
33.15	0.19	0.67	1.80
34.14	0.18	0.69	1.85
35.12	0.17	0.70	1.90
36.11	0.17	0.71	1.95
37.10	0.16	0.72	2.00
38.08	0.15	0.73	2.05
39.07	0.15	0.75	2.10
40.05	0.14	0.76	2.15
41.04	0.14	0.77	2.20

EV female

M	S	L	BSA
1.40	0.29	-0.03	0.20
2.00	0.28	-0.01	0.25
2.63	0.28	0.01	0.30
3.34	0.28	0.02	0.35
4.15	0.27	0.04	0.40
5.09	0.27	0.06	0.45
6.13	0.26	0.08	0.50
7.23	0.26	0.10	0.55
8.36	0.26	0.12	0.60
9.48	0.25	0.14	0.65
10.55	0.25	0.16	0.70
11.56	0.25	0.17	0.75
12.52	0.24	0.19	0.80
13.43	0.24	0.21	0.85
14.29	0.23	0.23	0.90
15.12	0.23	0.25	0.95
15.94	0.23	0.27	1.00
16.74	0.22	0.29	1.05
17.53	0.22	0.31	1.10
18.33	0.22	0.32	1.15
19.15	0.22	0.34	1.20
20.01	0.21	0.36	1.25
20.91	0.21	0.38	1.30
21.87	0.21	0.40	1.35
22.88	0.20	0.42	1.40
23.93	0.20	0.44	1.45
25.02	0.20	0.46	1.50

(*Continued*)

Supplemental Table 1 (*Continued*)

EV female

M	S	L	BSA
26.14	0.20	0.47	1.55
27.28	0.19	0.49	1.60
28.44	0.19	0.51	1.65
29.60	0.19	0.53	1.70
30.77	0.18	0.55	1.75
31.94	0.18	0.57	1.80
33.11	0.18	0.59	1.85
34.29	0.18	0.61	1.90
35.48	0.17	0.62	1.95
36.66	0.17	0.64	2.00

VpreA male

M	S	L	BSA
1.37	0.32	0.26	0.20
2.08	0.32	0.25	0.25
2.79	0.32	0.25	0.30
3.50	0.32	0.24	0.35
4.21	0.31	0.24	0.40
4.91	0.31	0.23	0.45
5.62	0.31	0.23	0.50
6.33	0.31	0.22	0.55
7.05	0.31	0.21	0.60
7.78	0.30	0.21	0.65
8.51	0.30	0.20	0.70
9.26	0.30	0.20	0.75
10.02	0.30	0.19	0.80
10.78	0.29	0.19	0.85
11.55	0.29	0.18	0.90
12.34	0.29	0.18	0.95
13.13	0.29	0.17	1.00
13.93	0.29	0.17	1.05
14.74	0.28	0.16	1.10
15.57	0.28	0.16	1.15
16.41	0.28	0.15	1.20
17.26	0.28	0.15	1.25
18.12	0.27	0.14	1.30
18.98	0.27	0.14	1.35
19.86	0.27	0.13	1.40
20.75	0.27	0.13	1.45
21.64	0.27	0.12	1.50
22.54	0.26	0.12	1.55
23.44	0.26	0.11	1.60
24.35	0.26	0.11	1.65
25.26	0.26	0.10	1.70
26.17	0.26	0.10	1.75
27.09	0.25	0.09	1.80
28.01	0.25	0.09	1.85
28.94	0.25	0.08	1.90

(*Continued*)

Supplemental Table 1 (*Continued*)

VpreA male			
M	**S**	**L**	**BSA**
29.86	0.25	0.08	1.95
30.79	0.25	0.07	2.00
31.72	0.24	0.07	2.05
32.64	0.24	0.06	2.10
33.57	0.24	0.06	2.15
34.50	0.24	0.05	2.20
VpreA female			
M	**S**	**L**	**BSA**
1.22	0.27	-0.02	0.20
1.85	0.27	0.00	0.25
2.48	0.27	0.02	0.30
3.11	0.27	0.04	0.35
3.75	0.27	0.06	0.40
4.39	0.27	0.08	0.45
5.04	0.27	0.10	0.50
5.69	0.27	0.12	0.55
6.36	0.27	0.14	0.60
7.03	0.27	0.16	0.65
7.72	0.27	0.18	0.70
8.41	0.27	0.20	0.75
9.11	0.28	0.22	0.80
9.82	0.28	0.24	0.85
10.54	0.28	0.26	0.90
11.27	0.28	0.28	0.95
12.01	0.28	0.30	1.00
12.75	0.28	0.32	1.05
13.49	0.28	0.34	1.10
14.25	0.28	0.36	1.15
15.00	0.28	0.38	1.20
15.76	0.28	0.40	1.25
16.53	0.28	0.42	1.30
17.30	0.28	0.44	1.35
18.07	0.28	0.46	1.40
18.84	0.28	0.48	1.45
19.61	0.29	0.50	1.50
20.39	0.29	0.52	1.55
21.17	0.29	0.54	1.60
21.95	0.29	0.56	1.65
22.73	0.29	0.58	1.70
23.50	0.29	0.60	1.75
24.28	0.29	0.62	1.80
25.06	0.29	0.64	1.85
25.84	0.29	0.66	1.90
26.62	0.29	0.69	1.95
27.40	0.29	0.71	2.00

Equations 1 and 2 can be used to calculate *z*-scores.

$$z = \frac{\left[\frac{y}{M(t)}\right]^{L(t)} - 1}{L(t)\,S(t)}, \quad L(t) \neq 0 \tag{1}$$

$$z = \frac{log\left[\frac{y}{M(t)}\right]}{S(t)}, \quad L(t) = 0 \tag{2}$$

M (t), *L (t)*, and *S (t)* are the parameters M, L, and S at the independent variable *t* (in this case BSA); *y* is the dependent variable (in this case the measured volume, e.g., Vmax).

Supplemental Table 2 Reference ranges of LA volumes by 3DE presented by sex and age groups

	0-24 mo (*n* = 55) (M = 24, F = 31)	>2-5 years (*n* = 82) (M = 46, F = 36)	>5-10 years (*n* = 130) (M = 60, F = 70)	>10-14 years (*n* = 95) (M = 53, F = 42)	>14-18 years (*n* = 70) (M = 44, F = 26)	*P* value
Vmax, mL:						
M	8.7 (5.1; 12.7)*	16.2 (14.3; 19.3)	25.9 (21.6; 29.1)*	37.4 (30.2; 48.6)*	51.7 (44.5; 62.1)*	<.0001
F	5.2 (3.3; 7.3)*	15.1 (12.2; 18.0)	22.2 (18.0; 27.4)*	31.2 (26.5; 40.6)*	42.1 (36.3; 50.8)*	<.0001
Overall	6.2 (3.4; 9.3)	15.7 (13.4; 18.8)	23.9 (19.9; 28.4)	33.8 (28.2; 45.0)	48.9 (41.2; 58.6)	<.0001
Vmin, mL:						
M	2.5 (1.9; 4.3)*	5.6 (4.6; 6.8)*	9.0 (7.7; 10.9)*	13.6 (10.3; 17.8)*	19.5 (14.5; 23.2)*	<.0001
F	1.8 (1.2; 2.7)*	4.7 (3.7; 6.1)*	7.8 (6.3; 10.0)*	10.7 (9.2; 15.0)*	14.5 (11.9; 18.3)*	<.0001
Overall	2.2 (1.2; 2.9)	5.4 (4.1; 6.6)	8.3 (6.7; 10.5)	12.6 (9.6; 16.6)	18.0 (13.6; 22.0)	<.0001
Total EV, mL						
M	5.7 (3.1; 7.9)*	10.2 (9.4; 12.8)*	16.5 (14.2; 19.4)*	24.1 (19.3; 29.7)*	33.6 (29.1; 37.9)*	<.0001
F	3.3 (2.1; 4.7)*	10.5 (8.4; 12.4)*	14.4 (11.7; 17.7)*	20.0 (17.1; 25.0)*	27.4 (25.3; 34.1)*	<.0001
Overall	4.2 (2.2; 5.8)	10.4 (9.3; 12.6)	15.1 (13.1; 18.6)	21.7 (18.0; 28.1)	31.4 (26.8; 36.3)	<.0001
Total EF, %						
M	64.1 (62.2; 69.0)	66.1 (62.7; 69.0)	64.2 (61.3; 66.6)	63.1 (61.3; 66.5)*	63.1 (60.6; 65.3)*	.011
F	62.1 (60.0; 69.0)	67.6 (64.0; 70.4)	64.5 (62.1; 67.2)	63.9 (61.4; 66.6)*	64.7 (62.8; 66.2)*	.0063
Overall	63.5 (60.7; 69.0)	66.8 (63.7; 69.7)	64.3 (61.7; 66.8)	63.4 (61.4; 66.6)	63.8 (61.3; 65.7)	.0002
Vmax/BSA, mL/m^2:						
M	21.0 (14.4; 26.9)*	24.2 (21.2; 29.8)	25.9 (22.8; 30.7)	28.5 (22.6; 32.9)*	28.8 (24.8; 34.5)	<.0001
F	14.4 (12.8; 17.2)*	24.3 (19.0; 27.3)	24.9 (20.7; 28.5)	24.7 (20.8; 29.3)*	26.9 (22.5; 31.8)	<.0001
Overall	15.8 (12.8; 21.0)	24.2 (21.0; 27.8)	25.5 (21.6; 30.1)	26.6 (21.5; 30.8)	27.9 (24.3; 33.1)	<.0001
Vmin/BSA, mL/m^2:						
M	6.8 (5.0; 9.8)*	8.4 (7.2; 10.3)	9.4 (8.1; 11.8)	10.2 (8.4; 11.9)*	10.8 (8.6; 13.3)	<.0001
F	5.3 (4.6; 6.1)*	7.4 (5.7; 9.7)	8.5 (7.1; 10.6)	8.6 (7.1; 10.8)*	9.2 (7.5; 11.5)	<.0001
Overall	5.5 (4.8; 6.9)	8.1 (6.2; 10.0)	9.0 (7.6; 10.9)	9.6 (7.9; 11.7)	10.3 (7.7; 12.8)	<.0001
Total EV/BSA, mL/m^2:						
M	14.2 (9.4; 17.2)*	16.3 (14.1; 19.2)	16.8 (14.7; 19.8)	18.0 (14.5; 21.4)*	18.3 (16.5; 20.9)	.0009
F	9.0 (8.0; 10.7)*	16.2 (12.7; 18.5)	16.1 (13.5; 18.8)	16.2 (13.7; 17.9)*	17.9 (14.8; 20.2)	<.0001
Overall	10.4 (8.1; 14.1)	16.2 (13.8; 18.7)	16.6 (13.9; 19.2)	17.3 (14.1; 19.5)	18.1 (15.6; 20.5)	<.0001

F, Female; *M*, male.

Data are presented as median and 25th and 75th quantiles. *P* values refer to age group differences. To test differences between the sexes in every age group, the Mann-Whitney-test was used. Differences between the age groups were tested using the nonparametric Kruskal-Wallis test.

*$P < .05$ for sex differences.

Supplemental Table 3 Reference ranges of LA phasic volumes and function by 3DE presented by sex and age groups

	0-24 mo (*n* = 24) (M = 8, F = 16)	>2-5 years (*n* = 63) (M = 35, F = 28)	>5-10 years (*n* = 114) (M = 55, F = 59)	>10-14 years (*n* = 83) (M = 46, F = 37)	>14-18 years (*n* = 66) (M = 40, F = 26)	*P* value
VpreA, mL:						
M	2.8 (1.3; 5.9)	8.0 (6.4; 9.2)	12.5 (10.6; 14.1)*	19.1 (15.2; 24.9)	28.2 (23.5; 35.0)*	<.0001
F	2.3 (1.8; 4.1)	6.9 (5.0; 8.4)	10.4 (8.3; 14.4)*	16.0 (13.3; 22.7)	23.2 (18.3; 26.6)*	<.0001
Overall	2.3 (1.7; 4.1)	7.2 (5.9; 9.0)	11.6 (9.3; 14.2)	18.2 (14.3; 24.5)	25.9 (21.5; 32.6)	<.0001
Passive EV, mL:						
M	2.1 (1.1; 5.3)	8.6 (7.7; 10.6)	13.1 (10.6; 15.9)*	19.2 (14.2; 23.4)*	23.6 (20.0; 27.4)*	<.0001
F	1.7 (1.2; 4.5)	9.0 (6.6; 10.3)	11.2 (8.8; 13.2)*	15.1 (13.3; 7.4)*	20.5 (17.3; 23.1)*	<.0001
Overall	1.7 (1.1; 4.5)	8.9 (7.6; 10.5)	11.9 (9.2; 15.1)	16.5 (13.6; 21.6)	22.5 (18.3; 25.7)	<.0001
Active EV, mL:						
M	1.0 (0.3; 1.7)	2.0 (1.5; 2.8)	3.3 (2.0; 4.8)	6.1 (4.0; 8.2)	10.0 (6.8; 12.0)	<.0001
F	0.8 (0.4; 1.2)	2.1 (1.2; 2.7)	3.2 (2.0; 4.6)	5.1 (3.8; 7.4)	8.2 (3.8; 10.5)	<.0001
Overall	0.8 (0.4; 1.4)	2.1 (1.3; 2.7)	3.2 (2.0; 4.7)	5.5 (3.8; 7.9)	9.0 (5.7; 11.4)	<.0001
Passive EV/total EV, %:						
M	70.7 (62.6; 82.3)	81.9 (80.0; 86.6)	80.0 (73.5; 85.7)	75.5 (68.9; 82.4)	71.0 (65.1; 77.3)	<.0001
F	77.7 (66.0; 83.3)	81.1 (73.8; 86.5)	77.4 (72.7; 84.4)	74.6 (70.3; 80.5)	74.2 (62.3; 83.3)	.0368
Overall	73.2 (64.8; 83.3)	81.9 (77.4; 86.6)	79.0 (73.3; 84.7)	74.7 (69.3; 81.9)	71.8 (64.8; 78.3)	<.0001
Active EV/total EV, %:						
M	29.3 (17.7; 37.4)	18.1 (13.4; 20.0)	20.0 (14.3; 26.5)	24.5 (17.6; 31.1)	29.0 (22.7; 34.9)	<.0001
F	22.3 (16.7; 34.0)	18.9 (13.5; 26.2)	22.6 (15.6; 27.3)	25.4 (19.5; 29.7)	25.8 (16.7; 37.7)	.0368
Overall	26.8 (16.7; 35.2)	18.1 (13.4; 22.6)	21.0 (15.3; 26.7)	25.3 (18.1; 30.7)	28.2 (21.7; 35.2)	<.0001
Passive EF, %:						
M	43.3 (40.8; 52.9)	53.1 (50.8; 58.7)	51.4 (48.4; 55.4)	48.9 (44.4; 51.9)	46.1 (40.9; 49.0)	<.0001
F	48.2 (44.7; 55.6)	54.9 (51.8; 58.6)	50.9 (46.7; 55.0)	47.8 (42.8; 51.9)	47.2 (41.5; 53.0)	<.0001
Overall	47.3 (42.0; 54.9)	54.1 (51.1; 58.7)	51.1 (46.9; 55.1)	48.0 (43.3; 51.9)	46.5 (41.4; 51.0)	<.0001
Active EF, %						
M	33.1 (22.9; 42.0)	25.7 (19.0; 30.1)	27.3 (16.7; 35.4)	29.8 (24.3; 37.7)	32.7 (26.9; 37.7)	.0109
F	29.9 (21.5; 41.9)	29.5 (21.8; 34.8)	29.0 (21.9; 35.5)	30.0 (24.7; 34.4)	31.1 (22.0; 43.5)	.6483
Overall	31.6 (21.5; 41.9)	27.0 (21.2; 32.3)	28.1 (20.5; 35.4)	30.3 (24.6; 36.7)	32.6 (25.7; 41.3)	.0087
VpreA/BSA, mL/m^2:						
M	9.9 (4.6; 14.8)	11.2 (9.7; 13.7)	12.5 (11.1; 14.1)	14.4 (11.5; 17.2)	16.0 (13.1; 19.5)	<.0001
F	8.1 (6.6; 9.1)	10.3 (7.8; 12.1)	11.7 (9.5; 14.4)	13.4 (10.2; 13.4)	13.8 (12.1; 16.7)	<.0001
Overall	8.1 (6.6; 9.9)	10.9 (9.1; 13.1)	12.2 (10.1; 14.1)	13.7 (11.0; 16.8)	15.5 (12.8; 17.8)	<.0001
Passive EV/BSA, mL/m^2:						
M	7.1 (5.4; 12.0)	12.9 (11.1; 15.9)	13.6 (11.0; 15.0)	13.5 (11.1; 16.3)*	13.4 (10.7; 14.8)	.0267
F	7.9 (4.7; 10.1)	13.5 (9.6; 15.1)	12.3 (9.8; 14.4)	12.0 (10.2; 13.4)*	12.5 (10.7; 14.6)	<.0001
Overall	7.9 (5.4; 10.2)	13.0 (11.0; 15.7)	13.2 (10.5; 14.8)	12.4 (10.4; 14.8)	12.8 (10.7; 14.7)	<.0001
Active EV/BSA, mL/m^2:						
M	2.5 (1.6; 5.3)	3.1 (2.1; 3.7)	3.4 (1.9; 4.6)	4.5 (2.8; 5.6)	5.2 (3.9; 6.4)	<.0001
F	2.2 (1.4; 3.4)	3.2 (2.0; 4.0)	3.4 (2.1; 4.8)	4.1 (2.8; 5.7)	5.1 (2.4; 6.4)	.0004
Overall	2.5 (1.5; 7.0)	3.1 (2.1; 3.8)	3.4 (2.0; 12.2)	4.2 (2.8; 5.6)	5.2 (3.4; 6.4)	<.0001

F, Female; *M*, male.
Data are presented as median and 25th and 75th quantiles. *P* values refer to age group differences. To test differences between the sexes in every age group the Mann-Whitney-test was used. Differences between the age groups were tested using the nonparametric Kruskal-Wallis test.
*$P < .05$ for sex differences.

Supplemental Table 4 Reference ranges of durations (msec) of the different phases of the atrial cardiac cycle and phasic function by 3DE presented by R-R interval groups

	345-500 (*n* = 16)	500-600 (*n* = 55)	600-750 (*n* = 154)	750-1,000 (*n* = 116)	1,000-2,000 (*n* = 9)	*P* value
Overall absolute atrial diastole, msec	277 (242; 340)	309 (279; 345)	327 (298; 354)	360 (335; 387)	369 (342; 389)	<.0001
Overall absolute atrial systole, msec	176 (111; 201)	257 (215; 279)	351 (305; 394)	481 (439; 539)	763 (671; 793)	<.0001
Overall atrial PE, msec	88 (63; 104)	145 (122; 171)	200 (175; 224)	262 (237; 297)	397 (292; 465)	<.0001
Overall atrial AE, msec	84 (48; 97)	104 (69; 128)	144 (113; 174)	210 (173; 245)	372 (210; 427)	<.0001
Overall atrial diastolic fraction of cardiac cycle, %	59.2 (56.9; 77.6)	53.4 (51.3; 60.6)	48.2 (44.0; 52.7)	41.9 (39.0; 46.0)	32.6 (30.8; 36.5)	<.0001
Overall atrial systolic fraction of cardiac cycle, %	40.8 (22.4; 43.1)	46.7 (39.4; 48.8)	51.8 (47.3; 56.0)	58.1 (54.0; 61.0)	67.4 (63.5; 69.2)	<.0001
Overall PE fraction of cardiac cycle, %	19.9 (14.0; 23.8)	25.7 (22.2; 29.6)	29.5 (26.9; 32.8)	31.4 (28.6; 35.2)	36.2 (26.5; 44.2)	<.0001
Overall AE fraction of cardiac cycle, %	19.9 (9.9; 22.3)	18.7 (12.0; 22.5)	21.1 (16.7; 25.9)	25.2 (21.0; 29.9)	33.9 (20.0; 38.0)	.0001
Overall PE fraction of atrial systole, %	58.3 (50.4; 66.5)	58.3 (54.8; 69.6)	58.4 (52.2; 65.1)	56.5 (50.0; 61.4)	51.8 (39.6; 68.8)	.0481
Overall AE fraction of atrial systole, %	41.7 (33.5; 49.6)	41.7 (30.4; 45.2)	41.6 (34.9; 47.5)	43.4 (38.6; 50.0)	48.2 (31.2; 60.4)	.0481
Overall passive EV/total EV, %	74.7 (66.0; 83.5)	81.1 (77.1; 89.5)	79.2 (72.2; 84.2)	74.2 (67.1; 80.2)	68.0 (57.5; 72.2)	<.0001
Overall active EV/total EV, %	25.3 (16.5/34.0)	18.9 (10.5; 22.9)	20.8 (15.8; 27.8)	25.8 (19.8; 32.9)	32.0 (27.8; 42.5)	<.0001
Overall passive EF, %	47.8 (44.4; 56.0)	55.5 (50.9; 58.7)	50.9 (46.7; 54.2)	46.9 (43.1; 51.2)	42.3 (36.9; 47.3)	<.0001
Overall active EF, %	34.4 (23.1; 43.1)	26.2 (17.8; 32.6)	28.2 (21.5; 35.1)	31.0 (25.8; 37.7)	37.0 (34.4; 43.2)	.0001

Data are presented as median and 25th and 75th quantiles. *P* values refer to R-R interval group differences.

9 Appendix C - Third study

Krell, K., Laser, K.T., Dalla-Pozza, R., Winkler, C., Hildebrandt, U., Kececioglu, D., Breuer, J. and Herberg, U. (2018). Real-time three-dimensional echocardiography of the left ventricle—pediatric percentiles and head-to-head comparison of different contour-finding algorithms: a multicenter study. Journal of the American Society of Echocardiography, 31(6), pp.702-711.

NORMAL PEDIATRIC VALUES FOR NEW ECHOCARDIOGRAPHIC TECHNIQUES

Real-Time Three-Dimensional Echocardiography of the Left Ventricle—Pediatric Percentiles and Head-to-Head Comparison of Different Contour-Finding Algorithms: A Multicenter Study

Kristina Krell, Kai Thorsten Laser, MD, Robert Dalla-Pozza, MD, Christian Winkler, Ursula Hildebrandt, MD, Deniz Kececioglu, MD, Johannes Breuer, MD, and Ulrike Herberg, MD,
Bonn, Bad Oeynhausen, and Munich, Germany

Background: Real-time three-dimensional echocardiography (RT3DE) is a promising method for accurate assessment of left ventricular (LV) volumes and function, however, pediatric reference values are scarce. The aim of the study was to establish pediatric percentiles in a large population and to compare the inherent influence of different evaluation software on the resulting measurements.

Methods: In a multicenter prospective-design study, 497 healthy children (ages 1 day to 219 months) underwent RT3DE imaging of the LV (ie33, Philips, Andover, MA). Volume analysis was performed using QLab 9.0 (Philips) and TomTec 4DLV2.7 (vendor-independent; testing high ($TomTec_{75}$) and low ($TomTec_{30}$) contour-finding activity). Reference percentiles were computed using Cole's LMS method. In 22 subjects, cardiovascular magnetic resonance imaging (CMR) was used as the reference.

Results: A total of 370/497 (74.4%) of the subjects provided adequate data sets. LV volumes had a significant association with age, body size, and gender; therefore, sex-specific percentiles were indexed to body surface area. Intra- and interobserver variability for both workstations was good (relative bias ± SD for end-diastolic volume [EDV] in %: intraobserver: QLab = −0.8 ± 2.4; $TomTec_{30}$ = −0.7 ± 7.2; $TomTec_{75}$ = −1.9 ± 6.7; interobserver: QLab = 2.4 ± 7.5; $TomTec_{30}$ = 1.2 ± 5.1; $TomTec_{75}$ = 1.3 ± 4.5). Intervendor agreement between QLab and $TomTec_{30}$ showed larger bias and wider limits of agreement (bias: QLab vs $TomTec_{30}$: end-systolic volume [ESV] = 0.8% ± 23.6%; EDV = −2.2% ± 17.0%) with notable individual differences in small children. QLab and TomTec underestimated CMR values, with the highest agreement between CMR and QLab.

Conclusions: RT3DE allows reproducible noninvasive assessment of LV volumes and function. However, intertechnique variability is relevant. Therefore, our software-specific percentiles, based on a large pediatric population, serve as a reference for both commonly used quantification programs. (J Am Soc Echocardiogr 2018;31:702-11.)

Keywords: 3D echocardiography, Nomogram, Pediatric, Children, Left heart, Volumetry

From the Department of Pediatric Cardiology, Children's Hospital, University of Bonn (K.K., C.W., U.H., J.B., U.H.), Bonn; Department of Congenital Heart Defects, Heart and Diabetes Center, North Rhine Westphalia Ruhr University Bochum (K.T.L., D.K.), Bad Oeynhausen; and Department of Pediatric Cardiology and Pediatric Intensive Care, Ludwig Maximilians University, Medical Hospital of the University of Munich (R.D.-P.), Munich, Germany.

K.K. and K.T.L. contributed equally to this work.

This study was part of the project, "Validation and Standardization of Real-Time-3D Echocardiography for the Functional Analysis of Pediatric Cardiac Valves," sponsored by the Fördergemeinschaft Deutsche Kinderherzzentren (Project No. W-BN/M/BAD-009/2009).

Conflicts of Interest: None.

Reprint requests: Ulrike Herberg, MD, PhD, Department of Pediatric Cardiology, University of Bonn, Adenauerallee 119, 53113 Bonn, Germany (E-mail: *ulrike.herberg@ukb.uni-bonn.de*).

0894-7317

https://doi.org/10.1016/j.echo.2018.01.018

Abbreviations

3D = Three-dimensional

BSA = Body surface area

CFA = Contour-finding activity

CMR = Cardiovascular magnetic resonance imaging

EDV = End-diastolic volume

EF = Ejection fraction

ESV = End-systolic volume

LOA = Limits of agreement

LV = Left ventricular

RT3DE = Real-time three-dimensional echocardiography

SV = Stroke volume

$TomTec_{30}$ = TomTec with low contour-finding activity

$TomTec_{75}$ = TomTec with high contour-finding activity

Echocardiographic assessment of left ventricular (LV) size and function is one of the most important tools in pediatric cardiology: it is essential for diagnosis, prognosis, and management in various congenital as well as acquired heart diseases.[1-4] Accurate and reproducible LV volume measurements and assessment of the ejection fraction (EF) in particular play an essential role in daily echocardiographic examination and decision making.[5,6]

Real-time three-dimensional echocardiography (RT3DE) with matrix transducer technology has become widely available for the assessment of cardiac anatomy and function and has been proven to be superior to conventional two-dimensional methods with regard to accuracy and reproducibility of LV volume calculations.[2,7-11] Further improvement of matrix technology with transducers of small aperture and improved near-field resolution by X7-2 and X5-1 transducers (Philips, Andover, MA) have led to the increased application of 3DRTE in children. However, although there is widespread clinical need for the calculation of 3D-related volumes, pediatric reference values derived from a large normal population are currently lacking.

For 3D volume calculation, several clinical software programs with a variety of postprocessing options and different benefits have been developed.[12] Currently, the most commonly used software programs for 3D quantification of the pediatric left ventricle are the vendor-independent software TomTec (TomTec, Unterschleissheim, Germany) and the vendor-specific QLab (Philips, Andover, MA), which can only be used for 3D volume data sets obtained by Philips ultrasound scanners. Both apply semiautomatic endocardial border-tracking algorithms and offer the opportunity to calculate values quickly, reproducibly, and in a practical workflow. Up until now, data regarding the intervendor agreement and consistency between the two software types have been limited to a small number of healthy children, as well as children with a single ventricle.[13,14]

The primary aim of our study is to provide reference values for LV indices in a large cohort of healthy children. In order to investigate whether a set of universal reference values could be applicable for both quantification software algorithms, intervendor agreement and the influence of different contour-finding adjustments were assessed for QLab as well as TomTec.

METHODS

Study Design and Data

In a prospective multicenter design, 497 children and adolescents from birth to 18 years of age were enrolled to undergo RT3DE of the left ventricle between April 2011 and November 2013. Normal cardiac anatomy and function as well as sinus rhythm were a precondition and confirmed by physical examination and echocardiography, according to standard recommendations.[1] The study was approved by the local ethics institutional review committee (Registration No. 226/06) and representative boards of all participating centers and conformed to the principles of the Declaration of Helsinki as well as German law. Written consent was given by the legal guardian or in person by young adults. Examinations were performed at three different centers by five different operators with five different sonographic units from the same manufacturer (iE33, Philips, using the transducers X7-2, $n=285$; X5-1, $n=6$; and X3-1, $n=6$). Prior to the start of the study, standardization of the acquisition procedure including presets and operator training took place. Insights regarding the use of real-time 3D matrix transducers[15] and restrictions in spatiotemporal accuracy of RT3DE in pediatrics[16] were incorporated into the acquisition procedures. Measurement accuracy of the ultrasound scanners was validated using calibrated, static, tissue-mimicking phantoms[17] as well as moving phantoms.[16] In the core lab in Bonn, all data were reviewed and quantified. Results were compared to the gold standard, cardiovascular magnetic resonance imaging (CMR), performed on volunteers (22 cases: 20 children, mean age 12.3 years, and two adults, ages 22 years and 43 years). Due to ethical reasons, CMR on young healthy children requiring sedation was not performed.

Real-Time Three-Dimensional Echocardiography

Image Acquisition. Image acquisition was implemented from an apical window based on standard recommendations.[18] A full-volume scan was acquired from four to seven R-wave triggered subvolumes during end-expiratory breath holding when necessary. Blinded 3D data sets were stored in a DICOM format on a DVD and sent to the core lab. In the core lab, the quality of the 3D data was rated, and any data sets containing artefacts due to movement, arrhythmia, or incomplete depiction of the left ventricle were excluded. Only those data sets that could be interpreted sufficiently, with complete delineation of the left ventricle and without disturbing artefacts, were processed and transferred to two different offline workstations (Figure 1A, 1B).

Data Analysis with QLab 9.0. Three-dimensional data sets of the LV were analyzed using offline QLab Version 9.0 (3DQ Advanced software, Philips). After initially adjusting a proper four-chamber view, the end-diastolic frame, presented by the one with maximum LV volume, was first determined. Ventricular trabeculae and papillary muscles were included in the LV cavity. Next the end-systolic frame showing the smallest volume, respectively the frame before mitral valve opening, was selected. After subsequently setting five points, at the apex, septal, lateral, anterior, and mitral annulus (Figure 1C), the cardiac cycle as well as minimal end-systolic volume (ESV), maximal end-diastolic volume (EDV), EF, and stroke volume (SV) were semiautomatically computed and the LV cavity was displayed as a 3D model. If delineation of the LV endocardial borders was unsatisfactory (Figure 1D), the operator manually adjusted the initial endocardial contour at the apex, septum, and mitral valve and repeated the automatic tracking throughout the cardiac cycle. Data analysis was performed by two raters who were blinded to results derived from TomTec (K.K. and U.H.).

Data Analysis with TomTec. TomTec 4DLV analysis software 2.7 (Image-Arena version 4.1; Build 4.1.1.30, TomTec, Unterschleißheim, Germany) was used to perform offline LV data analysis. All operators followed a standardized protocol for analysis of the data after interinstitutional operator training based on previous findings.[15,19] The data sets were adjusted in order to acquire maximal long-axis dimension.

HIGHLIGHTS

- Pediatric reference percentiles for 3D-RTE of the left ventricle are provided.
- Reference values are gender-specific and correlate with BSA, weight, and height.
- LV 3D volumes are dependent on the software algorithm used for 3D data analysis.

Using the four- and two-chamber views as well as the apical long-axis view, the end-systolic and end-diastolic delineations were traced manually. Ventricular trabeculae and papillary muscles were included in the LV cavity. EDV, ESV, and EF were calculated semiautomatically. Manual adjustments were made to the initial endocardial contour if the delineation of the LV endocardial borders was inadequate. Without changing previously performed manual tracing, the sensitivity of the contour-finding algorithm, to separate endocardial border from noise, was set for 30 ($TomTec_{30}$), respectively 75 ($TomTec_{75}$), intensity units (Figure 1E, 1F). The contour-finding activity (CFA) defines the intensity of the automatic differentiation between endocardial border and noise by the software. If low values are used, the automatic contour-finding process is decreased. $TomTec_{75}$ with high contour-finding activity relies heavily on automatic geometric assumptions, whereas $TomTec_{30}$ with low CFA prioritizes manual tracing.[15] $TomTec_{30}$ was chosen for all 370 cases. During the study, we performed an interim analysis of CMR and 3DRTE data. The findings confirmed those of an earlier study on 49 subjects with and without congenital heart disease, which showed only moderate correlation of $TomTec_{75}$ with CMR.[15] Subsequently, the number of cases calculated with $TomTec_{75}$ was limited to 252 cases. Three independent raters (not involved in QLab data quantification and blinded to the results from QLab) performed the data analysis (U.B., N.R., A.H.).

CMR Imaging Acquisition and Analysis. Twenty-two healthy subjects underwent CMR with vector electrocardiography and respiratory motion gating, using a 3.0-T whole body magnetic resonance imaging system (Achieva 3.0T TX; Philips Medical Systems) equipped with parallel radiofrequency signal transmission technology to enhance image uniformity (maximum gradient performance, 80 mT/m; slew rate 200 T/m/sec). A 32-element phased-array receive-only surface coil was used for signal detection. A stack of 15-21 short-axis slices was obtained by applying a segmented, multislice, multiphase vector, electrocardiographically triggered, steady-state, free-precession gradient-echo sequence (repetition time 2.7 msec, echo time 1.35 msec, excitation angle 40°, slice thickness 5-6 mm, no slice gap, matrix size 160 × 240, field of view 384 mm, in plane resolution, 1.6 × 1.6 mm, 25 cardiac phases under short breath-holding periods of <12 seconds of duration). These slices were used to assess the LV and right ventricular volumes.

Offline analyses of CMR volume measurements and quantitative flow CMR data sets were performed on a workstation using the HDZ MR-Tools software package, as reported elsewhere.[15,19] LV volumes, including papillary muscles and trabecular structures (to ensure comparability with the echocardiographic analysis), were generated from the summation of the cavity areas multiplied by the slice thickness in an algorithm for semiautomatic vessel border detection without geometric models or assumptions.

Statistical Analysis

Data Analysis with LMS. The data set includes the EDV, ESV, SV, weight, height, and age for each subject. The body surface area (BSA) was calculated using the Haycock formula, according to American Society of Echocardiography recommendations[1]: BSA (m^2) = 0.024265 × height (cm)$^{0.3964}$ × weight (kg)$^{0.5378}$. For the computation of reference curves, the LMS method by Cole and Green was applied in the software environment R in combination with the GAMLSS package for the computation.[20-22] The indexed EDV/BSA, ESV/BSA, and SV/BSA were selected as dependent variables, with age as an independent variable. Boys and girls were considered separately, and subjects were classified according to age group, using intervals of two months for children under 6 years and six months for children between the ages of 6 and 12. Children older than 12 years were classified into groups with intervals of one year. Statistical outliers detected in each group were removed from the data set for further calculations.

For the computation of reference curves, the function of GAMLSS fits a regression model to the data. For the LMS method, the regression model is based on the Box-Cox Cole and Green distribution with the parameters L (Box-Cox power), M (median), and S (coefficient of variation). While L represents the skewness of the distribution, S defines the variation for each age group. M is the median for each group, dividing it into two parts of equal amounts.

Penalized splines were used for L, M, and S in order to create smooth percentile curves. The smoothness of the penalized splines can be configured by their degree of freedom. The goodness of fit was assessed by the global deviance that indicates the deviation between model and data. We optimized our curves considering the smoothness (degree of freedom) and the goodness of fit (global deviance). Both features are in competition, and by optimizing, we made sure to find the optimal setting satisfying both an appropriate smoothness and a low global deviance.

Comparison of LV Volumes by QLab, TomTec, and CMR. For the assessment of agreement between QLab and TomTec as well as RT3DE and CMR, the Bland-Altman analysis was used, plotting the difference versus the average of the two methods, as well as the percentage difference (%) against the absolute mean. Statistical analyses were performed with Prism GraphPad Software (Version 6, GraphPad Software, CA) for all relevant data. Significance was tested using a Wilcoxon test, and P values ≤ .05 were considered statistically significant.

Intra- and Interobserver Variability. Intraobserver and interobserver variability was assessed in randomly selected subjects (QLab $n = 36$; $TomTec_{30}$ $n = 33$; $TomTec_{75}$ $n = 21$). All data sets were reanalyzed using raw data, starting with the definition of end diastole and end systole and tracing of the endocardial contours. For interobserver variability assessment, 3D data sets were processed independently by two raters, blinded to each other's measurements. For intraobserver variability, 6 months after the initial analysis, one of the evaluators blindly and randomly reprocessed the data sets. Agreement was expressed by the intraclass correlation coefficients (SPSS Version 22, SPSS, Chicago, IL) and Bland-Altman analysis (Prism GraphPad).

RESULTS

Study Subject Characteristics

Of 497 subjects enrolled, comparative analysis of LV volumes was feasible in 370 (194 male and 176 female; 74.4% feasibility). The

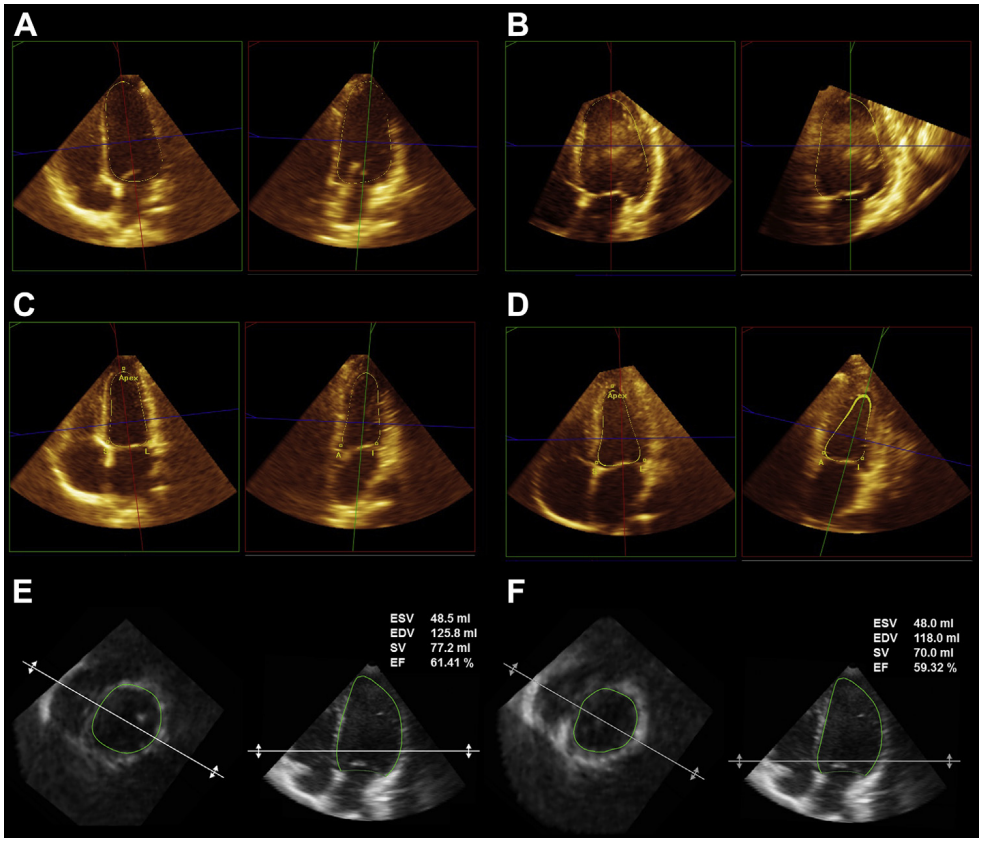

Figure 1 Representative 3D data sets with excellent **(A)** and usable **(B)** image quality. Multiplanar review with a reformatted four-chamber view and corresponding two-chamber view. The *yellow line* depicts the automatically detected endocardial borders at end diastole using QLab. The 3D data set not requiring **(C)** and requiring **(D)** data correction at end systole using the QLab software analysis package. The 3D data set analyzed with TomTec using low (**E**, $TomTec_{30}$) and high (**F**, $TomTec_{75}$) sensitivity of contour finding.

subject characteristics are presented in Table 1, and age distribution is shown in Figure S1. The remaining subjects had to be excluded due to poor imaging quality or trigger artefacts ($n = 116$), incomplete demographic data ($n = 3$), or missing images ($n = 8$).

Percentiles

Reference values and percentiles for LV volumes generated by QLab and TomTec could be obtained from 370 healthy children. LV volumes correlated to sex, age, weight, height, and BSA. A nonlinear relationship between the LV volumes and age was noted, for example, in small children due to the altering growth process (selected scatterplots shown in Figure S2). For this reason, the LMS method based on penalized splines for the global range of the data was applied. The application of the LMS method resulted in smooth curves that were fitted to the data. Sex-specific percentiles for ventricular volumes indexed to BSA are shown in Figure 2 (QLab) and Figure 3 ($TomTec_{30}$), respectively. Reference percentile curves for absolute ventricular volumes related to age, height, weight, and BSA are computed in the supplement (Figures S3 and S4). Systolic function, as calculated by EF, is consistent from birth to puberty; mean and SD were 61.5% ± 5.1% for QLab, 62.7% ± 5.3% for $TomTec_{30}$, and 62.0% ± 5.9% for $TomTec_{70}$.

When indexing ventricular volumes to BSA, there is a steady rise with increasing age, reaching an initial plateau at the age of 5-7 years, using TomTec. A second plateau is found at the age of 8-11 years. SVs, as derived parameters, display the slope more prominently.

Table 1 Subject characteristics and frame rate ($N = 370$)

Characteristic (176 females and 194 males)	Median	Range
Age (months)	91.5	0.03-219
Height (cm)	130	40-192
Weight (kg)	26.4	2.2-92.7
BSA (m^2)	0.97	0.1-3.1
Heart rate (min^{-1})	86	43-182
3D volume rate/heart cycle	16	7-35

Intra- and Interobserver Variability

Intra- and interobserver variability was assessed for all software modifications separately. Intraobserver variability showed good results for QLab and $TomTec_{30}$ with a small bias of less than 2.1% (0-1.1 mL) and moderate 95% limits of agreement (LOA) ranging between 4% and 21% (Tables 2 and S1). Of note, $TomTec_{75}$—despite using high automatic adjustment—showed the highest intraobserver variability for ESV with 5.5%. Interobserver variability was slightly higher, resulting in an overall bias of less than 5% (0-2.3 mL) and comparable LOA. Intraclass correlation for EDV, ESV, and SV was excellent for both QLab and TomTec with correlation coefficients between 0.91 and 0.99 (Table S1).

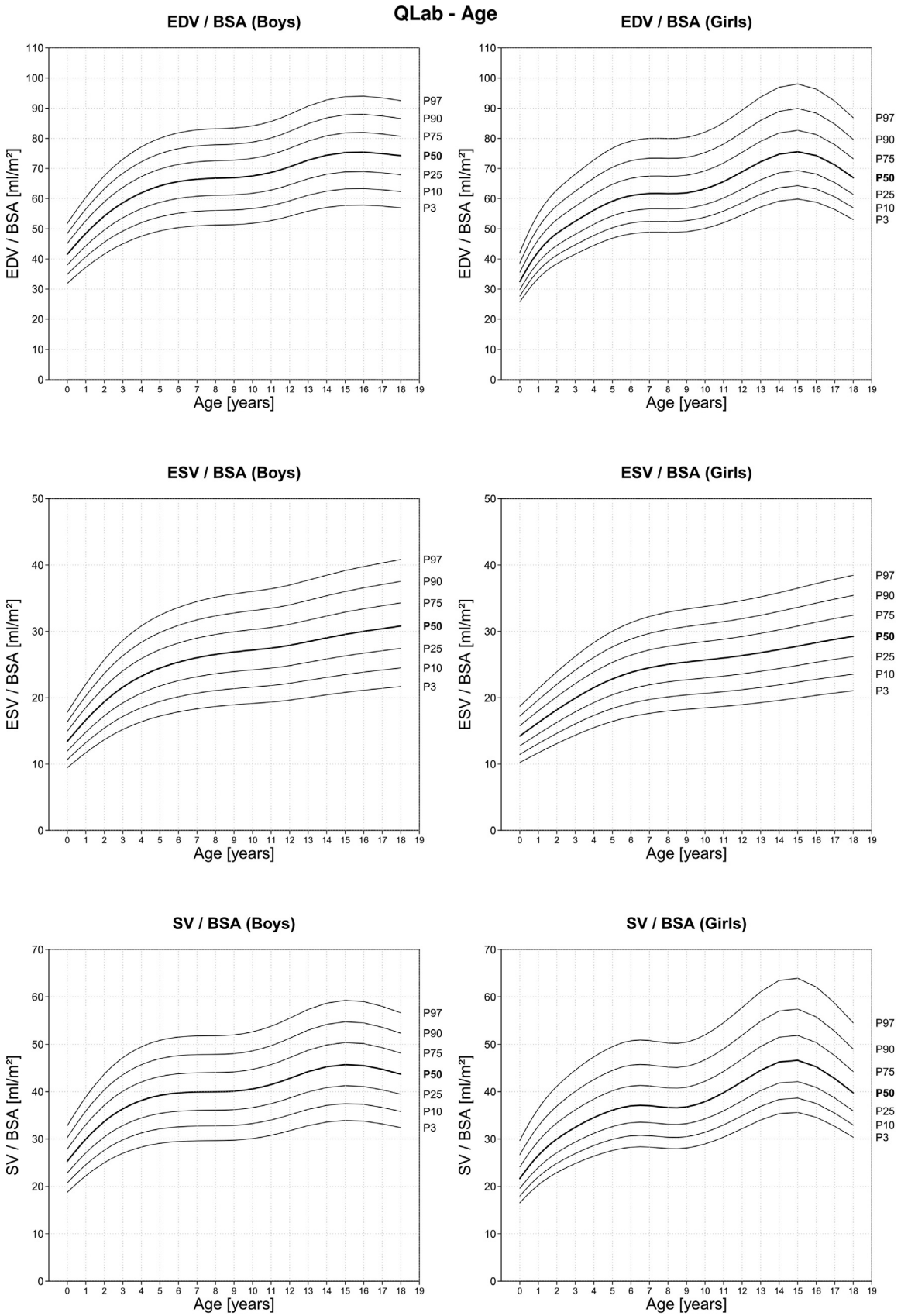

Figure 2 Gender-specific percentiles for QLab with EDV, ESV, and SV indexed to BSA in relation to age. P indicates the percentile value, e.g., P50 = 50th percentile value.

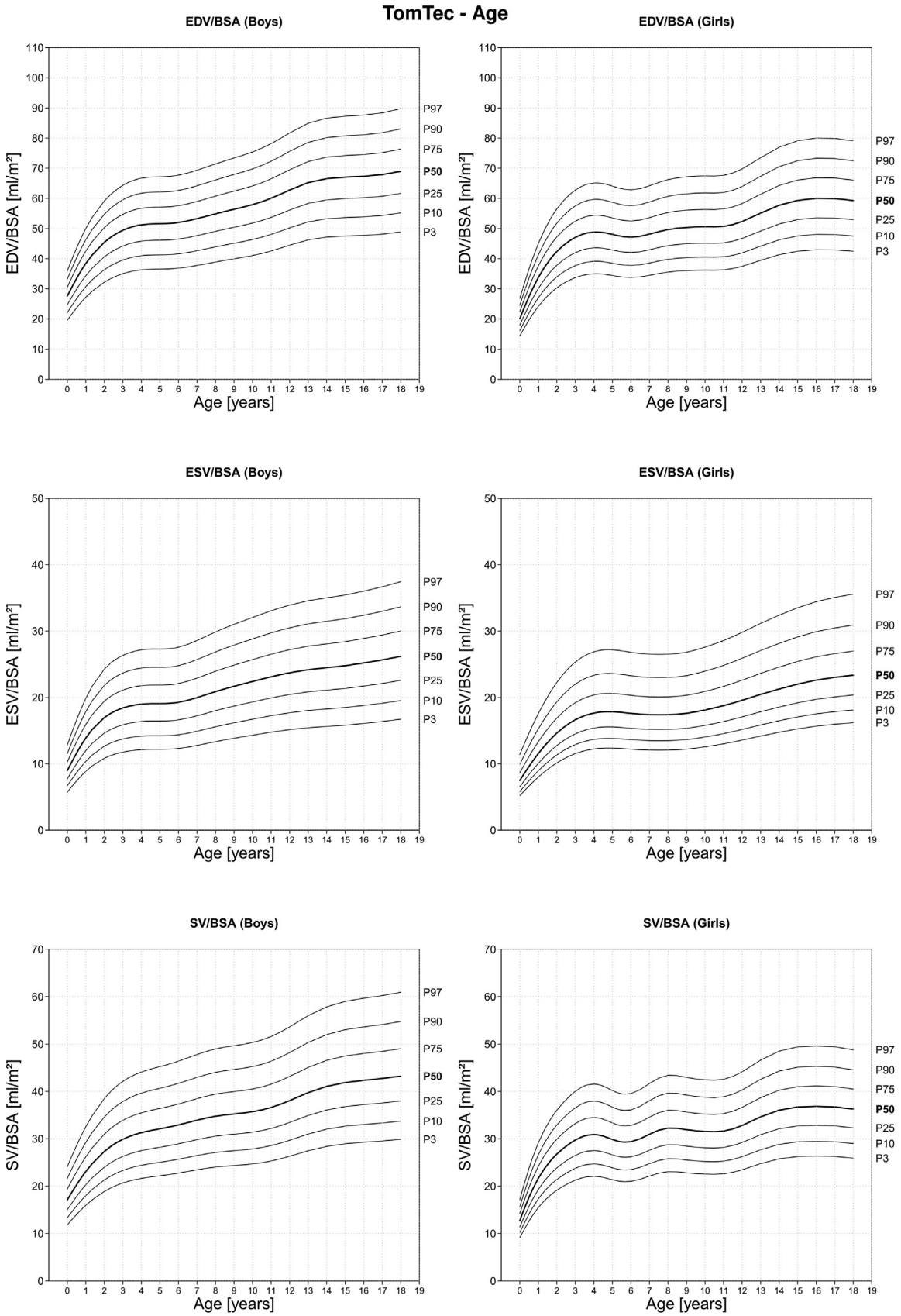

Figure 3 Gender-specific percentiles for $TomTec_{30}$ with EDV, ESV, and SV indexed to BSA in relation to age. P indicates the percentile value, e.g., P50 = 50th percentile value.

Table 2 Intraobserver and interobserver variability

	Intraobserver variability		Interobserver variability	
	Bias (%)	95% LOA (%)	Bias (%)	95% LOA (%)
ESV				
QLab	1.1	−9 to 11.1	−1.6	−24.0 to 21.0
$TomTec_{30}$	−1.3	−20.5 to 17.9	1.8	−17.0 to 21.0
$TomTec_{75}$	−5.5	−21.6 to 10.7	4.2	−16.3 to 24.8
EDV				
QLab	−0.8	−5.4 to 3.9	2.4	−12.0 to 17.0
$TomTec_{30}$	−0.7	−14.8 to 13.4	1.2	−8.7 to 11.0
$TomTec_{75}$	−1.9	−15.0 to 11.2	1.3	−7.5 to 10.1
SV				
QLab	−2.1	−10.9 to 6.7	4.8	−17.0 to 27.0
$TomTec_{30}$	0.0	−17.4 to 17.4	0.8	−12.0 to 14.0
$TomTec_{75}$	−0.1	−14.2 to 14.0	0.4	−13.0 to 13.8

Comparison of Different Software Algorithms

$TomTec_{30}$ and $TomTec_{75}$. Analysis of identical 3D data sets with the same software but different settings had a significant impact. Use of $TomTec_{75}$ instead of $TomTec_{30}$ with lower automatic adjustments resulted in significantly smaller EDV, ESV, and SV ($P < .001$; relative values Table 3, left column, absolute values Table S2). For measurement of EF, there was no bias between the modalities, and a significant difference could not be determined (Table S2).

QLab and $TomTec_{30}$. Agreement between QLab and $TomTec_{30}$ was assessed in all 370 cases (Tables 3 and S2). Bland-Altman analysis showed bias ranging from 0.8% (ESV) to 4.2% (SV), with larger values for ESV and smaller values for EDV using QLab. A significant difference ($P < .001$) existed for SV (calculated by the difference between EDV and ESV) and EF. The 95% LOA were relatively wide, ranging between 11% and 47%. In individual cases of very young children with small ESV, intervendor differences exceeded 50% (Figure S5A).

QLab and $TomTec_{30}$—Good Quality Only. In order to examine the impact of image quality on the measurement of LV volumes, we finally compared only the data sets with excellent quality ($n = 104$ patients). Using these data sets, the bias for ESV was smaller, while EDV, SV, and EF showed significant differences between QLab and $TomTec_{30}$ ($P < .001$; Tables 3 and S2). The 95% LOA were moderately smaller, and, in small children, intraindividual bias of LV volumes >50% did not occur (Figure S5B).

QLab and $TomTec_{75}$. Compared to $TomTec_{30}$, the bias between QLab and $TomTec_{75}$ was significantly higher ($P < .001$ for ESV, EDV, SV; Table 3). Statistical differences for EF could not be confirmed.

Figure 4 summarizes the bias and 95% LOA for intra- and interobserver as well as intertechnique variability. As the LOA for intertechnique variability were considerably larger than inter- and interobserver variability, it seems that the choice of software algorithm has a relevant influence on volume calculation.

Validation with CMR. Independent of the quantification software, LV volumes and EF were underestimated by RT3DE when compared to the gold standard CMR. Overall, we observed the smallest bias between QLab and CMR, followed by $TomTec_{30}$ and CMR. The largest differences were found between $TomTec_{75}$ and CMR. The 95% LOA showed highest deviation for SV, which is calculated from EDV and ESV (Tables 4 and S3).

DISCUSSION

This study presents the results of a multicenter approach designed to provide normative values for LV volumes using state-of-the-art RT3DE, based on a large cohort of healthy children. We were able to provide percentiles for LV volumes for the two most commonly used quantification software programs. Considering the observed correlation of LV size and function with age, height, and weight, the percentiles provide a long-awaited comparison for users of the two software algorithms. These percentiles may play an essential role in the longitudinal as well as horizontal follow-up of pediatric patients with, for example, cardiomyopathy, LV volume load, or borderline left ventricle.

This study is the first to provide sex- and age-related nomograms on a large cohort of children. Ventricular volumes indexed to BSA demonstrated gradual enlargement from childhood to adolescence in which volumes reached plateaus before puberty at the age of 8-11 years. Children do not grow at a constant rate from year to year as they progress from neonates to young adults. Therefore, after the rapid growth during puberty, the indexed EDV did not increase further. This observation is consistent with the speediest body growth and correlates to CMR findings.[23] When computing the percentiles, a data-driven approach was used. The smoothing parameters were kept deliberately low in order to detect trends during the growth phases. This is particularly valuable when assessing the different onset and speed of growth between girls and boys.[20] As a result, the percentile curves represent the characteristic course of the data. Despite the high number of cases included in our study and the statistical design used, the number of subjects still plays a pivotal role for the creation of percentiles and may influence the shape of the curves as well.

Our data are in line with previous studies on smaller series using RT3DE and semiautomatic software analysis packages,[2,9,14,24,25] but the number of subjects studied, the age range, and the equipment used varied. This is reflected by the variation of published normal values for adolescents ranging between 57 and 72 mL/m^2 for EDV, 19 and 28 mL/m^2 for ESV, and 57% and 66% for EF.[2,9,24,25]

Two of the most commonly used quantification software programs were compared, and data were evaluated against CMR in a subset of patients. In concordance with previous data,[14,15] good intra- and interobserver variability proved that these software algorithm provide reproducible measurements of LV volumes. We could also demonstrate agreement of QLab- and TomTec-derived volumes with volumes generated by CMR, despite a well-known underestimation of both RT3DE software algorithms.

In a head-to-head comparison, LV volumes derived from QLab only moderately correlated to $TomTec_{30}$. Although bias between the vendors was low, intertechnique variability may be of particular importance. As reflected by Figure 4, intervendor LOA exceeded those of intra- and interobserver variability, bearing in mind that measurement variability can be relevant as well. The individual differences between software algorithms can be considerably relevant especially in younger children with very small volumes. Therefore, percentiles specific for each software algorithm seem to be needed

Table 3 Calculation of LV 3D volume data using different software algorithm—agreement among QLab, $TomTec_{30}$, and $TomTec_{75}$

	$TomTec_{30}$ vs $TomTec_{75}$	QLab vs $TomTec_{30}$	QLab vs $TomTec_{30}$ Good quality only	QLab vs $TomTec_{75}$
ESV				
Bias (%)	9.8	0.8	0.1	8.1
95% LOA (%)	−18.4 to 38.0	−45.5 to 47.0	−39.6 to 39.7	−39.7 to 55.8
P	<.001	.051	.932	<.001
EDV				
Bias (%)	8.9	−2.2	−4.6	7.0
95% LOA (%)	−11.8 to 29.6	−35.5 to 31.2	−33.8 to 24.7	−25.4 to 39.4
P	<.001	.065	.006	<.001
SV				
Bias (%)	9.3	−4.2	−7.2	6.7
95% LOA (%)	−16.4 to 34.9	−43.9 to 35.5	−43.4 to 29.1	−36.2 to 49.6
P	<.001	<.001	<.001	<.001

and have been calculated. Using a data-driven approach, the shape of the percentiles differed and plateaus were more pronounced in percentiles for $TomTec_{30}$ than in QLab. When data were related to age, there was a steady rise, which reached a plateau at the age of 5-7 years and a second plateau at the age of 8-11 years. The shapes of the percentiles for SVs, which are calculated volumes (SV = EDV − ESV), result from the additional effects of the plateaus found in EDV and ESV.

Therefore, results obtained by different quantification software packages have to be interpreted accordingly. The clinical management of children with congenital heart disease relies on the serial assessment of LV size and function. Comparison of serial data may be not valid if different measurement algorithms have to be used. To obtain reliable and reproducible data, measurement algorithm should not be changed and software specific nomograms should be used.

Intervendor variability of both semiautomatic software packages, QLab and TomTec, has been assessed by Hascoet *et al.* in a group of 40 healthy pediatric subjects, revealing small biases but high LOA.[14] In a challenging study in 32 children with single ventricle,[13] QLab 8.1 was compared to TomTec 4DLV 3.0 without further specification of CFA. The reported bias between QLab and TomTec for EDV and ESV was significantly larger than in our study (Zhong *et al.*, $n = 32$, relative bias ± SD: EDV −10.7% ± 11.3%, ESV −14.9% ± 17.1%; our study: EDV −2.2% ± 17.1%, ESV 0.8% ± 23.6%), which may have been due to the different software settings and definition of endocardial border used.

The most likely reasons for the reported vendor variability include endocardial border detection algorithms.[15] High automatic adjustments ($TomTec_{75}$), as recommended by the manufacturer, underlie stronger geometric assumptions and therefore depend only moderately on the operator and image quality. Although $TomTec_{30}$ has been shown to be more operator dependent and influenced by data set quality,[15] the use of lower automatic adjustment settings with a focus on manual tracing in our data leads to better agreement with values acquired by CMR and correlates better to CMR-derived EDV, which is an important parameter for clinical decision making in pediatric cardiology. In addition, image quality plays a pivotal role. Both types of software track the endocardial surface of the LV throughout the cardiac cycle and consequently depend on image quality. Our data confirm findings shown in adults that poor image quality is associated with less agreement and greater bias.[26] Although data sets with relevant artefacts or incomplete image depiction were excluded, we tried to process as much data as possible in order to test feasibility in routine clinical practice, which might explain the high intervendor differences in several individual patients. In fact, Bland-Altman analysis of data with excellent imaging quality (104 subjects) did not reveal extreme outliers, but intervendor variability and individual differences between both software types remained. Finally, in small children with high heart rates, spatial and temporal resolution influences accurate determination of true ESV and EDV and may explain the high bias in this group. This is concordant with the fact that bias and LOA in our study are slightly higher than those reported in prior studies on older children[14] or adults.[27]

In our study, we intended to minimize data variability by using ultrasound scanners and transducers of the same type and from the same vendor, testing the performance of the individual ultrasound machines by static tissue mimicking as well as moving phantoms,[16,17] the definition of similar presets for data acquisition, and the qualification and training of sonographers and readers. Nevertheless, operator experience on data acquisition and analysis plays an important role.[28]

In order to determine the agreement between RT3DE and the gold standard technique, results of both software types were compared to CMR. Previous studies confirmed a correlation between volumes derived from RT3DE and CMR,[8,10,11,15,27,29-31] as long as intermodality differences are considered.[12,32] As in all previous studies, RT3DE tends to underestimate volumes obtained by CMR, and EDV was underestimated by a greater degree than ESV.[2,8,26,27,32] Still QLab as well as $TomTec_{30}$ showed the closest correlation to CMR data.

Limitations

Despite an already high number of subjects, creation of percentiles is characterized by statistical assumptions, and further studies may be needed to validate the quality of created percentiles. In addition, the ideal measure of body size to be related to the volumetric variables has to be defined and may not be height, weight, or BSA.[23]

Three-dimensional echocardiography and CMR were obtained within one day, but not simultaneously, and therefore LV volumes and EF may be affected by prolonged breath holding or sympathetic stimulation due to stress under CMR examination. In addition, CMR was obtained in a small number of volunteers but, for ethical reasons,

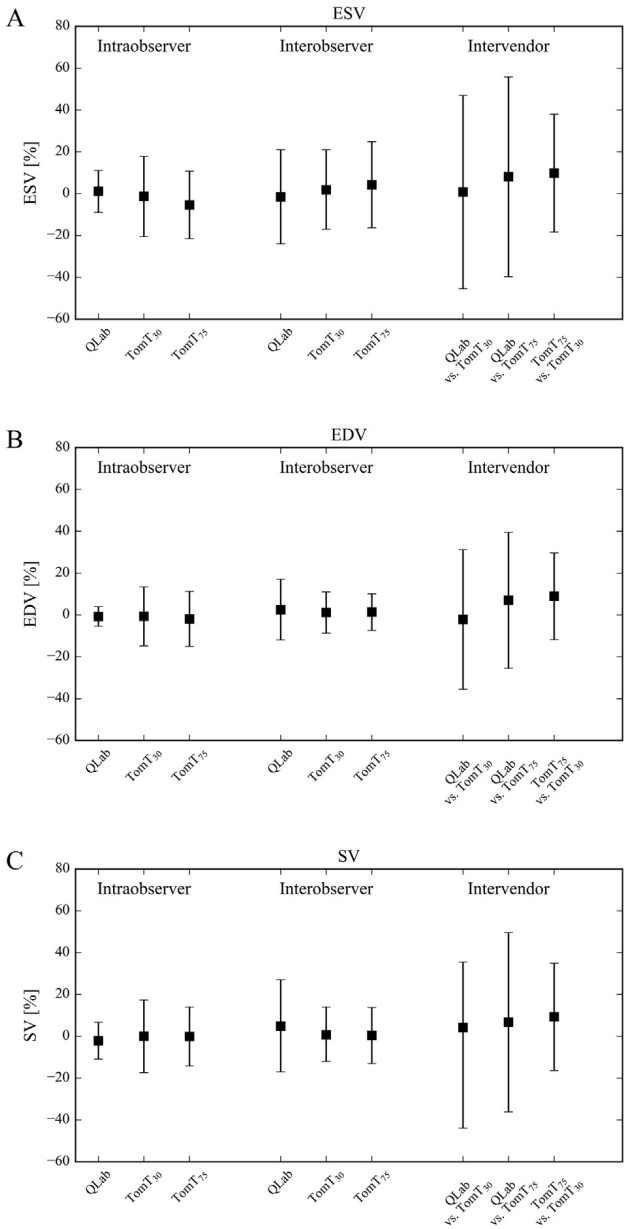

Figure 4 Intra- and interobserver-variability in relation to intervendor variability. The plots depict the relative bias (*box*) and 95% LOA (*bars*) in percents. LOA for intervendor variability for ESV **(A)**, EDV **(B)**, and SV **(C)** are larger than inter- and intraobserver variability.

not on neonates or smaller children. In our previous studies, the accuracy of RT3DE for quantification of small volumes was assessed by static as well as moving small phantoms.[16]

Children with acquired or congenital heart disease were excluded from this study, as we sought to build normative percentiles. In order to assess intervendor differences in hearts with altered geometry, further studies in children with congenital heart disease are needed.

CONCLUSION

The calculation of LV dimensions on RT3DE by semiautomated border detection software is feasible and allows reproducible and noninvasive evaluation of LV volumes and EF in pediatric cardiology.

Table 4 Agreement between CMR and RT3DE (QLab and TomTec$_{30/75}$)

	CMR and QLab	CMR and TomTec$_{30}$	CMR and TomTec$_{75}$
ESV			
Bias (%)	4.8	−2.2	0.8
95% LOA (%)	−24.0 to 33.6	−38.1 to 33.6	−46.9 to 48.4
P	.07	.375	.614
EDV			
Bias (%)	10.6	12.2	18.3
95% LOA (%)	−15.4 to 36.6	−16.2 to 40.5	−18.8 to 55.3
P	.003	.008	.004
SV			
Bias (%)	12.9	21.1	29.7
95% LOA (%)	−30.3 to 56.1	−17.8 to 60.0	−13.0 to 72.5
P	.075	<.001	<.001

This study provides percentiles of RT3DE for LV volumes as a reference for all users of the vendor-specific software QLab, as well as the vendor-independent TomTec. Furthermore, in a large cohort of healthy children, it has been shown that 3DE quantification can be influenced by the analysis package and software settings used. Therefore, results obtained by different quantification software algorithms have to be interpreted accordingly. For longitudinal follow-up, as well as cross-sectional series in practice and research, software-specific nomograms should be used.

ACKNOWLEDGMENTS

We thank Ute Baur (study nurse), Nicola Rieder (federal volunteer service), Anna Hoppe (student assistant), Hannah Kulka (student assistant), and Sophie Peiseler (student assistant) for their support; Brigitte Peters (Department of Biometry and Medical Informatics, Otto-von-Guericke University, Magdeburg, Germany) for statistical analysis; and Emma Raderschadt for editorial assistance.

SUPPLEMENTARY DATA

Supplementary data related to this article can be found online at https://doi.org/10.1016/j.echo.2018.01.018.

REFERENCES

1. Lopez L, Colan SD, Frommelt PC, Ensing GJ, Kendall K, Younoszai AK, et al. Recommendations for quantification methods during the performance of a pediatric echocardiogram: a report from the pediatric measurements writing group of the American Society of echocardiography pediatric and congenital heart disease Council. J Am Soc Echocardiogr 2010;23:465-95.
2. Ylanen K, Eerola A, Vettenranta K, Poutanen T. Three-dimensional echocardiography and cardiac magnetic resonance imaging in the screening of long-term survivors of childhood cancer after cardiotoxic therapy. Am J Cardiol 2014;113:1886-92.

3. Balluz R, Liu L, Zhou X, Ge S. Real time three-dimensional echocardiography for quantification of ventricular volumes, mass, and function in children with congenital and acquired heart diseases. Echocardiography 2013;30:472-82.
4. Schwartz ML, Gauvreau K, Geva T. Predictors of outcome of biventricular repair in infants with multiple left heart obstructive lesions. Circulation 2001;104:682-7.
5. Cantinotti M, Scalese M, Molinaro S, Murzi B, Passino C. Limitations of current echocardiographic nomograms for left ventricular, valvular, and arterial dimensions in children: a critical review. J Am Soc Echocardiogr 2012;25:142-52.
6. Lang RM, Badano LP, Mor-Avi V, Afilalo J, Armstrong A, Ernande L, et al. Recommendations for cardiac chamber quantification by echocardiography in adults: an update from the American Society of echocardiography and the European Association of cardiovascular imaging. J Am Soc Echocardiogr 2015;28:1-39.
7. Lu X, Xie M, Tomberlin D, Klas B, Nadvoretskiy V, Ayres N, et al. How accurately, reproducibly, and efficiently can we measure left ventricular indices using M-mode, 2-dimensional, and 3-dimensional echocardiography in children? Am Heart J 2008;155:946-53.
8. Simpson J, Lopez L, Acar P, Friedberg MK, Khoo NS, Ko HH, et al. Three-dimensional echocardiography in congenital heart disease: an expert consensus document from the European Association of cardiovascular imaging and the American Society of echocardiography. J Am Soc Echocardiogr 2017;30:1-27.
9. Buccheri S, Costanzo L, Tamburino C, Monte I. Reference values for real time three-dimensional echocardiography-derived left ventricular volumes and ejection fraction: review and meta-analysis of currently available studies. Echocardiography 2015;32:1841-50.
10. Friedberg MK, Su X, Tworetzky W, Soriano BD, Powell AJ, Marx GR. Validation of 3D echocardiographic assessment of left ventricular volumes, mass, and ejection fraction in neonates and infants with congenital heart disease: a comparison study with cardiac MRI. Circ Cardiovasc Imaging 2010;3:735-42.
11. Riehle TJ, Mahle WT, Parks WJ, Sallee D, Fyfe DA. Real-time three-dimensional echocardiographic acquisition and quantification of left ventricular indices in children and young adults with congenital heart disease: comparison with magnetic resonance imaging. J Am Soc Echocardiogr 2008;21:78-83.
12. Leung KY, Bosch JG. Automated border detection in three-dimensional echocardiography: principles and promises. Eur J Echocardiogr 2010;11:97-108.
13. Zhong SW, Zhang YQ, Chen LJ, Wang SS, Li WH. Evaluation of left ventricular volumes and function by real time three-dimensional echocardiography in children with functional single left ventricle: a comparison between QLAB and TomTec. Echocardiography 2015;32:1554-63.
14. Hascoet S, Brierre G, Caudron G, Cardin C, Bongard V, Acar P. Assessment of left ventricular volumes and function by real time three-dimensional echocardiography in a pediatric population: a TomTec versus QLAB comparison. Echocardiography 2010;27:1263-73.
15. Laser KT, Bunge M, Hauffe P, Argueta JR, Kelter-Klopping A, Barth P, et al. Left ventricular volumetry in healthy children and adolescents: comparison of two different real-time three-dimensional matrix transducers with cardiovascular magnetic resonance. Eur J Echocardiogr 2010;11:138-48.
16. Herberg U, Klebach C, Faller J, Trier HG, Breuer J. Spatiotemporal accuracy of real-time 3D echocardiography in the neonatal and pediatric setting-validation studies using small dynamic test objects. Ultraschall Med 2013;34:580-9.
17. Herberg U, Brand M, Bernhardt C, Trier HG, Breuer J. Variables influencing the accuracy of 2-dimensional and real-time 3-dimensional echocardiography for assessment of small volumes, areas, and distances: an in vitro study using static tissue-mimicking phantoms. J Ultrasound Med 2011;30:899-908.
18. Lang RM, Badano LP, Tsang W, Adams DH, Agricola E, Buck T, et al. EAE/ASE recommendations for image acquisition and display using three-dimensional echocardiography. J Am Soc Echocardiogr 2012;25:3-46.
19. Laser KT, Barth P, Bunge M, Dachner G, Esdorn H, Fischer M, et al. Model versus non-model based left ventricular volumetry—a matter of imaging modality or quantification software? J Biomed Graph Comput 2013;3:54-66.
20. Cole TJ, Green PJ. Smoothing reference centile curves: the LMS method and penalized likelihood. Stat Med 1992;11:1305-19.
21. Team RDC. R: a language and environment for statistical computing. Vienna, Austria: R Foundation for Statistical Computing; 2015.
22. Rigby RA, Stasinopoulos DM. Generalized additive models for location, scale and shape. J R Stat Soc Ser C Appl Stat 2005;54:507-54.
23. Sarikouch S, Peters B, Gutberlet M, Leismann B, Kelter-Kloepping A, Koerperich H, et al. Sex-specific pediatric percentiles for ventricular size and mass as reference values for cardiac MRI: assessment by steady-state free-precession and phase-contrast MRI flow. Circ Cardiovasc Imaging 2010;3:65-76.
24. Kaku K, Takeuchi M, Tsang W, Takigiku K, Yasukochi S, Patel AR, et al. Age-related normal range of left ventricular strain and torsion using three-dimensional speckle-tracking echocardiography. J Am Soc Echocardiogr 2014;27:55-64.
25. Kaku K, Takeuchi M, Otani K, Sugeng L, Nakai H, Haruki N, et al. Age- and gender-dependency of left ventricular geometry assessed with real-time three-dimensional transthoracic echocardiography. J Am Soc Echocardiogr 2011;24:541-7.
26. Miller CA, Pearce K, Jordan P, Argyle R, Clark D, Stout M, et al. Comparison of real-time three-dimensional echocardiography with cardiovascular magnetic resonance for left ventricular volumetric assessment in unselected patients. Eur Heart J Cardiovasc Imaging 2012;13:187-95.
27. Soliman OI, Krenning BJ, Geleijnse ML, Nemes A, van Geuns RJ, Baks T, et al. A comparison between QLAB and TomTec full volume reconstruction for real time three-dimensional echocardiographic quantification of left ventricular volumes. Echocardiography 2007;24:967-74.
28. Douglas PS, DeCara JM, Devereux RB, Duckworth S, Gardin JM, Jaber WA, et al. Echocardiographic imaging in clinical trials: American Society of echocardiography standards for echocardiography core laboratories: endorsed by the American College of Cardiology Foundation. J Am Soc Echocardiogr 2009;22:755-65.
29. Dorosz JL, Lezotte DC, Weitzenkamp DA, Allen LA, Salcedo EE. Performance of 3-dimensional echocardiography in measuring left ventricular volumes and ejection fraction: a systematic review and meta-analysis. J Am Coll Cardiol 2012;59:1799-808.
30. Nikitin NP, Constantin C, Loh PH, Ghosh J, Lukaschuk EI, Bennett A, et al. New generation 3-dimensional echocardiography for left ventricular volumetric and functional measurements: comparison with cardiac magnetic resonance. Eur J Echocardiogr 2006;7:365-72.
31. Soliman OI, Kirschbaum SW, van Dalen BM, van der Zwaan HB, Mahdavian Delavary B, Vletter WB, et al. Accuracy and reproducibility of quantitation of left ventricular function by real-time three-dimensional echocardiography versus cardiac magnetic resonance. Am J Cardiol 2008;102:778-83.
32. Mor-Avi V, Jenkins C, Kuhl HP, Nesser HJ, Marwick T, Franke A, et al. Real-time 3-dimensional echocardiographic quantification of left ventricular volumes: multicenter study for validation with magnetic resonance imaging and investigation of sources of error. JACC Cardiovasc Imaging 2008;1:413-23.

APPENDIX

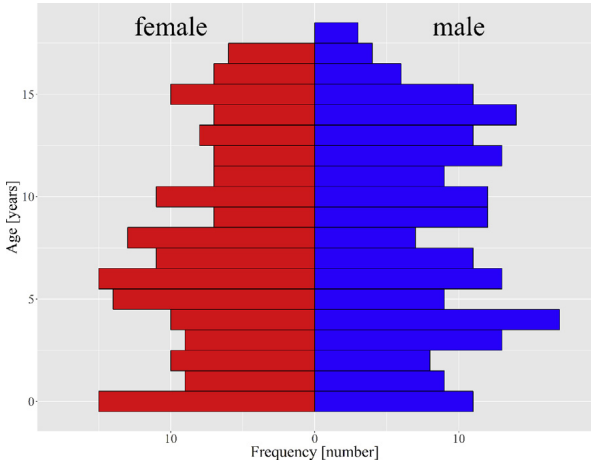

Figure S1 Sex and age distribution, study group differentiated between boys and girls.

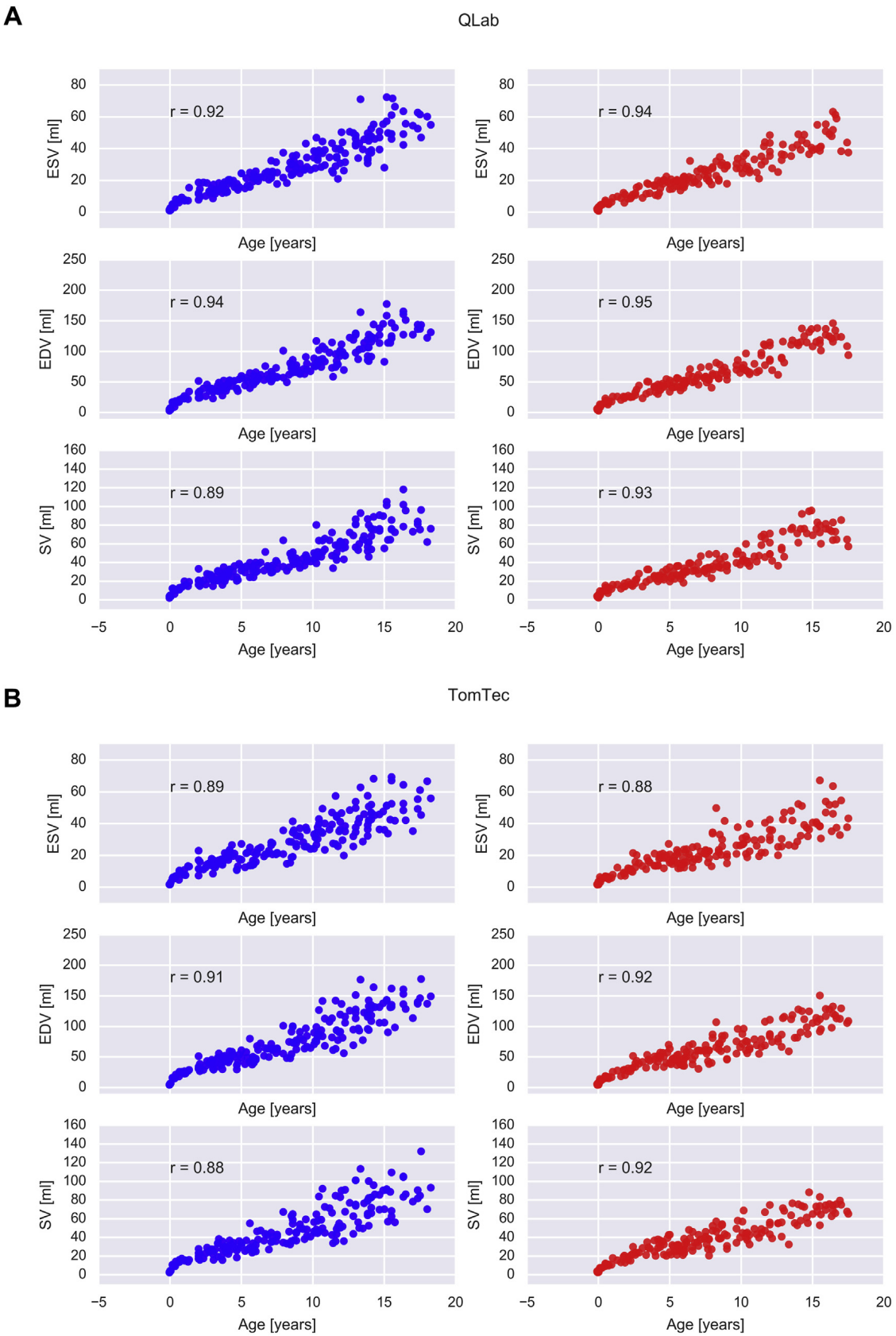

Figure S2 Gender-specific (*blue* = male, *red* = female) scatterplots for LV indices generated by QLab **(A)** and $TomTec_{30}$ **(B)** correlated to age.

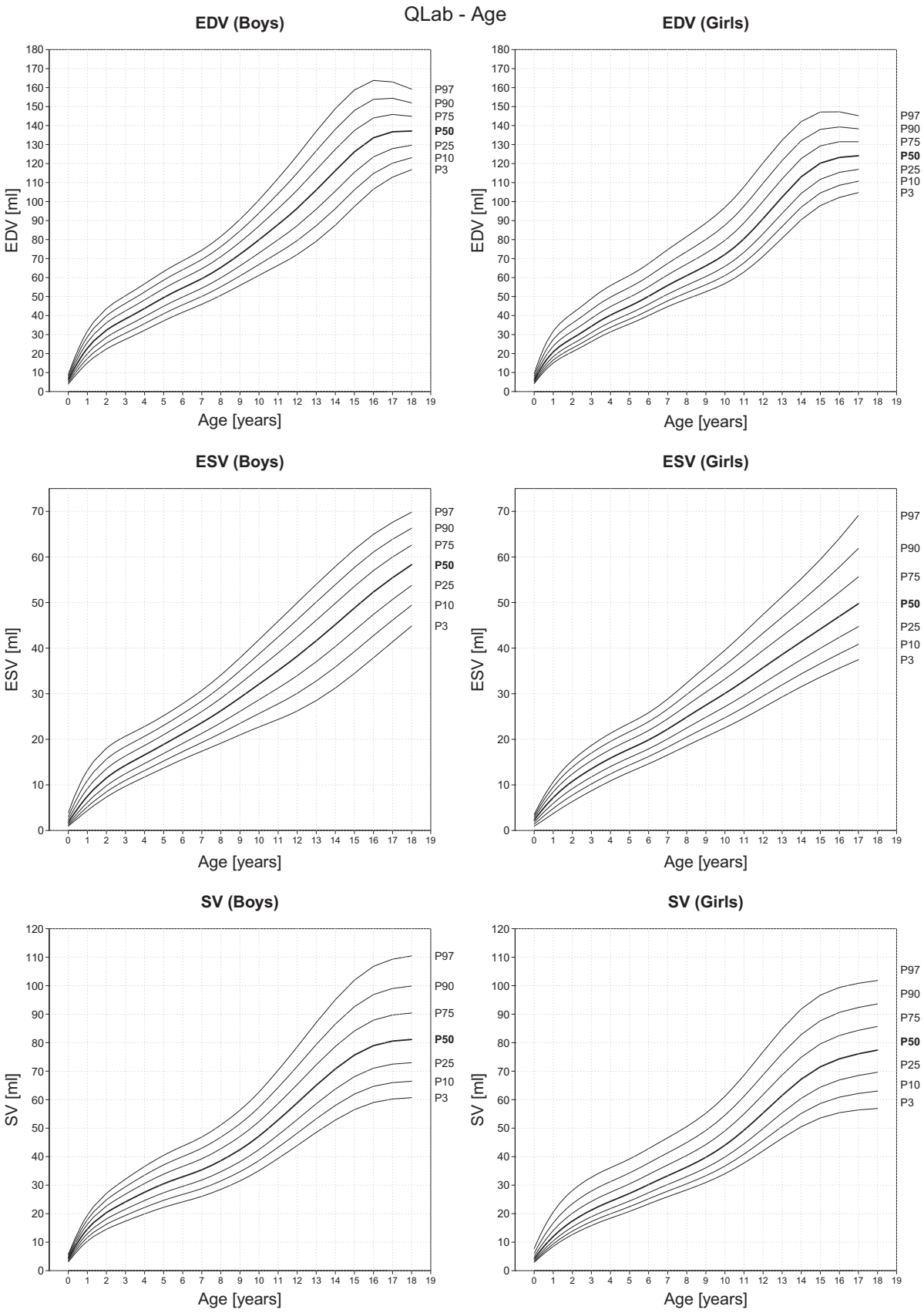

Figure S3 Gender-specific percentiles for QLab: EDV, ESV, and SV in relation to age, height, weight, and BSA (Haycock). P indicates the percentile value, e.g., P50 = 50th percentile value.

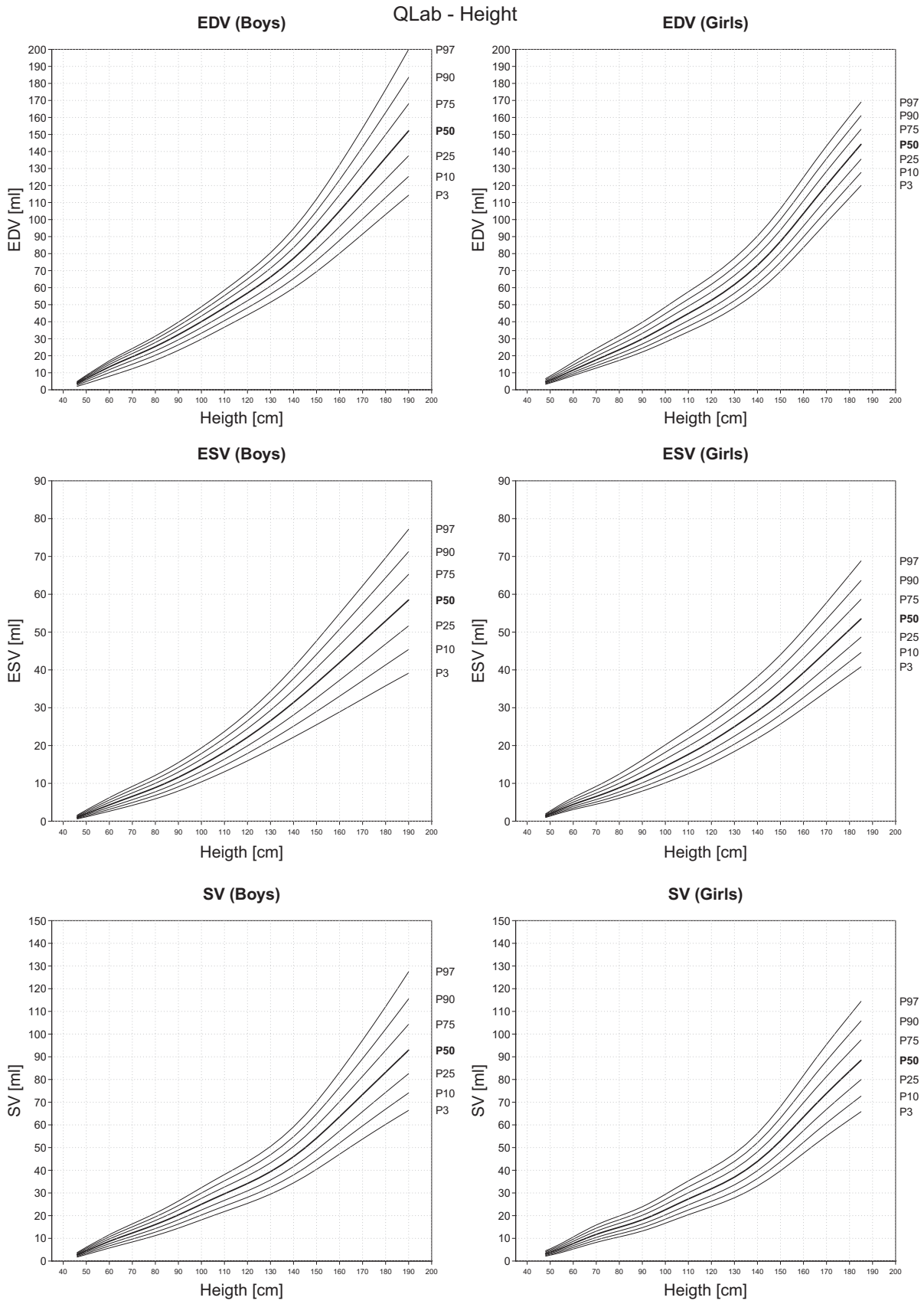

Figure S3 Continued.

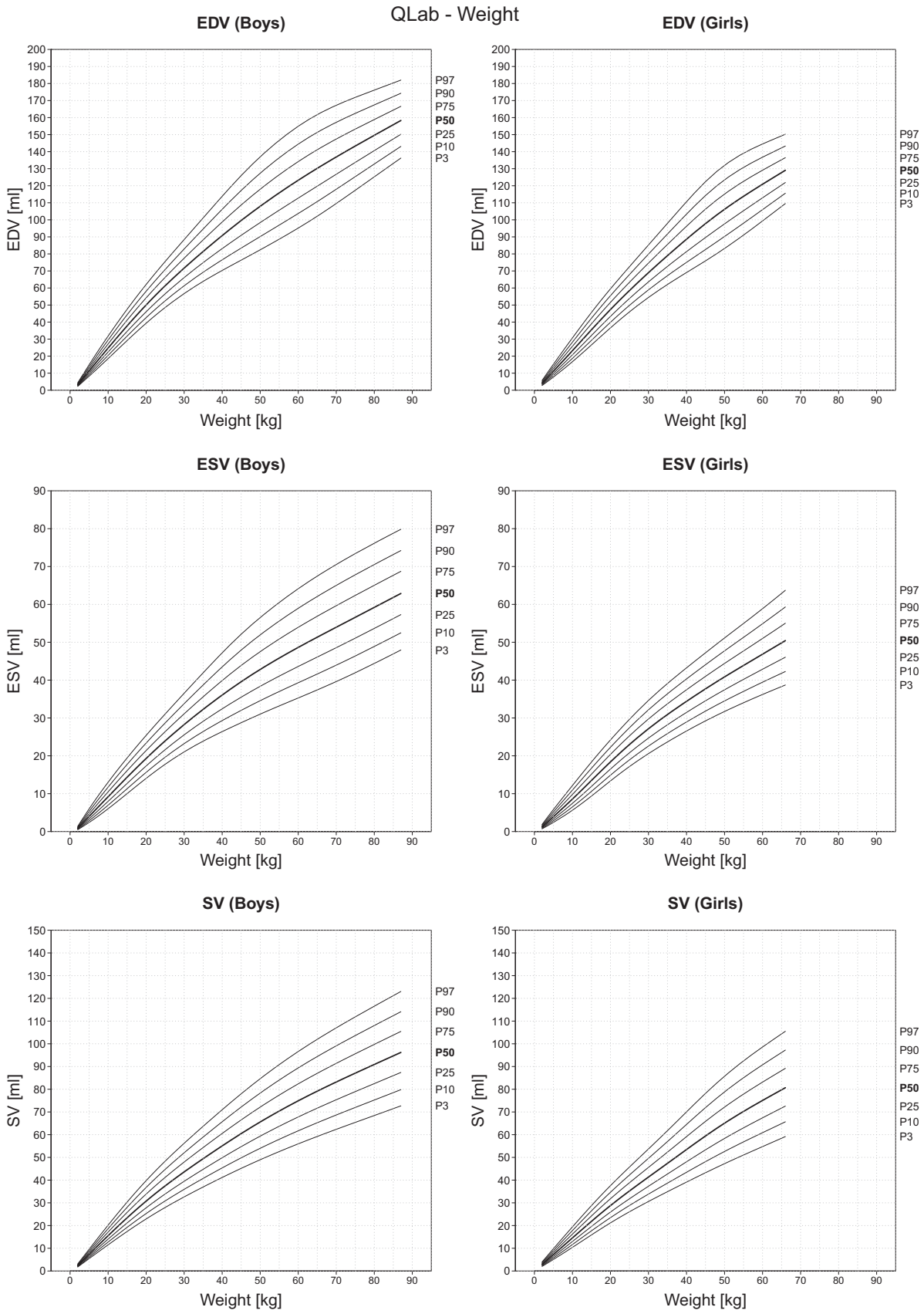

Figure S3 Continued.

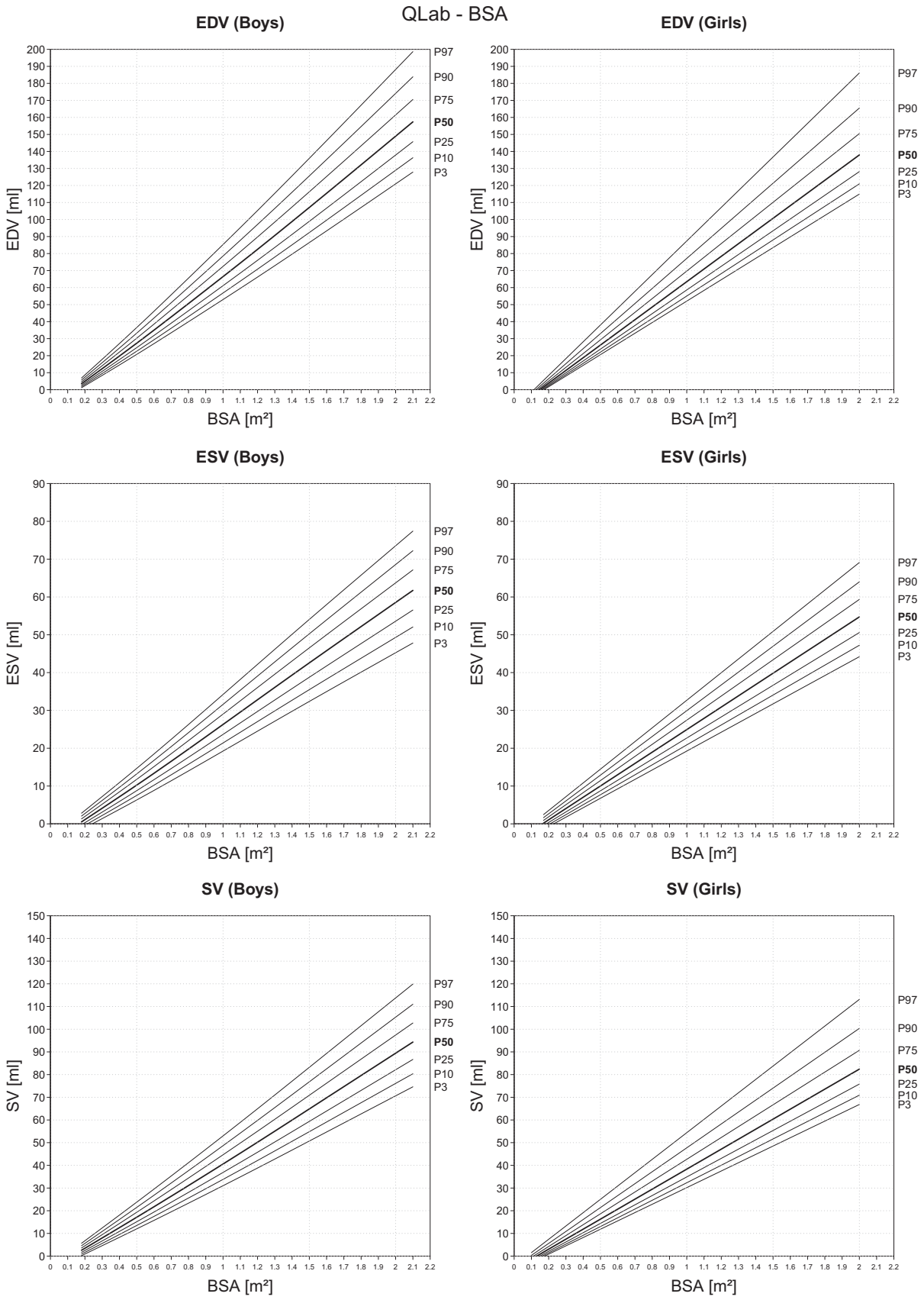

Figure S3 Continued.

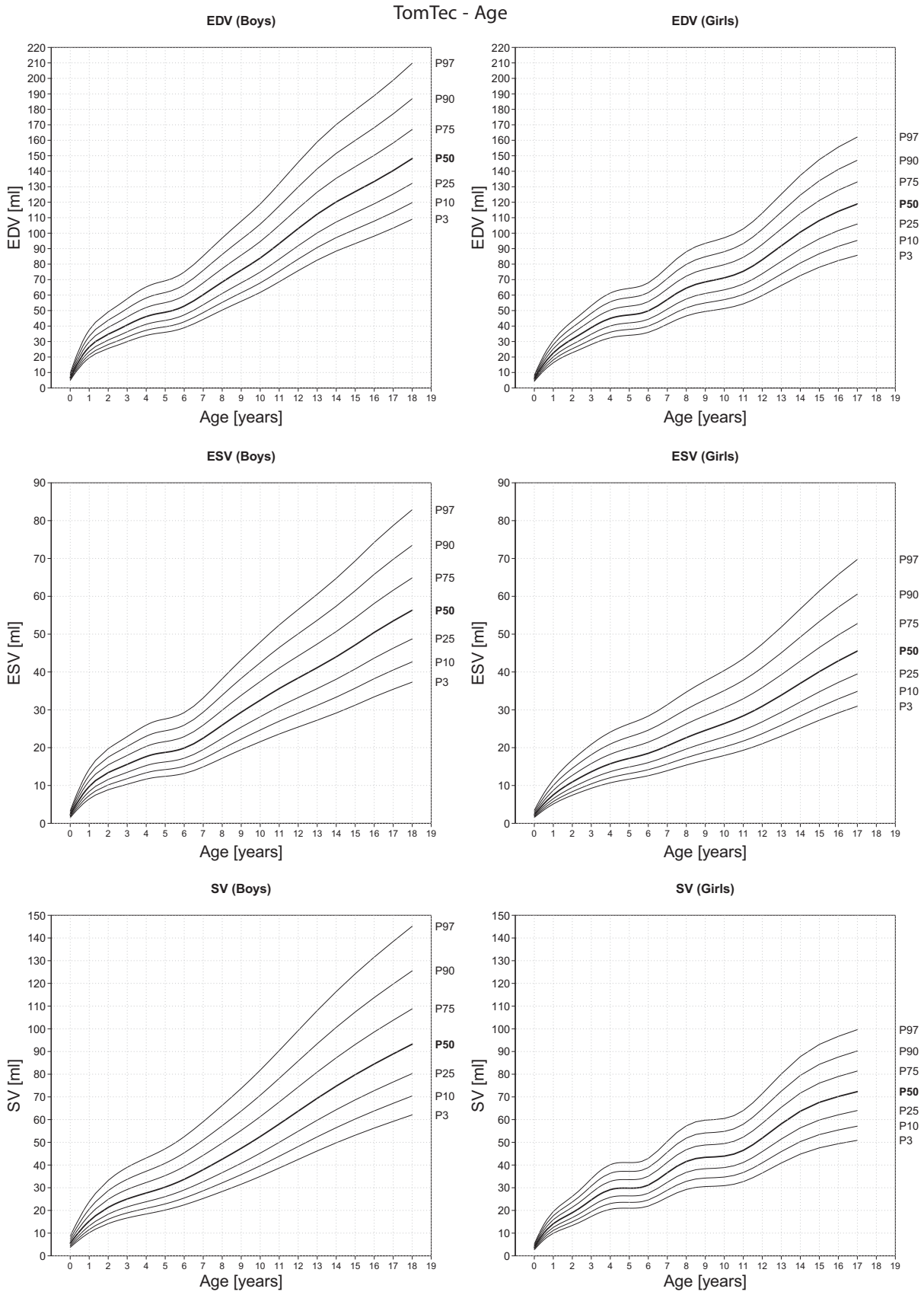

Figure S4 Gender-specific percentiles for $TomTec_{30}$: EDV, ESV, and SV in relation to age, height, weight, and BSA (Haycock). P indicates the percentile value, e.g., P50 = 50th percentile value.

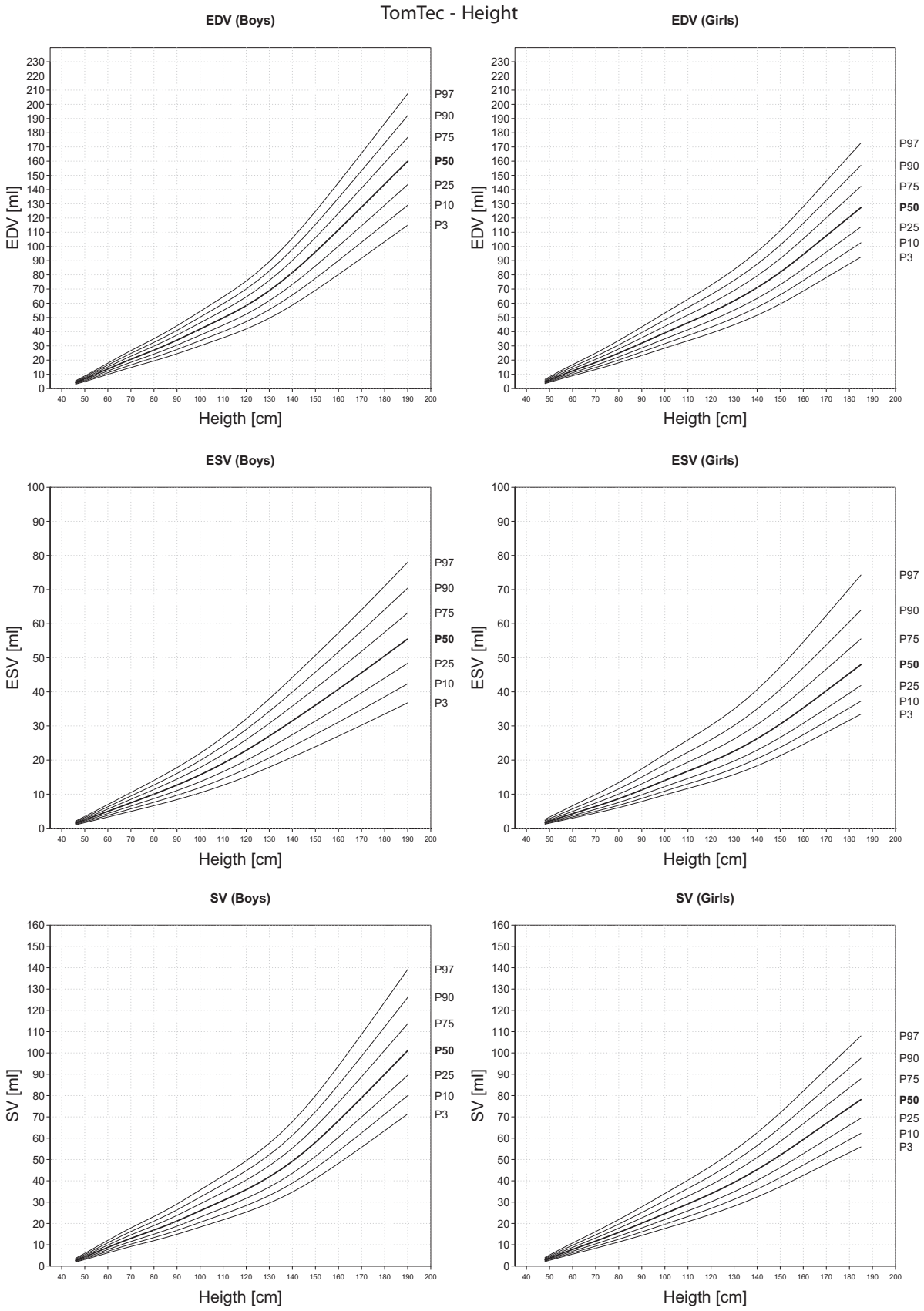

Figure S4 Continued.

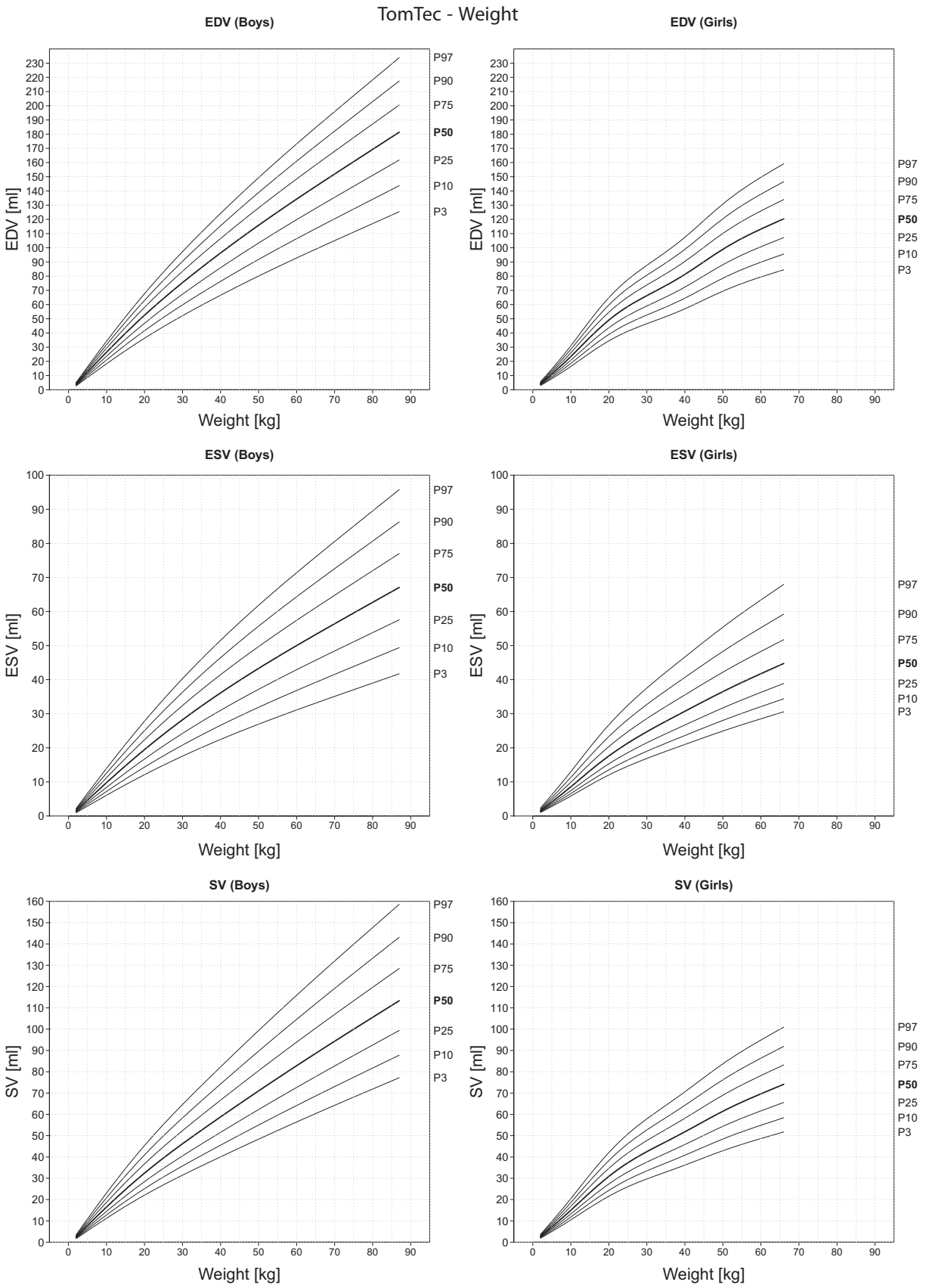

Figure S4 Continued.

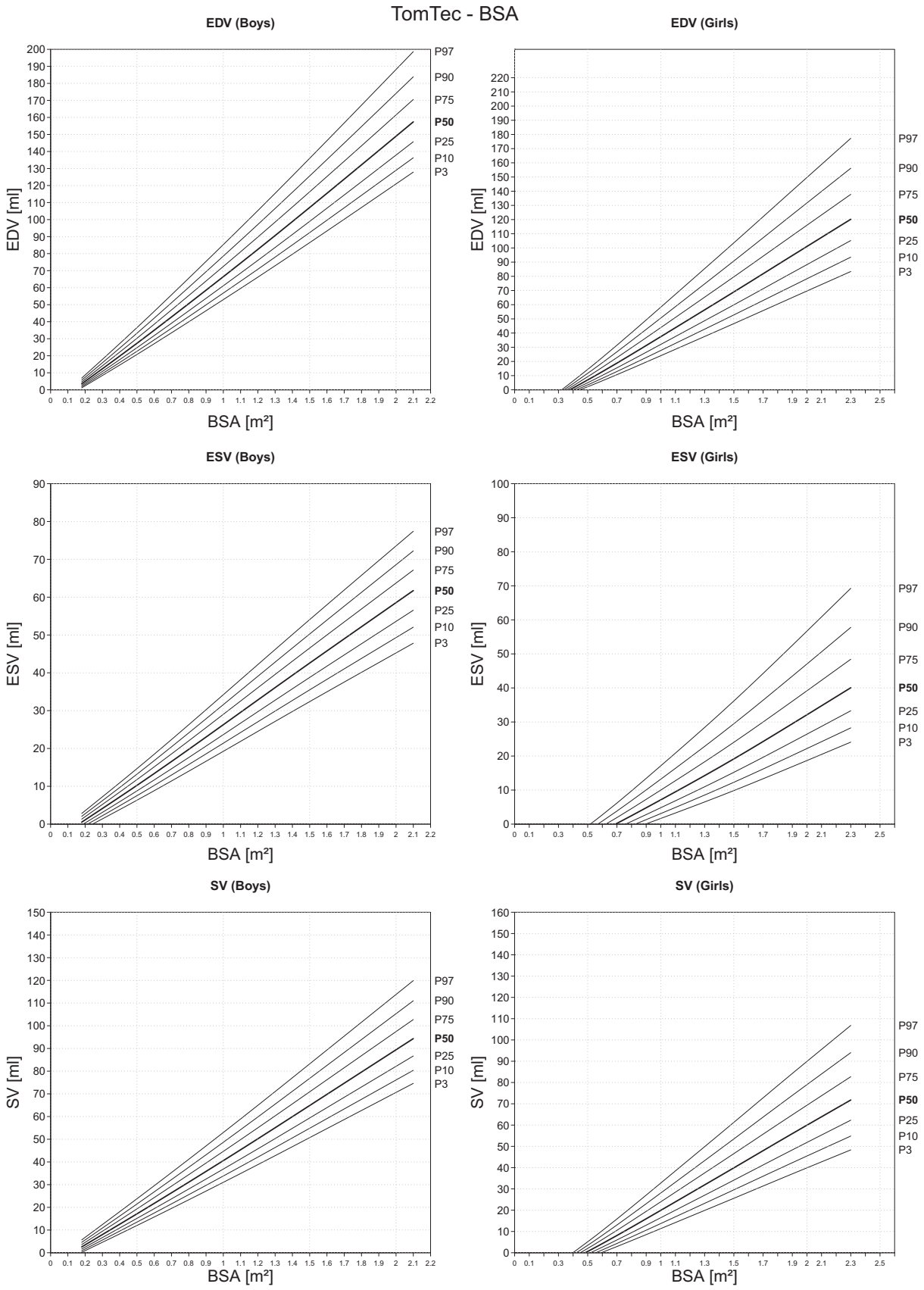

Figure S4 Continued.

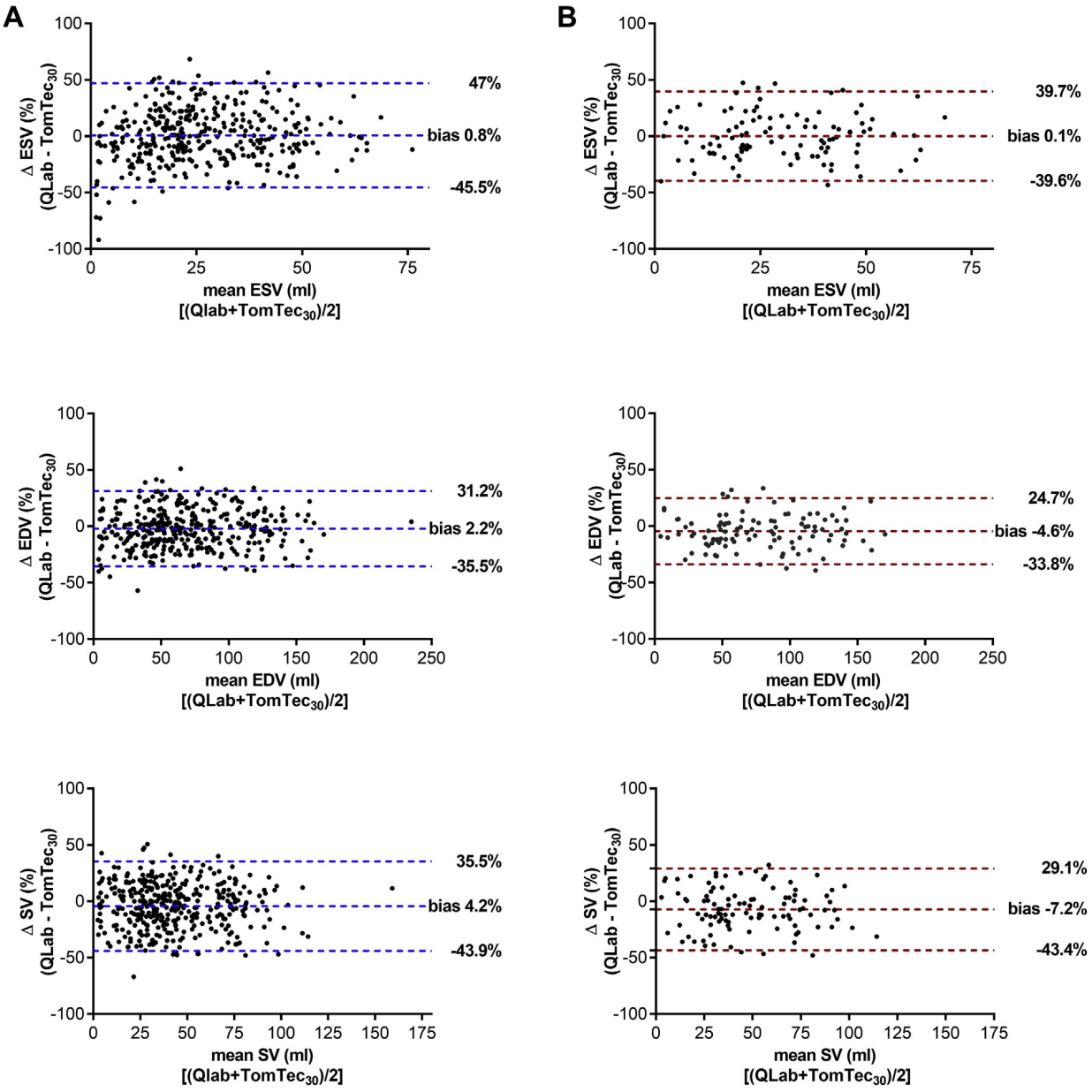

Figure S5 Bland-Altman plots by RT3DE using Qlab 9.0 and TomTec with low CFA ($TomTec_{30}$) derived from data sets of 370 healthy children **(A)** and data sets with good quality only (n = 104) **(B)**.

Table S1 Intra- and interobserver variability

	Intraobserver variability		Interobserver variability	
	Intraclass correlation 95% CI	Bias 95% LOA	Intraclass correlation 95% CI	Bias 95% LOA
ESV (mL)				
QLab	0.997 0.994 to 0.998	0.4 −3.2 to 3.9	0.983 0.969 to 0.991	−0.3 −7.9 to 4.4
$TomTec_{30}$	0.997 0.995 to 0.999	0.0 −4.6 to 4.6	0.994 0.988 to 0.997	−0.1 −5.8 to 5.5
$TomTec_{75}$	0.983 0.966 to 0.993	−0.8 −4.4 to 2.8	0.996 0.991 to 0.999	0.8 −3.5 to 5.1
EDV (mL)				
QLab	0.998 0.997 to 0.998	−0.6 −4 to 2.7	0.998 0.997 to 0.998	2.1 −7.7 to 12.0
$TomTec_{30}$	0.998 0.997 to 0.999	0.4 −8.1 to 8.9	0.998 0.996 to 0.999	0.1 −8.0 to 8.2
$TomTec_{75}$	0.999 0.998 to 1.000	−1.1 −7.6 to 5.4	0.999 0.998 to 1.000	0.4 −4.8 to 5.7
SV (mL)				
QLab	0.999 0.998 to 0.999	−1.1 −5.4 to 3.3	0.98 0.953 to 0.990	2.3 −8.0 to 13.0
$TomTec_{30}$	0.997 0.995 to 0.999	0.0 −7.2 to 7.1	0.996 0.993 to 0.998	0.0 −6.9 to 6.8
$TomTec_{75}$	0.998 0.996 to 0.999	−0.3 −5.0 to 4.4	0.998 0.995 to 0.999	0.2 −1.2 to 4.6
EF (%)				
QLab	0.934 0.918 to 0.947	−0.8 −4.6 to 3.1	0.571 0.218 to 0.776	1.6 −7.0 to 10.0
$TomTec_{30}$	0.952 0.914 to 0.975	0.4 −5.5 to 6.4	0.935 0.867 to 0.968	−0.1 −5.6 to 5.4
$TomTec_{75}$	0.91 0.814 to 0.916	2.4 −5.2 to 9.9	0.911 0.780 to 0.964	−7.0 −7.1 to 5.2

Table S2 Calculation of LV 3D volume data using different software algorithm—agreement among QLab, $TomTec_{30}$, and $TomTec_{75}$

	$TomTec_{75}$ vs $TomTec_{30}$	QLab vs $TomTec_{30}$	QLab vs $TomTec_{30}$, good quality only	QLab vs $TomTec_{75}$
ESV (mL)				
Bias	1.9	0.7	0.1	2.0
95% LOA	−4.5 to 8.3	−12 to 13.3	−13.3 to 13.4	−9.5 to 13.6
P	<.001	.051	.932	<.001
EDV (mL)				
Bias	5.4	−1.2	−3.6	4.5
95% LOA	−6.6 to 17.0	−26.3 to 23.8	−29.6 to 22.4	−16.5 to 25.5
P	.000	.065	.006	<.001
SV (mL)				
Bias	3.7	−2.0	−3.7	2.5
95% LOA	−7.1 to 15.0	−21.2 to 17.2	−23.4 to 16.0	−16.1 to 21.2
P	<.001	<.001	<.001	<.001
EF (%)				
Bias	−0.1	−1.2	−1.6	−0.3
95% LOA	−8.4 to 8.2	−14.1 to 11.7	−13.4 to 10.3	−14.7 to 14.2
P	.821	.000	.009	.55

Table S3 Agreement between CMR and RT3DE (QLab and $TomTec_{30/75}$)

	CMR and QLab	CMR and $TomTec_{30}$	CMR and $TomTec_{75}$
ESV (mL)			
Bias	2.3	−1.9	−1.4
95% LOA	−8.9 to 13.6	−21.0 to 17.0	−27.2 to 24.3
P	.07	.375	.614
EDV (mL)			
Bias	8.3	8.9	14.0
95% LOA	−14.5 to 31.1	−19.0 to 37.0	−26.0 to 53.9
P	.003	.008	.004
SV (mL)			
Bias	5.3	11	15.4
95% LOA	−20.8 to 31.5	−9.0 to 31.0	−9.2 to 40.0
P	.075	<.001	<.001
EF (%)			
Bias	2.0	5.5	6.9
95% LOA	−11.7 to 15.6	−7.1 to 18	−5.8 to 19.6
P	.195	.001	<.001